A STUDY OF A NEW ELECTROMECHANICAL ENERGY CONVERSION PROCESS USING SUPERCONDUCTING FREQUENCY MODULATED RESONATORS

Thesis by

Huan-chun Yen

In Partial Fulfillment of the Requirements

for the Degree of

Doctor of Philosophy

California Institute of Technology

Pasadena, California

1977

(Submitted May 18, 1977)

To Pauline and Our Parents

ACKNOWLEDGEMENT

I would like to express my sincere appreciation to the following persons who have made this work possible.

Professor J.E.Mercereau for his valuable advice, constructive criticism and continuous interest throughout this research.

Dr. G.J.Dick for his ingenious insight to this problem and many other things that he has taught me.

Dr. K.W.Shepard for his continuous interest, encouragement and help toward this research.

Dr. T.Yogi for his numerous personal advices and assistance in carrying out the experiment.

Dr. H.Notarys for his general help in the daily operation of the laboratory.

Mr. J.R.Delayen for his generosity of sharing his apparatus and data with me.

All the previous and present graduate student colleagues for making the laboratory also a pleasant place to work at nights.

Mr. S.Santantonio for his skillful machining of various resonators used for this study.

Mr. E.P.Boud for his helpful and kind advice in addition to the technical assistance.

Ms. G.Kusudo for her enthusiastic administrative and general assistance for all my years as a graduate student.

I also like to thank the Institute of Electrical and Electronics

Engineers, Inc. for the kind permission to reproduce the following figures;2.1, 2.9, 2.10, 3.1, 3.2, 3.3 which originally appeared in IEEE Trans MAG-11 and MAG-13.

The financial assistance throughout my graduate study is provided by the California Institute of Technology and is greatly appreciated.

Last, but not least, I would like to thank my wife Pauline, not only for the fine typing of this dissertation, but also for her patience and encouragement throughout the course of my graduate study.

ABSTRACT

Experimental demonstrations and theoretical analyses of a new electromechanical energy conversion process which is made feasible only by the unique properties of superconductors are presented in this dissertation. This energy conversion process is characterized by a highly efficient direct energy transformation from microwave energy into mechanical energy or vice versa and can be achieved at high power level. It is an application of a well established physical principle known as the adiabatic theorem (Boltzmann-Ehrenfest theorem) and in this case time dependent superconducting boundaries provide the necessary interface between the microwave energy on one hand and the mechanical work on the other. The mechanism which brings about the conversion is another known phenomenon - the Doppler effect. The resonant frequency of a superconducting resonator undergoes continuous infinitesimal shifts when the resonator boundaries are adiabatically changed in time by an external mechanical mechanism. These small frequency shifts can accumulate coherently over an extended period of time to produce a macroscopic shift when the resonator remains resonantly excited throughout this process. In addition, the electromagnetic energy inside the resonator which is proportional to the oscillation frequency is also accordingly changed so that a direct conversion between electromagnetic and mechanical energies takes place. The intrinsically high efficiency of this process is due to the electromechanical interactions involved in the conversion rather than a process of thermodynamic nature and therefore is not limited by the thermodynamic value.

A highly reentrant superconducting resonator resonating in the range of 90 to 160 MHz was used for demonstrating this new conversion technique. The resonant frequency was mechanically modulated at a rate of two kilohertz. Experimental results showed that the time evolution of the electromagnetic energy inside this frequency modulated (FM) superconducting resonator indeed behaved as predicted and thus demonstrated the unique features of this process. A proposed usage of FM superconducting resonators as electromechanical energy conversion devices is given along with some practical design considerations. This device seems to be very promising in producing high power ($\sim$ 10W/cm^3) microwave energy at 10 - 30 GHz.

Weakly coupled FM resonator system is also analytically studied for its potential applications. This system shows an interesting switching characteristic with which the spatial distribution of microwave energies can be manipulated by external means. It was found that if the modulation was properly applied, a high degree (>95%) of unidirectional energy transfer from one resonator to the other could be accomplished. Applications of this characteristic to fabricate high efficiency energy switching devices and high power microwave pulse generators are also found feasible with present superconducting technology.

TABLE OF CONTENTS

Chapter I

INTRODUCTION

This thesis concerns a new process of energy conversion which is made feasible only by the unique properties of superconductors. The main thrust for this study is that with present-day superconductivity technology, this application appears quite practical. In this dissertation we will not deal with the fundamental aspects of the superconductivity phenomena, instead, we will study the underlying principles for this application using our knowledge of superconductivity and achievable technical expertise.

Superconductivity is a manifestation of a macroscopic coherent electronic state in certain metals, alloys and compounds when cooled below 23°K or so. It is characterized by the absence of d.c. electrical resistance (the perfect electrical conductivity) and by a perfect or near perfect diamagnetism (the Meissner effect). During the last three decades, a great deal of progress has been made both in understanding the fundamental processes involved in the superconductivity and in advancing technologies for superconducting material processing. As a result, numerous practical applications based on these unique properties of superconductors have been proposed, demonstrated and realized, ranging from tiny quantum devices to huge superconducting magnet systems. Among these applications, the latter has been undoubtedly the most successful application so far (1,2). Despite these notable achievements, almost all branches of applied superconductivity are still being actively pursued (3,4).

As noted above the electrical resistance of a superconductor is

identically zero for direct currents. It becomes finite however for time varying currents (a.c) even though it can remain quite small up to frequencies in the infrared region. Physically this finite a.c. loss can arise because of the inertia of the superconducting electrons inside the superconductor which prevents them from responding to the external electric field instantaneously. The lagging in response results in incomplete screening of external field which allows the field to penetrate into a thin layer (called penetration depth, usually about several hundred Å thick) on the superconductor surface. The loss occurs when the normal electrons which coexist with superconducting ones at finite temperature are driven by this residual field inside the penetration depth. However, this loss mechanism based on the superconducting-normal electron model (two fluid model) is only a phenomenological account of the possible mechanism. In 1957 Bardeen, Cooper and Schrieffer advanced a microscopic theory of superconductivity based on quantum mechanics (BCS theory) (5). There a new, dominant loss mechanism involving the excitation of quasiparticles across a non-zero energy gap out of the condenstate of a superconductor was proposed. Experimentally only part of the observed surface resistance can be explained in terms of this microscopic mechanism. The origin of the remaining part (residual surface resistance) continues to be a controversial subject (6,7,8,9). Nevertheless, it has been demonstrated that at 1 GHz the surface resistance of a superconductor can be 5 or 6 orders of magnitude smaller than the corresponding value of room temperature copper at low field level (10). In addition to the temperature dependence,

the surface resistance generally was also found to depend on the magnetic and/or electric field that the superconductor surface experienced (6,7,8,9).

Experimental studies at high field level have previously been associated with the effort to generate intense rf* fields inside superconducting resonators for charged particle accelerators. These studies have shown that the residual surface resistance R_s possibly is due to dielectric loss on the surface, magnetic flux trapped inside superconductor, or acoustic phonon generation or any combination of them (6,7,8,9). Furthermore, these studies also showed that intense rf magnetic fields up to 1600 gauss and rf electric fields up to 70 MV/m were obtainable inside microwave resonators, even exceeding the thermodynamic values in some cases (6,10,11).

The implication of this spectacular reduction in rf surface resistance as well as the ability to support intense electromagnetic fields inside a resonator, is that superconductors can be used to fabricate devices and machinery operated at high rf power level. Such a development is now possible since the material technology for producing large high quality superconducting surfaces has become "routine" in many laboratories. This field is now known as "high power rf superconductivity." Almost all previous high power rf applications have been centered around building superconducting particle accelerators and related devices. Resonators of fixed resonant frequency have been exclusively used in these applications and a good understand-

---

* Throughout this dissertation, radio frequency (rf) is loosely defined as from 80 MHz to 10 GHz for our purpose.

ing of their electromagnetic characteristics has been achieved. Prototype superconducting accelerators are under development at several places both in the United States and abroad.

Tunable superconducting resonators whose resonant frequencies can be continuously tuned or modulated on the other hand have not drawn similar attention. The main reason seems to be lack of obvious applications of frequency modulated (FM) resonators. There has been a proposed application of FM resonator as an ultra sensitive displacement transducer in the past (12). However the motivation behind the present work is to demonstrate the development of FM resonators as a new class of novel high power devices. In this dissertation, analytic and/or experimental foundations are laid illustrating the principle and its implementation via superconductivity as well as some possible applications which are in turn evaluated with existing superconductivity technologies. Among these applications are efficient electromechanical energy conversion devices; microwave energy switches and high power microwave pulse generators. Although basic physical concepts underlying these applications have been known for sometime and often appear in other contexts of physics, the subtleties of applying these concepts in conjunction with extraordinary properties of superconductors to build useful devices and machinery are unique and less familiar and will be explored in this dissertation.

The content of each chapter is outlined below: Chapter II deals with analytical and experimental studies on the properties of a single FM resonator, using a highly reentrant resonator as an example. An efficient electromechanical energy conversion scheme is then present-

ed along with some practical considerations. Chapter III discusses the behavior of a system composed of coupled FM resonators. The spatial and temporal energy distribution among the resonators are derived with the results applied to energy switching and pulse generation applications.

All the units used in this dissertation are the rationalized MKS units unless otherwise specified.

References

1. V.L.Newhouse, Applied Superconductivity Vol. 1 & 2. (Academic Press, New York, 1975).
2. S.Foner and B.Schwartz, Superconducting Machines and Devices (Plenum Press, New York, 1974).
3. 1974 Applied Superconductivity Conference, IEEE Trans. Mag. MAG-11, 95-883 (1975).
4. 1976 Applied Superconductivity Conference, IEEE Trans. Mag. MAG-13, 11-887 (1976).
5. J.Bardeen, L.N.Cooper and J.R.Schrieffer, Phys. Rev. 108, 1175-1204 (1957).
6. T.Yogi, Ph.D. Thesis, California Institute of Technology (1977).
7. J.Halbritter, IEEE Trans. Mag. MAG-11, 427-430 (1975).
8. J.M.Pierce, J. Appl. Phys. 44, 1342-1347 (1973).
9. J.R.Delayen, H.C.Yen, G.J.Dick, K.W.Shepard and J.E.Mercereau, IEEE Trans. Mag. MAG-11, 408-410 (1975).
10. J.P.Turneaure and N.T.Viet, Appl. Phys. Lett. 16, 333-335 (1970).
11. K.Schnitzke, H.Martens, B.Hillenbrand and H.Diepers, Phys. Lett. 45A, 241-242 (1973)
12. G.J.Dick and H.C.Yen, Proceedings of 1972 Applied Superconductivity Conference Annapolis, Md. 684-686 (1972).

Chapter II

FREQUENCY MODULATED (FM) SUPERCONDUCTING RESONATORS AND THEIR APPLICATIONS AS ELECTROMECHANICAL ENERGY CONVERSION DEVICES

2.1 Introduction

Resonators of fixed boundaries have been well studied in conventional microwave electronics. The resonant frequencies and corresponding mode configurations are determined by the resonator geometry and are mathematically obtained by solving Maxwell equations with appropriate fixed boundary conditions. For an ideal resonator, a particular nondegenerate mode once excited will persist indefinitely in time. Since the resonator modes are standing wave modes, the electromagnetic energy associated with an excited mode is completely confined to within the ideal conducting enclosure of the resonator. The fixed conducting boundaries of the resonator provide an isolating barrier across which no energy can flow into or out of the resonator.

Frequency modulated (FM) resonators on the other hand behave quite differently from those described in the preceding paragraph. The frequency modulation of our interest is accomplished by slow motion of the resonator boundaries in time. Conventional wisdom of solving well defined boundary value problems fails in this case because the boundaries themselves are constantly changing. In fact, the resonator can not be separated from the modulation mechanism and form an isolated subsystem by itself any more. The consequence of changing from fixed to moving boundaries is that energy can now flow into or out of the resonator in either direction depending on the nature of modulation. Since mechanical means are employed to modulate

the resonator, mechanical energy can be exchanged with the electromagnetic energy via a moving boundary. This mode of energy exchange is characterized by a direct conversion of low frequency mechanical energy into high frequency electromagnetic energy or vice verse.

The mechanism which brings about this energy conversion scheme can be understood in terms of the familiar Doppler effect. To illustrate this point, let us consider a specific example, namely an ideal cylindrical resonator of radius R and height h whose TE_{111} mode is excited. The radius R is assumed to be fixed but the height can be varied by making one end movable so that the resonator can be tuned (modulated). This mode whose frequency depends only on the position of the movable end for a given radius is characterized by the absence of a longitudinal electric field along the axial direction of the cylinder. The longitudinal magnetic field has the usual standing wave pattern which can be regarded as composed of two waves travelling oppositely to each other and being reflected at the two ends of the cylinder. If the movable end is slowly moved inward, the resonant frequency f is increased. But each time the wave is reflected from the moving end, its frequency is Doppler shifted by a very small amount. The shift is such that the new oscillation frequency matches the instantaneous resonant frequency to a high degree of accuracy. The mismatch depends on the rate at which the end boundary is moved and can be made infinitesimally small if the rate is extremely slow. Even though the individual shift is quite small ($\Delta f < 10^{-6} f$ for mechanical modulation),

it nevertheless can accumulate from many reflections over a long period of time to produce a macroscopic frequency change. Concurrently with the frequency change, the time averaged electromagnetic energy associated with the oscillation inside the resonator is also changed by the same factor, because it can be shown quite generally the electromagnetic energy is proportional to the oscillation frequency in this adiabatic limit (see further discussion in Sec. 2.2). The increase in energy comes from the mechanical work done by the external modulation mechanism on the high frequency electromagnetic force which is the counterpart of the Lorentz force at low frequencies indicating the energy exchange with outside is now possible.

In order for the aforementioned accumulation to take place, we have tacitly assumed that the electromagnetic oscillation is sustained forever. This actually requires that two conditions be satisfied. The first condition which has already been assumed is that modulation must be done slowly so that over one period of the electromagnetic oscillation, the change in frequency is infinitesimally small. Under this adiabatic condition, the resonant oscillation will adjust to and follow the quasi-static change of the boundary. The second condition which bears directly to the usage of superconductors is that the electromagnetic energy inside the resonator should not decay significantly throughout the modulation process. If a normal resonator were used, this scheme would never be operative because the electromagnetic energy inside would have been completely dissipated before any appreciable accumulation could take place. Only superconducting resonators can approximately satisfy this condition. Consequences

of these two conditions are further discussed later in Sec.2.2, Sec. 2.4 and Sec. 2.5.

In this chapter, experimental evidence is presented to demonstrate the unique features of this new electromechanical energy conversion process using a superconducting resonator. The application of this scheme to fabricate practical devices is then discussed. The outline of each section is as follows: Section 2.2 reviews the fundamental principle governing slowly frequency modulated resonators. Section 2.3 covers the experimental methods employed to study this conversion scheme. Section 2.4 discusses the experimental results. Section 2.5 introduces an efficient electromechanical energy conversion device using an FM superconducting resonator as a component. The characteristics of this type device are then evaluated. A brief comparison with more familiar parametric amplifiers is also presented in Sec. 2.6.

2.2 Adiabatic Principle (Boltzmann-Ehrenfest Theorem)

The adiabatic principle is one of the important basic physical principles underlying this electromechanical energy conversion scheme. A general treatment leading to the Boltzmann formula and its application to an adiabatic transformation resulting in adiabatic invariants of Ehrenfest has been given by L.Brillouin(1). Since we are interested in a system executing quasi-sinusoidal harmonic oscillation at frequency f, the adiabatic principle will be reviewed here in terms of harmonic oscillation parameters.

In Appendix A, the Boltzmann-Ehrenfest theorem is shown with a resonant circuit consisting of an inductor L and a slowly varying capacitor C. Since this theorem is quite general and certainly appli-

cable to an adiabatically frequency modulated resonator, the results obtained there are also applicable here. This is not completely unexpected because after all the resonator is the counterpart of LC resonant circuit at high frequency and quite often the essential resonator characteristics can be obtained from its equivalent LC circuit without the detailed knowledge of the field configurations. In any case, the same results can be obtained from the first principle with a given resonator geometry even though in reality this can be a very complicated exercise. If we briefly summarized the results obtained in Appendix A, the Boltzmann-Ehrenfest theorem can be stated as follows: when a transformation is carried out on an ideal periodic system of period $T \equiv 1/f$ by a very slow and continuous change of its constraint parameters, the product $T\overline{W}$ remains constant and constitutes an adiabatic invariant of the transformation, where $\overline{W}$ is the total energy of the system averaged over one period of oscillation.* Mathematically, this theorem states that if the adiabatic condition

$$\frac{1}{f(t)} \frac{df(t)}{dt} << f(t) \qquad (2.1)$$

is satisfied then for a dissipationless system the quantity $\overline{W}(t)/\overline{f(t)}$ is an adiabatic invariant. This comes about because as shown in Appendix A,

$$\frac{d}{dt} \ln(W/f) = \frac{W(0)}{\omega(0)} \cdot \omega^2 \left(s \cdot \cos\left(2 \int_0^t \omega dt + 2\theta_0\right)\right.$$

---

* Strictly speaking, frequency is not defined for non-periodic oscillations. However an averaged frequency over several oscillations has an operational meaning and it is understood to be interpreted as such.

$$- \frac{s^2}{2} \sin(2\int_0^t \omega\, dt + 2\theta_0) + O(s^3)) \qquad (2.2)$$

where $W(0)$,$\omega(0)$ and θ_0 are respectively the initial energy, angular frequency and phase. $s \equiv \frac{1}{\omega^2}\frac{d\omega}{dt}$ is a dimensionless parameter characterizing the slowness of the adiabatic process. It can be seen from Eq.(2.1) that s is a very small number in the adiabatic limit. If we average Eq.(2.2) over one oscillating period, the right hand side of Eq.(2.2) becomes vanishingly small because the averaged trigonometric terms are essentially zero to a high degree of accuracy * (in addition to the smallness of s). Therefore we have

$$\frac{\overline{W}(t)}{\overline{f}(t)} = \text{constant} \qquad (2.3)$$

The bar indicates an averaging over one intrinsic oscillation period has been performed.

In this system, there are two scales of time variation that differ by several orders of magnitude from each other (adiabatic condition). The rapid time variation takes place approximately over the intrinsic oscillation period, in this example, the rf oscillation period. The slow time variation takes place approximately over the time scale during which the constraint parameters change significantly. The detailed electric and magnetic field distributions (or equivalently, the charge and current distributions) belong to the former and the total instantaneous energy, the oscillating frequency etc. belong to the

---

*Only the rapidly changing trigonometric terms need to be averaged. The other time dependent quantities vary over a much slower scale (5 or 6 order of magnitude slower) and can be regarded as constant for this purpose.

latter category.*

Equation (2.1) shows that the theorem requires the frequency change during one period of oscillation be infinitesimally small compared to the frequency itself. In general a quantity A(t) is said to be adiabatically varied if it satisfies the following relationship:

$$\frac{1}{f(t)}\frac{dA(t)}{dt} \ll A(t) \tag{2.4}$$

A dimensionless parameter s_A as defined by Eq(2.5) can then be used to measure the slowness of the changing in A(t).

$$S_A \equiv \frac{1}{f(t)} \cdot \frac{d}{dt}(\ln A(t)) \tag{2.5}$$

If A(t) is the instantaneous angular frequency, we have for a mechanically modulated microwave resonator at 1 GHz

$$s_\omega \sim \frac{1}{\omega(t)\cdot\tau_m} \leqslant \frac{1}{2\pi\cdot 10^9\cdot 10^{-4}} \sim 10^{-6} \tag{2.6}$$

where τ_m is the characteristic mechanical modulation time. The value of 10^{-4} sec for τ_m is considered as near the upper limit achievable with present rotating machines. This shows s_ω is indeed a very small number as assumed before. Thus when an adiabatically varying quantity A(t) can be expanded into an ascending power series in s_A, second or

---

*Since quantities that vary appreciably only over many rf oscillating periods are of main interest, let it be understood that whenever they are expressed in the form A(t), an average over one rf period is assumed unless otherwise stated. In that limit, they can be considered as the instantaneous values. Hereafter the bar over an averaged slowly varying quantity will be dropped.

higher order terms can be completely neglected. Quite often even the first order terms are negligible too, This gives us some insights into the nature of the adiabatic invariant. An invariant strictly speaking is not a constant, rather its difference from a constant value can be made as small as we wish and for practical purpose can be treated as a constant.

If dissipations are present in the quasiperiodic system, adiabatic invariants no longer exist. In Appendix A, it is shown that in the presence of dissipation, Eq.(2.3) is replaced by Eq. (2.7).

$$\frac{W(t)}{f(t)} = \text{constant} \cdot \exp\left(-\int_o^t \frac{dt}{\tau_p(t)} \right) \qquad (2.7)$$

where $\tau_p(t)$ is the instantaneous energy decay time which can depend on the frequency and therefore the time. The exponent of Eq.(2.7) shows the integral effect of all the losses up to the time t when started with a fixed amount of energy at t = 0.

Take time derivative of Eq.(2.7) we obtain

$$\frac{dW}{dt} = W \left(\frac{1}{\tau_m} - \frac{1}{\tau_p} \right) \qquad (2.8)$$

where $\tau_m = \left(\frac{d}{dt} \ln f\right)^{-1}$ is previously identified as the characteristic modulation time. Clearly if the dissipation is so excessive that $\tau_p << \tau_m$, the system behavior is dominated by the irreversible decaying process without noticeable modulation effect at all. On the other hand, if the energy does not dissipate significantly (such as the case with a superconducting resonator) so that $\tau_p >> \tau_m$ the system is practically dominated by the modulation effect. As noted before, in the adiabatic limit, the modulation causes both the oscillation frequency

and energy to change gradually as a result of continuous Doppler's shift upon reflecting from a moving boundary many times. As for the moving boundary, the modulation causes it to experience a continuous net momentum and energy transfer across the boundary because both the total energy and momenta are conserved for the whole system (electromagnetic fields, resonator and modulation source). The net momentum transfer across the boundary results in a pressure exerted upon it, while the net energy transfer results in the energy conversion between electromagnetic and mechanical forms. This conversion process based upon Doppler effect is intrinsically highly efficient and if done adiabatically is also reversible. The reason is that the interplay of the energy conversion is purely electromechanical in nature rather than thermodynamical, therefore ordinary thermodynamic limitation does not apply here. If we borrow the concept of "entropy" from thermodynamics, this process can be viewed from a different angle. The state when an ideal fixed resonator is at resonance is no doubt a very special state of the system (the familiar notion of eigenstate). In order for an oscillation to sustain itself indefinitely, the phase change over an "oscillating path" has to be exactly a multiple of 2π. In a way,the state meeting this requirement represents a highly "ordered" state with a minimal "entropy". When the boundary is adiabatically modulated, the oscillation inside is sustained and made to follow external modulation. The phase relationship is preserved through continuous change in frequency. Thus for this process, the system remains highly "ordered" and the system "entropy" is unchanged. Furthermore, the slowness is necessary to assure reversibility of the process because a too rapid

modulation can cause sufficiently large phase change so that the instantaneous state of the oscillation depends very critically on the detail nature of the modulation. It is interesting to note that the requirement of reversibility and its consequence of no increase in "entropy" are the same for a reversible thermodynamic process. However, the similarity ends here. For an electromechanical conversion there is no fundamental limitation on how much mechanical energy can be converted into electromagnetic energy through modulations or vice versa; while for a thermodynamic conversion it is limited by the temperature of the two thermal baths which are employed in the process in a very fundamental way. The reason that the temperature plays such an important role in the thermodynamic conversion is that the mechanical work available is extracted from the internal energy of the working medium used in the conversion process. Microscopically the internal energy comes from the highly incoherent thermal energies associated with the internal degrees of freedom. Temperature is merely a macroscopic parameter used to characterize this internal energy. Thus the thermodynamic conversion actually converts a highly incoherent internal energy into a highly coherent mechanical energy. On the contrary, our electromechanical conversion converts an already coherent oscillation energy into another coherent form (mechanical energy) or vice versa.

2.3 Experimental Studies of the New Electromechanical Energy Conversion Scheme.

A highly reentrant superconducting resonator was used to study this new electromechanical energy conversion scheme. Even though

the static electromagnetic properties of this resonator have been studied in great detail, the results will be concisely presented only to the extent which is useful for our purpose of demonstrating this conversion technique.* The dynamic electromagnetic properties are then presented to show the time dependent behavior of the stored electromagnetic energy inside the resonator as a result of the electromechanical energy conversion.

2.3.1 Tunable Reentrant Resonator

Cross sectional view of the reentrant resonator used in this study is shown in Fig. 2.1. The resonator consists of three demountable pieces -- a circular base with a post located at the center, a cylindrical housing and a thin top plate. They were machined out of oxygen free high conductivity copper (OFHC) for easy lead electroplating and assembly. Indium gaskets were exclusively used for vacuum seals as well as rf current carrying joints.

The electromagnetic properties of this reentrant cavity were evaluated in terms of a lumped parameter model consisting of a capacitance terminated coaxial transmission line. Because of strong capacitive loading of this reentrant design, the resonant frequency was determined to a large extent by the size of the capacitive gap between the top plate and the central pole.

The thickness of the top plate was reduced to 50 mils in an annular region as shown in Fig.2.1 in order to maximize the mechanical compliance of this element. The minimum thickness was determined by the necessity of conducting the heat generated by rf losses in the rf

* The detailed results of that study have been published and can be found elsewhere (2).

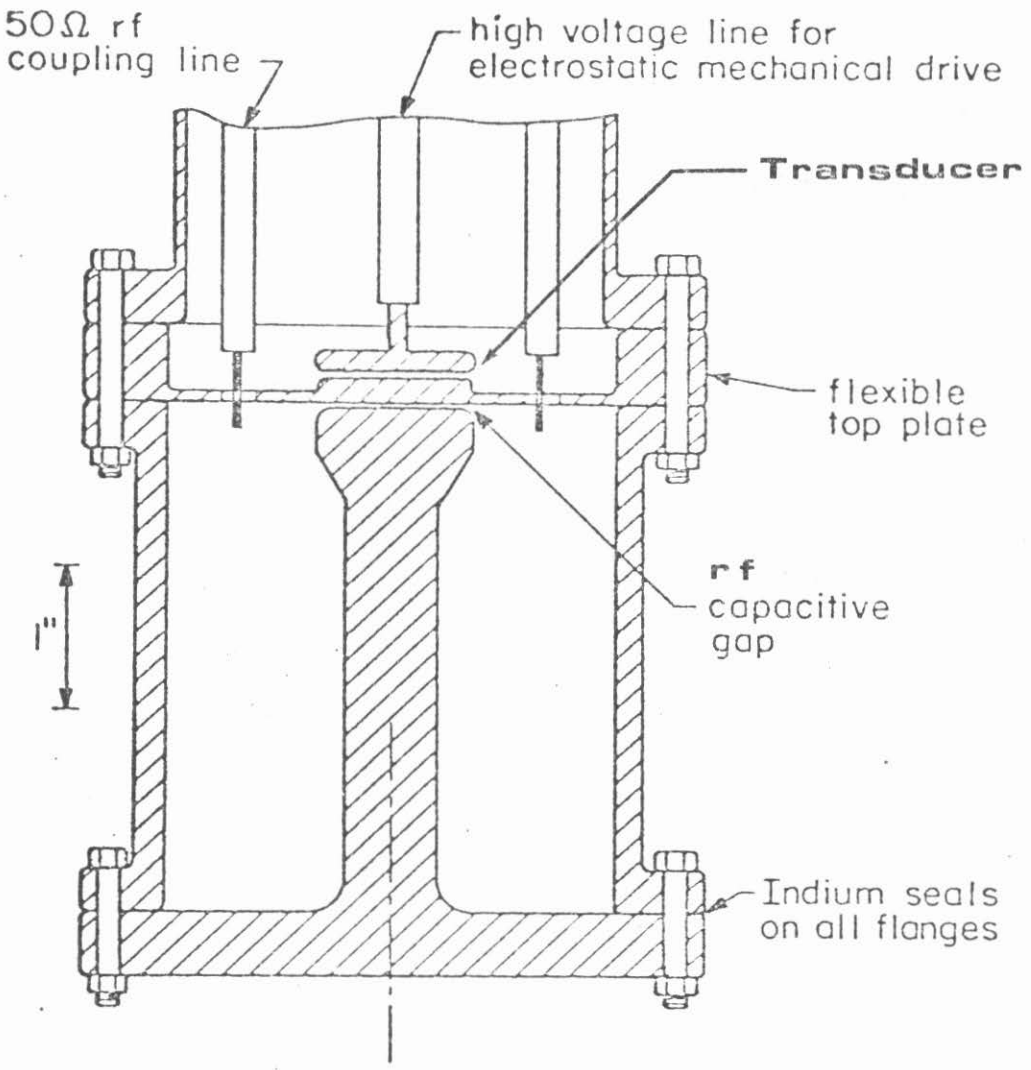

Fig. 2.1 Cross sectional view of the tunable reentrant resonator. It consists of three demountable copper pieces with lead-plated inner surfaces. The rf coupling lines and electrostatic mechanical drive are also schematically shown.

capacitive region to the external helium bath. The present design provides a thermal conductivity of about one watt per °K temperature rise in the center of the top plate and a mechanical compliance of 2.5×10^6 newton/m.

Frequency tuning of the resonator was accomplished by changing the rf gap size through mechanical deformation of the top plate both statically and dynamically. For the former, the top plate was statically loaded through a mechanical linkage causing it to deflect with an amplitude of a few mils which corresponds to a frequency range of 80 to 300 MHz. Any frequency within that range could be obtained reproducibly to within 20 KHz. All the static frequency dependent electromagnetic properties were studies with this method.

For dynamic tuning, the fundamental mechanical mode (drumhead mode) of the top plate was excited by an electrostatic transducer as shown in Fig.2.1.* The plate was excited to vibrate with a few mil amplitude by an alternating voltage of a few kilovolts at the frequency of its fundamental mode (about two kilohertz). Thus the cavity could be frequency modulated rapidly at the rate of about 10^{12} Hz/sec. The time dependent electromagnetic properties and electromechanical energy conversion were studied with this method.

In order to understand the experimental results, the relationship between the rf capacitive gap size and the resonant frequency is needed. This was found experimentally by putting various circular brass shims of known thickness between the top plate and the cylindrical

---

*Brief discussion of the transducer is given in Appendix B.

housing so that the gap size d could be known before the resonant frequency f was measured. The functional relationship between f and d was then found by fitting experimental data pairs (f,d) with the best fitting given by

$$\frac{1}{f^2} = \frac{0.4357}{d} + 0.037 \qquad (2.9)$$

where f is in 100 MHz and d in 10^{-4}m. Eq.(2.9) is plotted in Fig.2.2.

Because the geometry of our cavity is much smaller than the free space wavelength at the resonant frequency, lumped parameter approximation consisting of an equivalent inductance L and a capacitance C is expected to be sufficient for most first order calculations. The equivalent inductance L is equal to the total inductance of the coaxial section and does not change with the frequency. Its value was calculated from the geometry of the coaxial section and found to be 2.62×10^{-8} h. The equivalent capacitance C consists of two parts C_1 and C_2: C_1 comes from the capacitance of the coaxial section and is a constant (about 3.43 pf), while C_2 comes from the "parallel plate capacitance" of the gap region and is time dependent. Over the frequency range of interest, C_2 becomes the dominant part with C_1 accounting for only 4% to 8% of the total equivalent capacitance.

From the known equivalent inductance L and capacitance C, the resonant frequency was found by the usual relationship $(2\pi f)^2 = \frac{1}{LC}$, and was given by

$$\frac{1}{f^2} = \frac{0.436}{d} + 0.0355 \qquad (2.10)$$

(again f in 100 MHz and d in 10^{-4} m). It can be seen Eq.(2.10)

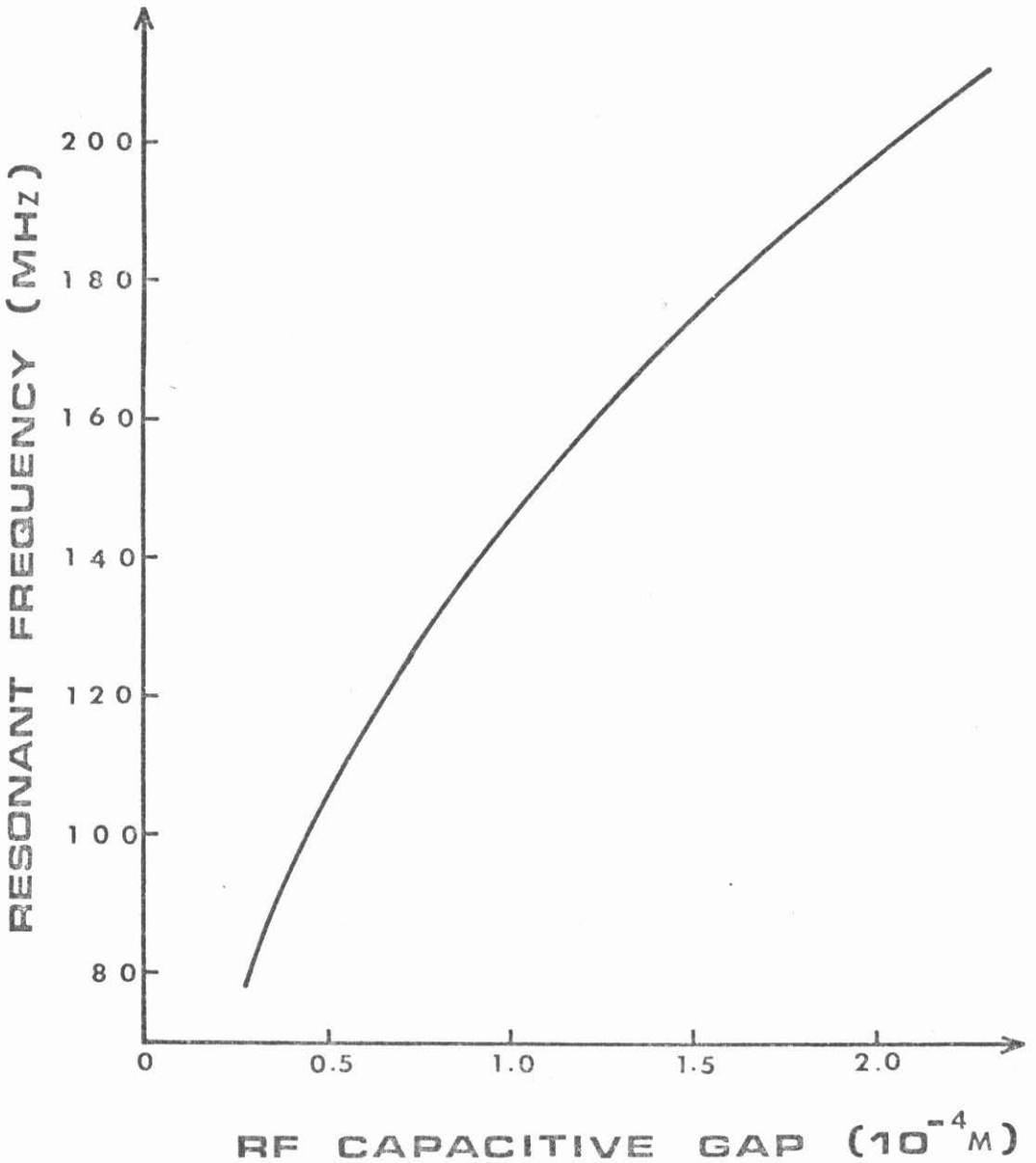

Fig. 2.2 Best fit of the experimentally determined resonant frequency versus the rf capacitive gap as given by Eq.(2.9).

compares very favorably with Eq.(2.9), indicating lumped parameter approximation is indeed adequate.

The field distributions in the resonator are characterized by a highly concentrated axial electric field in the gap region and a vanishingly small radial electric field in regions far from it. A schematic diagram showing the field lines of the fundamental mode is given in Fig.2.3. The magnetic field was deliberately made small everywhere inside the resonator because the resonator was originally designed to study the electrical properties of lead surface, therefore magnetic field was minimized to suppress its effects. It turns out this arrangement is also suitable for our present purpose. Not only is large frequency modulation easily achieved, but the modulation process is simple enough to make model calculation possible as illustrated below.

The energy content W(t) inside the resonator at any instant t is given by

$$W(t) = \int_{vol} \left(\frac{\varepsilon}{2} \vec{E}^2(\vec{r},t) + \frac{\mu}{2} \vec{H}^2(\vec{r},t) \right) dV \qquad (2.11)$$

where the integral is carried out over the resonator volume at that instant. $\vec{E}(\vec{r},t)$* and $\vec{H}(\vec{r},t)$ are respectively the instantaneous electric and magnetic field inside. ε and μ are respectively the permittivity and the permeability of the volume V. The energy change in W(t) can be realized by changing the field strengths as well as the field volume such as the case under our study. Since we are interested

---

* $\vec{E}(\vec{r},t) = \vec{E}_o(\vec{r},t)\sin\left(\int_o^t \omega dt + \theta\right)$ etc.

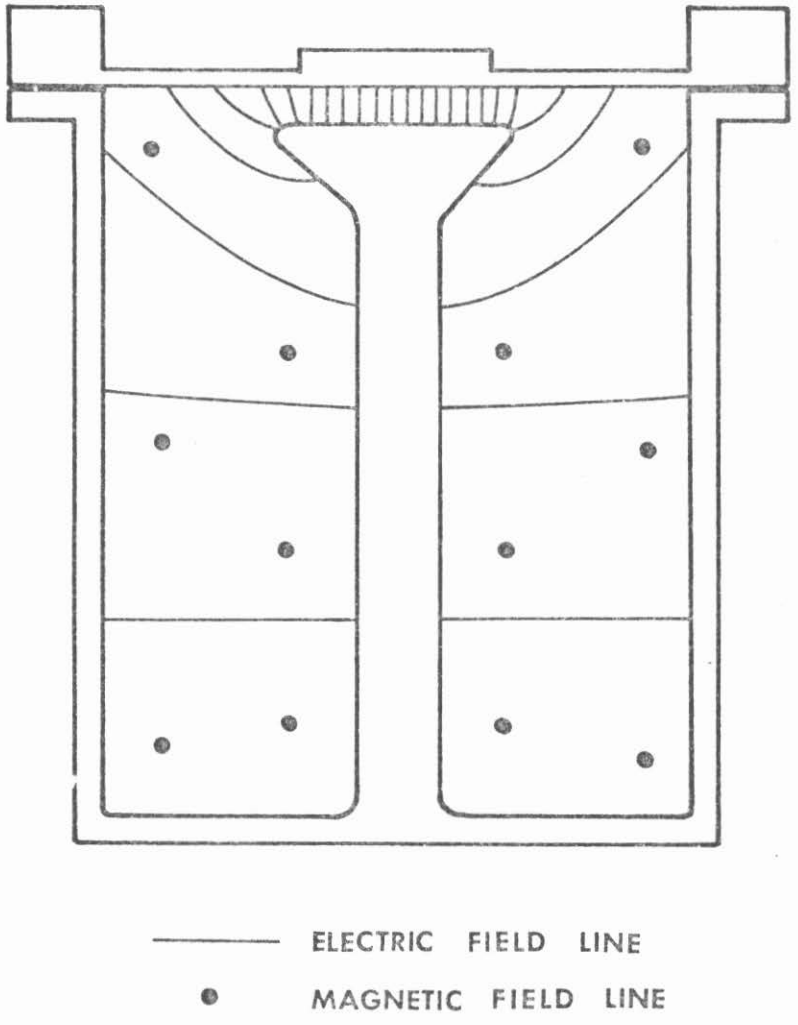

Fig. 2.3 Schematic drawing of the field profiles of the fundamental resonant mode. It shows a large axial electric field concentrated in the rf gap region and generally weak field elsewhere. The gap size is exaggerated for clarity.

in the adiabatic limit, the volume change is extremely small over one intrinsic oscillation period (refer to previous discussion in Sec. 2.1 and 2.2). If we average Eq.(2.11) over one rf period, and take into account the fact the contribution from either term is almost identical*, we have

$$W(t) = \int_{vol} \frac{\varepsilon}{2} \vec{E}_o^{\,2}(\vec{r},t)dV \qquad (2.12)$$

where our averaging convention has been used. It should be pointed out that all the time variations in Eq.(2.12) which include the changing in the field amplitude and volume are now on a much slower scale. If we define an "instantaneous" effective volume V_{eff} so that

$$W(t) = \int_{vol} \frac{\varepsilon}{2} \vec{E}_o^{\,2}(\vec{r},t)dV = \frac{\varepsilon}{2} E_{pk}^2(t) \cdot V_{eff}(t) \qquad (2.13)$$

where $E_{pk}(t)$ is the uniform peak electric field across the parallel plate gap region. As noted before, since the electric field is highly concentrated in the gap region for this resonator, the effective volume V_{eff} is expected to be roughly equal to the instantaneous gap volume (refer to Fig. 2.1).

Equation (2.13) is in consistency with the lumped parameter approximation because under the same conditions, the energy is given by

$$W(t) = \frac{1}{2} C(t) V_g^2(t) \qquad (2.14)$$

---

* The difference is vanishingly small and for practical purpose can be neglected. See further discussion in Appendix A.

where C(t) is the instantaneous equivalent capacitance, and $V_g(t)$ is the peak voltage across the gap.

Since the field is quite uniform in the gap region, Eq.(2.14) can be further written as

$$W(t) = \frac{1}{2}(C_1+C_2(t)) \cdot (E_{pk}(t)\cdot d(t))^2$$

$$= \frac{1}{2}(1 + \frac{C_1}{C_2(t)}) \cdot C_2(t)\cdot d^2(t) E_{pk}^2(t) \qquad (2.15)$$

with $C_2(t) = \frac{\varepsilon A}{d(t)}$

$$W(t) = (\frac{\varepsilon}{2} E_{pk}^2(t))\cdot(A\cdot d(t))\cdot(1 + \frac{C_1}{C_2(t)})$$

$$= (\frac{\varepsilon}{2} E_{pk}^2(t))\cdot V_{gap}\cdot(1 + \frac{C_1}{C_2(t)}) \qquad (2.16)$$

where A is the area of the parallel plate and V_{gap} is the gap volume enclosed by the area A and height d(t). Compared with Eq.(2.13) we get

$$V_{eff} = V_{gap}(1 + \frac{C_1}{C_2(t)}) \qquad (2.17)$$

Because the factor $(1 + \frac{C_1}{C_2(t)})$ varies from 1.042 to 1.087 in this study, using a constant of value of 1.065 only incurs an error of less than 2.2% in the energy over the entire range. Later we will use these results for data analysis.

2.3.2 Preparation of Superconducting Surface

After the required parts were machined out of OFHC copper, they were mechanically polished first with emery paper down to 600 grade,

then with levigated alumina polishing compound (grain size 1-3 μ). Subsequent lead electroplating essentially followed the standard industrial procedures* with minor modifications. Since detailed information is available elsewhere (3), only a brief description is given below:

(1) Cleaning: After mechanical polishing, organic material was removed with organic solvents such as acetone and trichloroethylene. The copper surface was then electropolished in a phosphoric acid bath** with a lead cathode to remove among other things the copper oxide.

(2) Electroplating: Immediately after electropolishing, the solution was rinsed away and the work piece was placed in a lead fluoroborate bath*** with lead electrodes made out of 99.9% purity lead foil. Initially a few short D.C. pulses (∿1 sec) were applied at a current density of 80 A/cm^2 to insure a complete coverage. Subsequently plating was continued at reduced current density of 8 mA/cm^2 until desired thickness was obtained.

(3) Chemical polishing: After plating, work piece was rinsed with deionized water before being chemically polished with an acid mixture**** and chelated with diluted EDTA.

(4) Drying: The surface was then treated with 7.5% ammonia and rinsed with acetone before being blown dry with dry nitrogen gas.

---

* Electroplating Engineering Handbook. ed. by A. Kenneth Graham (Reinhold Publishing Corporation).

** The electropolishing solution is a mixture of one part Electro-Glo "200" (Electro-Glo Co. Chicago) and three parts 85% phosphoric acid by volume.

*** One part "Shinol LF-3" (Harstan Chemical Company Brooklyn, N.Y.), 23 parts of 50% lead fluoborate and 26 parts of H_2O by volume.

(To be continued)

(5) Preserving: Before the resonator was assembled, the plated pieces were kept in vacuum or inside a pressured chamber filled with dry nitrogen gas to preserve the fresh lead surface.

The properties of superconducting lead surface obtained in this method have been published and can be found elsewhere (2).

2.3.3 Cryogenic Apparatus

After electroplating, the resonator was assembled before it was attached to the bottom of a dewar insert and pumped down to a pressure of 10^{-5} Torr or lower to prevent further surface deterioration. Indium gaskets were used for vacuum seals. A schematic diagram of the dewar, the insert and their accessories is shown in Fig.2.4.

The insert consisted mainly of three verticle probes: two were 50Ω coaxial lines for rf circuits; the third was used either as a high voltage line or a mechanical linkage. For low temperature experiments, a 4 inch stainless steel dewar was used along with standard cryogenic equipment as shown. Ambient earth magnetic field was reduced with a mu-metal shield to below 15 milligauss over the experimental region. The temperature of the helium bath was varied by pumping on its vapor in conjunction with a pressure regulation system. The temperature was determined by monitoring the equilibrium vapor pressure by a Wallace and Trernan pressure gauge, and converting by the 1958 He^4 scale of temperature. Typical temperature variation covered in the experiments ranged from 4.2 °K to 2 °K. During the

---

(continued from previous page)
**** One part of glacial acetic acid, 2 parts of 70% nitric acid, 6 parts of 30% H_2O_2, 9 parts of saturated EDTA, and 480 parts of H_2O, all by volume.

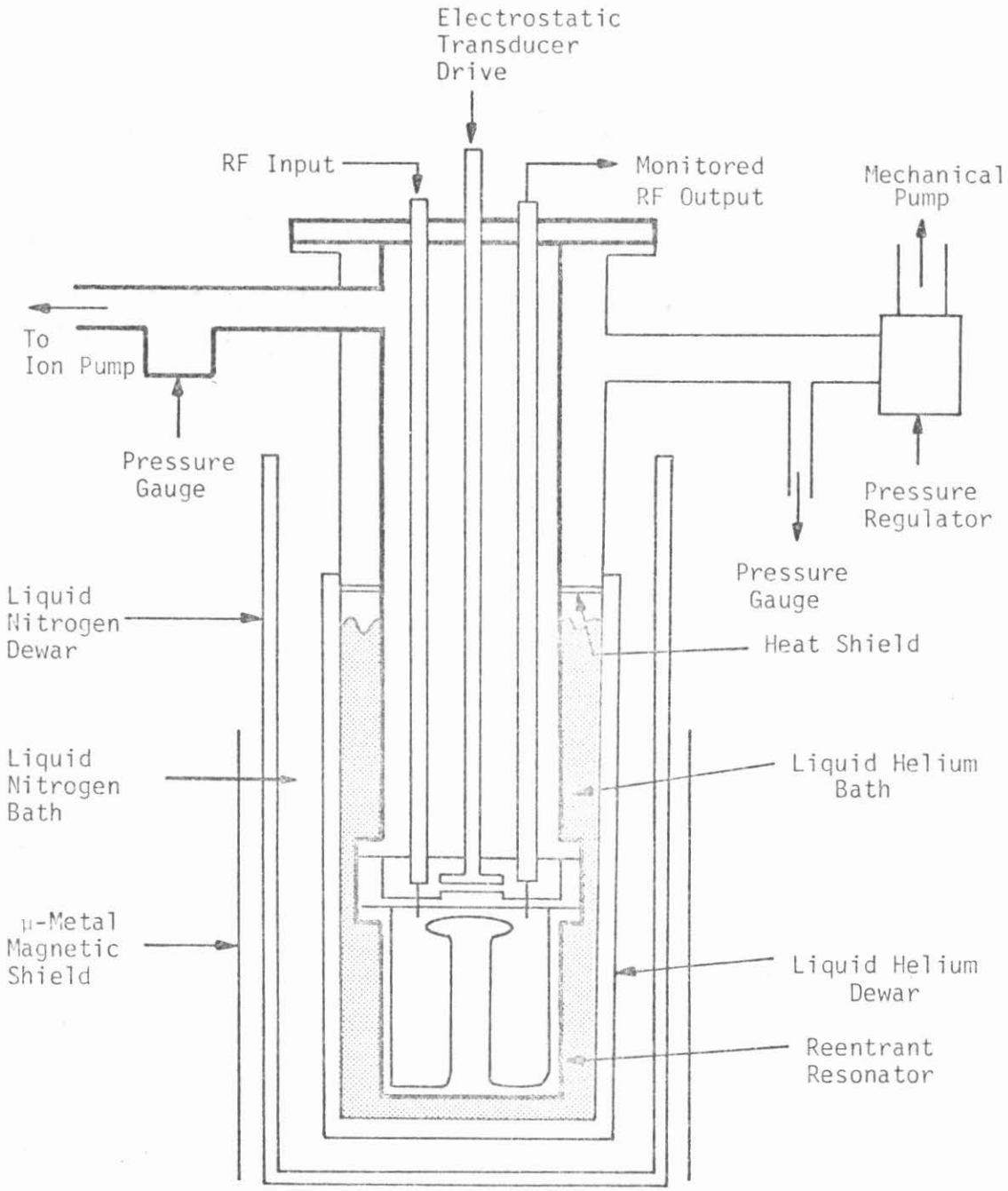

Fig. 2.4 Dewar Insert (in bold lines) and associated cyrogenic apparatus used in this study. Normally the resonator was operated at 4.2 K. For lower-temperature operation, a mechanical pump was used to pump on the helium vapor in connection with a pressure regulation system.

experiments, the pressure inside the resonator was maintained below 10^{-7} Torr with a differential ion pump.

2.3.4 RF Measurements

Standard rf instrumentation was used for all the experiments. To insure proper impedance matching, all the electronics including coaxial lines were made to have characteristic impedance of 50Ω. For a study of the static frequency dependent properties, the technique followed standard procedures for exciting a superconducting resonator of fixed resonant frequency discussed below in subsection (a). For the study of the time dependent properties, an electronic scheme was designed to inject and monitor the time dependent rf energy inside the resonator as discussed below in subsection (b).

(a) Statically tuned resonators:

When the resonator was statically tuned, rf excitation was accomplished by one of the following methods; namely the phase-locked loop or a self-oscillation loop. The block diagrams showing the electronic components and arrangements for both methods are given in Figs.2.5 and 2.6 respectively. Since the detailed theory of the loop operations and measurement techniques are discussed extensively in the literature (4), only a simplified theory of operation relating the measured quantities to the properties of the resonator is given here. Our notations will follow those in (5).

Measurements consisted of sending rf energy into the resonator through one coaxial line and monitoring the field inside through another. Both lines are capacitively coupled to the resonator. The

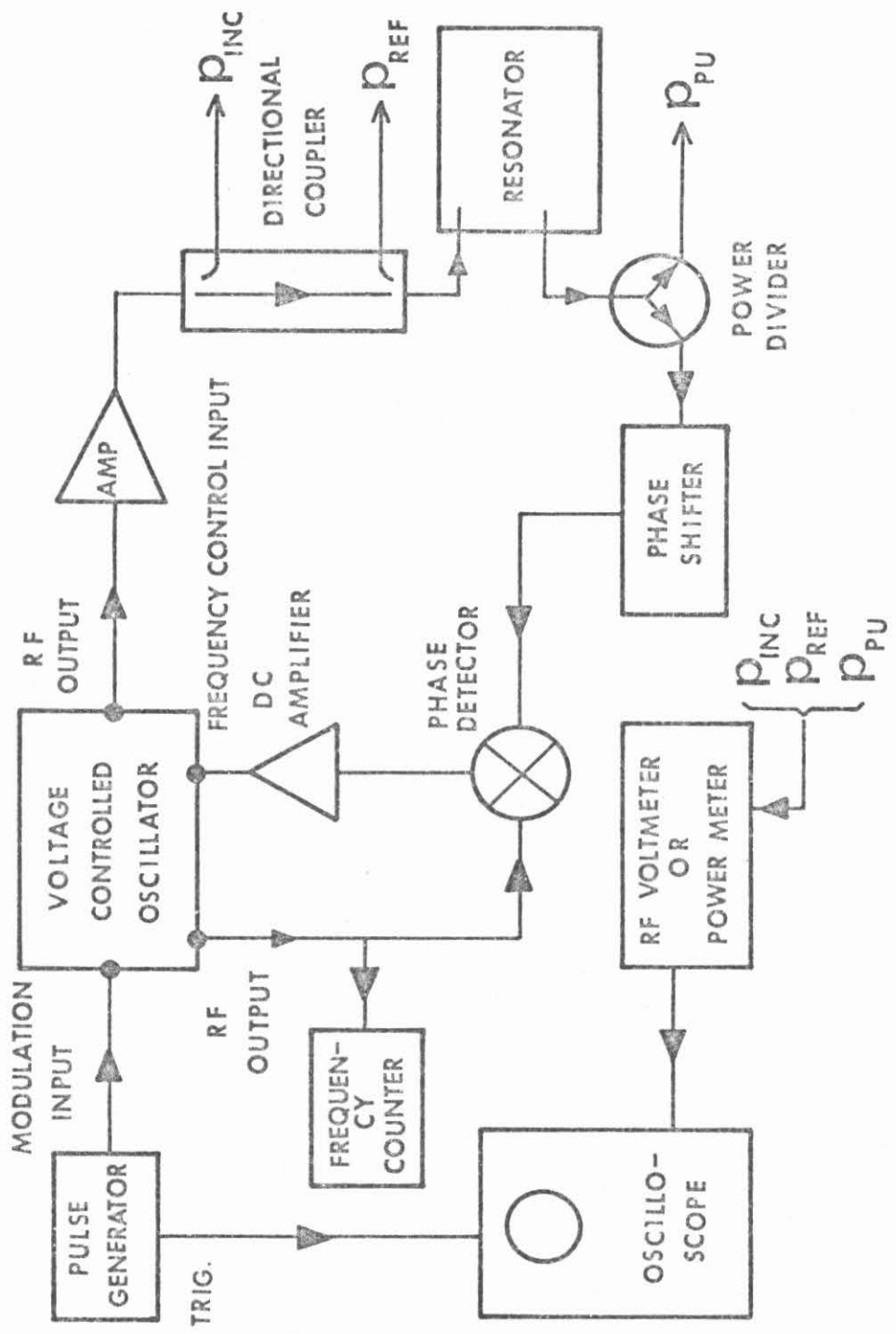

Fig. 2.5 Block diagram of a phase-locked loop for exciting a high Q resonator of fixed resonant frequencies

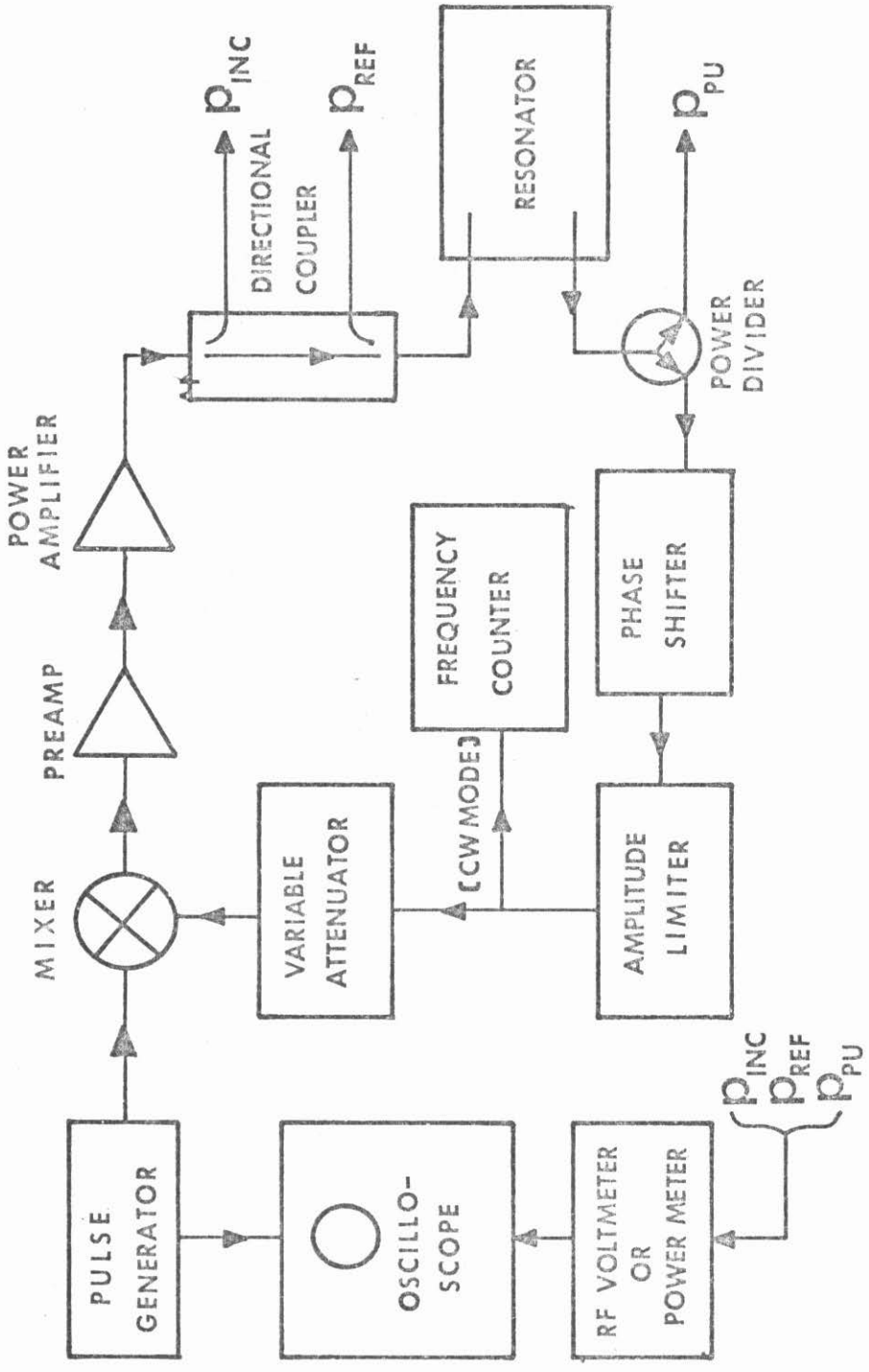

Fig. 2.6 Block diagram of a self-oscillation loop for exciting a high Q resonator of fixed resonant frequencies.

measured quantities were the unloaded power decay time τ_{po}, the incident power P_{inc}, the reflected power P_{ref} and the monitored signal P_{pu} (refer to Figs.2.4 and 2.5 for definitions of these quantities).

Conservation of energy requires

$$P_{inc}(t) - P_{ref}(t) = P_{diss}(t) + P_{pu}(t) + \frac{dW(t)}{dt} \qquad (2.18)$$

where P_{diss} is the power dissipated in the resonator itself, $\frac{dW}{dt}$ is the time rate of change of the field energy stored inside the resonator.

For a fixed coupling, the monitored signal P_{pu} is proportional to the energy content W(t), i.e.,

$$P_{pu} = K \cdot W \qquad (2.19)$$

From the definition of the unloaded quality factor Q_o

$$Q_o \equiv \frac{\omega W}{P_{diss}} = \omega \tau_{po} \qquad (2.20)$$

we get

$$\frac{1}{Q_o} = \frac{k}{\omega} \left(\frac{P_{inc} - P_{ref}}{P_{pu}} - 1 - \frac{1}{k} \frac{d}{dt}(\ln P_{pu}) \right) \qquad (2.21)$$

Once the proportional constant k (coupling parameter) is known, the energy content, and therefore the rf voltage across the capacitive gap at steady state can be determined by the measured quantity P_{pu} as indicated by Eqs. (2.10) and (2.14).

Experimentally, two methods were available for determining the coupling parameter K. Their simplified derivations are given below:

Method I. At steady state, with incident rf energy probe critically coupled to the resonator (i.e., when $\frac{d}{dt} = 0$ and $P_{ref} = 0$), we have

$$P_{inc} = P_{diss} + P_{pu} \tag{2.22}$$

Since the monitoring probe was extremely weakly coupled to the resonator

$$P_{pu} << P_{diss}$$

therefore

$$P_{inc} \simeq P_{diss}$$

and

$$Q_o = \omega\tau_{po} = \frac{\omega W}{P_{diss}} \simeq \frac{\omega W}{P_{inc}}$$

i.e.,

$$W \simeq P_{inc} \cdot \tau_{po} \tag{2.23}$$

and

$$k = \frac{P_{pu}}{W} = \frac{P_{pu}}{\tau_{po} \cdot P_{inc}} \tag{2.24}$$

Thus by measuring P_{inc}, P_{pu}, τ_{po}, one can determine k.

Method II

From Eq.(2.14) the energy content of the resonator is equal to

$$W = \frac{1}{2} CV_g^2$$

where C is the equivalent capacitance and V_g is the peak voltage across the capacitive gap. Suppose an rf voltage is directly applied across the capacitive gap with a 50Ω tramsmission line through a

small hole in the center of the top plate. If the resonator is assumed to be an ideal open circuit at resonance, then the incident voltage V_+ and the reflected voltage V_- at the resonator are related to the voltage across the gap V_g by the following equation:

$$V_+ = V_- = V_g/2 \tag{2.25}$$

Experimentally what was measured were the incident and reflected voltages at the respective ports of a directional coupler: V'_+ and V'_-. After taking into account the attenuation properly, we can relate (V'_+, V'_-) to (V_+, V_-) with two attenuation coefficients α and β so that

$$\begin{aligned} V'_+ &= \alpha V_+ \\ V'_- &= \beta V_- \end{aligned} \tag{2.26}$$

Equation (2.25) can be written as

$$V_g = 2\sqrt{V_+ V_-} = 2\sqrt{\frac{V'_+ V'_-}{\alpha\beta}} \tag{2.27}$$

that is, V_g is determined by the measured V'_+, V'_-, α and β.
The coupling parameter k is finally obtained as follows:

$$k = \frac{P_{pu}}{W} = \frac{P_{pu}}{\frac{1}{2}CV_g^2} = (2L\omega^2)\cdot\frac{P_{pu}}{V_g^2} \tag{2.28}$$

At a particular frequency, P_{pu} is measured for a given V_g and apply Eq.(2.28) to obtain the value of k.

(b) Dynamically modulated resonators

For a dynamically frequency modulated resonator, the previously

described schemes for exciting the resonator become impractical because the resonant frequency is continuously changing rapidly in time. Our usual understanding of microwave resonator systems derived from solving Maxwell's equations with appropriate fixed boundary conditions can no longer directly apply. With boundaries constantly changing, the problem generally becomes not so well defined and harder to handle. However, in the limit of very slow change (adiabatic limit), the boundaries can be regarded as quasi-static and the corresponding instantaneous boundary value problem can be solved. The solution so obtained is assumed to approach the real situation in the slow limit.

Experimentally, an electronic scheme whose block diagram is shown in Fig. 2.7 was used to accomplish the excitation of the resonator. The thin top plate was driven to vibrate at its fundamental mechanical mode at a rate of about two kilohertz. The corresponding rf resonant frequency could thus be modulated over a wide range (up to a factor of two in resonant frequency) in the region of one to two hundred megahertz. RF pulses of various durations ranging from 5 to 20 μs were injected into the resonator through the incident probe at a specific point of the mechanical cycle when the frequency of the incident rf pulse matched the instantaneous resonant frequency. It was found pulses with width less than 5μs coupled poorly to the resonator. It is believed to be due to insufficient coupling to build up a noticeable amplitude. This is plausible because the typical voltage decay time is about 1.5 ms (see Eq.(2.34)), while the pulse duration is less than 5 μs. Even in the unmodulated case with perfect frequency match this duration will produce only a fraction of the steady state amplitude

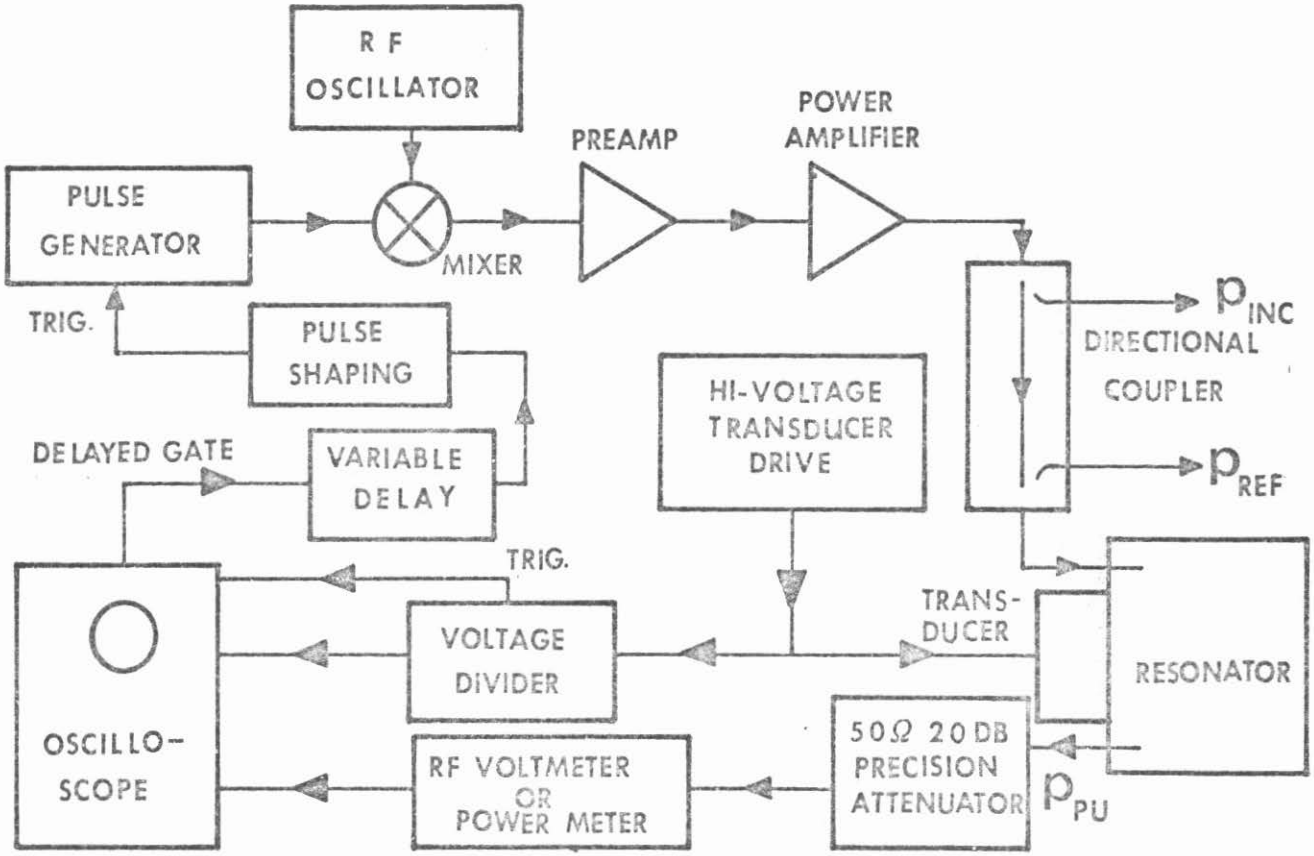

Fig. 2.7 Block diagram of the electronic scheme for injecting rf energy pulses into a highly frequency modulated superconducting resonator. To coordinate the injection and the plate vibration, a signal derived from the transducer drive was phase shifted before being used to trigger a pulse generator which in turn gated the rf energy.

which is obtained when the resonator is driven by a CW source of the same strength. Furthermore, within 5 μs, the resonator frequency changes by about 1 MHz which which may be sufficient to cause some frequency mismatch between the input and the resonator. Therefore the effective pulse duration is much less than 5 μs, and the oscillation amplitude is further reduced.

After injection, rf input ceased and the subsequent time evolution of the stored electromagnetic energy inside the FM resonator was monitored through another probe weakly coupled to the resonator. The monitored signal was then fed into a calibrated rf voltage measuring device for amplitude measurement. The corresponding instantaneous frequency was determined by beating this signal with a local oscillator (detailed information given below). To coordinate the rf energy injection and the plate vibration, an attenuated signal from the transducer drive was fed into a variable phase shifter. The phase shifted signal triggered a pulse generator which in turn gated the rf energy. The amount of delay was adjusted manually to achieve resonance. The interval between injections was made to be longer than the power decay time, so that the observed signal was due to one event only. The scheme was also modified so that multiple pulses of different frequencies could be injected into the resonator at different mechanical phase points to examine their possible interaction.

The measurement consisted of measuring a pair of time dependent

quantities (V(t), f(t)), where V(t) is the monitored voltage amplitude*, and f(t) is the instantaneous frequency. Operationally the voltage observed through the monitoring probe was first fed into a terminated rf voltage measuring system which had a bandwidth of at least 400 MHz (the frequency of the modulated signal ranges from 95 MHz to 155 MHz in this study). This terminated signal was displayed on a Tektronix scope which had a bandwidth of about 150 MHz. For each rf energy pulse injected, the corresponding evolution of the stored energy was displayed on the scope. A polaroid picture of this trace was taken for amplitude measurement later. A typical trace is shown in Fig. 2.11. The amplitude measured from the expanded polaroid picture at any time was corrected for any possible frequency dependence of the voltage measurement system. This was done by feeding a calibrated rf signal from a Hewlett-Packard 608F signal generator into the voltage measurement system to produce the same amplitude at the same frequency on the scope (frequency determination is discussed below). The calibrated output of the oscillator was then read from an rf voltmeter. For frequency measurement, the same monitored voltage V(t) was beat with a local oscillator first before being displayed on the scope. Marks showing the zero beat were used for frequency identification at these instants. Because of finite time resolution on the scope screen as well as finite width of zero beat mark, the frequency so determined was an averaged frequency over at least two hundred rf cycles. The

---

* That is, an actual voltage consists of two multiplicative factors: the amplitude V(t) and the phase factor $\sin(\int_0^t \omega dt + \theta)$.

amplitude measurement described above was carried out for each instant where the frequency was also known.

Before proceeding to discuss the evolution of the stored energy, the nature of our measured quantities V(t) and f(t) should be carefully examined. This was necessary because on one hand the measurements made actually represented information of what had already taken place a while ago (typically 6 ns) at the resonator site. On the other hand, the voltage V(t) contained frequency components that were distributed over a wide spectrum. For the voltage V(t) to represent truthfully the history of the stored energy inside the resonator, the time delay between the observation and actual event must be the same for each frequency component, that is, the propagation medium in between must be non-dispersive. Generally speaking, a signal containing a wide range of frequency components can be distorted by the dispersion as well as the attenuation of the propagation medium. The attenuation aspect (frequency response) can be corrected with a calibrated source as explained above for the amplitude correction. The dispersion effect however is much harder to eliminate unless a non-dispersive medium can be found. An experiment was done to check the dispersion properties of our measuring system. Signals from a generator were fed directly into the measuring system, the resultant time delay was measured for each frequency. It was found the delays were within 4ns of each other for all frequencies of interest. This small amount of difference in delay time causes no actual difficulty in interpreting the observed voltage because the measured voltage

change is on the time scale of the mechanical period which is about 500 μs, and the time resolution of each voltage amplitude measurement from the polaroid picture is about 2 μs during which the frequency change is much less than 1 MHz. Obviously the voltage so measured was an averaged value over several hundred rf cycles too.

There was another subtle point which had to be clarified before the measured values could be used without ambiguity. As noted before the voltage measurement and the frequency measurement were separately carried out with the same monitored signal but slightly different electronic circuits. The time delay between these two different circuitry paths must be small enough so that it is legitimate to correlate the frequency measurement to voltage measurement at apparently the same point. Even though experimental determination of this relative delay was done with somewhat large uncertainty due to the difficulty of comparing two quite different signals, it is nevertheless conservatively estimated to be no more than several ns by considering the behavior of the mixer used here for the frequency mixing. With 2-3 μs time resolution for actual measurement, this kind of delay was completely buried inside the measurement error itself and causes no additional uncertainty and ambiguity.

In order to study the time behavior of the stored energy W(t), the relationship between the corrected voltage V(t) and W(t) has to be known. Since the monitoring line was extremely weakly capacitively coupled to the resonator before the top plate was induced to vibrate, it was expected that the coupling would remain very weak for a not too large modulation (though it could become dependent on the frequency),

A separate calibration was done to determine this frequency dependence. During the calibration the monitoring probe was clamped to a fixed position and was weakly coupled to the resonator. The resonant frequency was then changed by statically deforming the top plate*. For each frequency, the resonator was critically driven so that the peak voltage across the gap V_g was known (see subsection (a)). Plotting the ratio of the monitored voltage $V(t)$ to V_g versus the frequency, a linear relationship was found from 100 MHz to 175 MHz, indicating a lumped circuit approximation (see Fig. 2.8) with a constant coupling capacitance was adequate as elaborated further below.

In this lumped circuit approximation, the voltage amplitude $V(t)$ and the peak voltage across the gap V_g are related by the following equations

$$V_1(t) = V_2(t) + \frac{1}{RC_o}\int_{-\infty}^{t} V_2(t)dt \qquad (2.29)$$

where $V_1(t)$ and $V_2(t)$ are respectively the instantaneous voltages across the variable capacitor C and the termination resistor R and are defined by the following equation

$$V_1(t) \equiv V_g(t)\sin\left(\int_o^t \omega dt + \theta_1\right)$$

$$V_2(t) \equiv V\ (t)\sin\left(\int_o^t \omega dt + \theta_2\right)$$

---

* Because of the thickened central portion of the plate upon which the force was uniformly applied, the configurations for static and dynamic deformation are approximately the same to the first order.

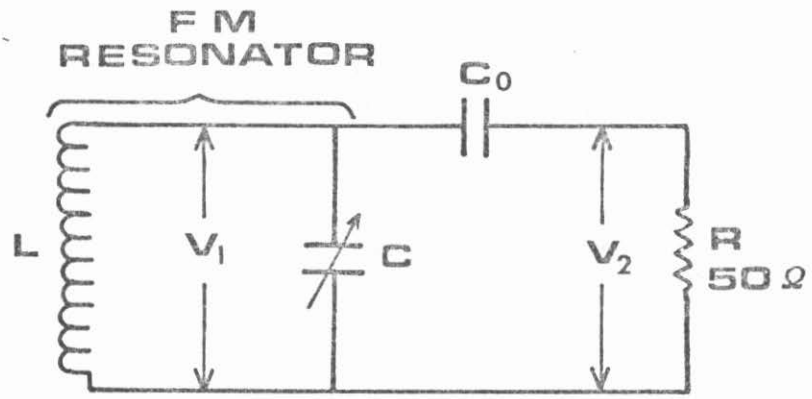

$$V_1(t) = V_2(t) + \frac{1}{RC_o}\int_{-\infty}^{t} V_2(t)dt$$

where

$$V_1(t) \equiv V_g(t)\sin\left(\int_0^t \omega dt + \theta_1\right)$$

$$V_2(t) \equiv V(t)\sin\left(\int_0^t \omega dt + \theta_2\right)$$

Fig. 2.8 The equivalent circuit showing the relationship between the instantaneous voltage across the rf capacitive gap $V_1(t)$ to that across the termination resistor $V_2(t)$. $V_g(t)$ and $V(t)$ are respectively the time dependent voltage amplitudes of V_1 and V_2.

where θ_1 and θ_2 are the initial phases.

Thus if V(t) is known, $V_g(t)$ and therefore W(t) can then be obtained from Eqs.(2.29) and (2.14). The calibration asserted that the coupling capacitance C_o is essentially constant. This is made clearer if we take liberty of Fourier analysis and treat the circuit as if it were time independent, then V and V_g are related by

$$V = \frac{j\omega C_o R}{1+j\omega C_o R} V_g \qquad (2.30)$$

Since monitoring line was weakly coupled to the resonator, C_o was found to be much less than 1 pf.* With $R = 50\Omega$, $\omega RC_o \simeq 10^{-3} \sim 10^{-4}$ Eq.(2.30) can be approximately written as

$$|V| \simeq \omega C_o R |V_g| \qquad (2.31)$$

which is consistent with the calibration result.

It should be pointed out though that it is not immediately clear that Eq.(2.30) is also valid for a frequency modulated voltage source V_g. In any case, Eq.(2.29) is the fundamental equation relating V_g and V. It will be shown next that in the adiabatic limit, Eq.(2.31) is the zeroth order solution of Eq.(2.29).

Because Eq.(2.29) involves quantities which vary either rapidly or slowly in time, it is awkward to deal with them simultaneously. Since we are more interested in the slowly varying quantities, we

---

* Perform one static measurement and with known values of V_g, V, ω and R, C_o can be solved from Eq.(2.30).

shall set up equations which contain them only.

Define

$$\chi = \int_0^t \omega dt + \theta_1$$

$$\eta = \theta_2 - \theta_1$$

Differentiate Eq.(2.29) and equate the coefficients of $\sin\chi$ and $\cos\chi$ terms on both sides we obtain the desired set of equations

$$\frac{dV_g}{dt} = -\omega V \sin\eta + \left(\frac{dV}{dt} + \frac{V}{RC_o}\right)\cos\eta$$

$$\omega V_g = \omega V \cos\eta + \left(\frac{dV}{dt} + \frac{V}{RC_o}\right)\sin\eta$$

Eliminating η from these two equations, we have

$$\left(\frac{dV_g}{dt}\right)^2 + (\omega V_g)^2 = (\omega V)^2 + \left(\frac{dV}{dt} + \frac{V}{RC_o}\right)^2$$

Since $\frac{dV_g}{dt} \sim \frac{V_g}{\tau_m} << \omega V_g$

$$\frac{dV}{dt} \sim \frac{V}{\tau_m} << \omega V << \frac{V}{RC_o} \qquad (\because \omega RC_o << 1)$$

therefore $(\omega V_g)^2 \simeq \left(\frac{V}{RC_o}\right)^2$

i.e. $|V| \simeq \omega C_o R |V_g|$

which is identical to Eq.(2.31).

Finally the stored energy is related to the measured quantities V(t), f(t) as follows:

$$W(t) = \frac{1}{2} C(t)\, V_g^2(t)$$

$$= \frac{1}{2L(4\pi^2 C_o R)^2} \cdot \frac{V^2(t)}{f^4(t)} \qquad (2.32)$$

Equation (2.32) will form the basis of our comparison in Section 2.4.

2.3.5 Error Estimations

Errors of various measured quantities were estimated and classified in the following categories.

(a) For both types of experiments, static and dynamic, the voltage was determined by comparison with a known signal through precision variable attenuator, wideband band amplifiers and oscilloscope. Each measurement was compared to the output of a calibrated rf source producing the same amount of response at the same frequency. The voltage was estimated to have an error of less than 1%.

(b) For power measurement, in the CW mode, a power meter was used. The reading error plus calibration error was about 1%. For pulsed mode, the voltage comparison described in (a) was used resulting in an error in power of about 3%.

(c) The power decay time τ_p was measured from a photographed decaying oscilloscope trace. The error was estimated to be 3% or less.

(d) For dynamic modulation experiment, the frequency was limited by

the time resolution of the zero beat mark. The error ranges from 0.5 to 2.0 MHz depending on the frequency itself, worse at places where frequencies change rapidly. This amounts to 0.3% to 1.5% error in frequency.

(e) The total energy inside an FM resonator W(t) was calculated from the measured amplitude V(t) according to Eq.(2.32). V(t) was measured from a photographed oscilloscope trace and compared with the output of a calibrated source as described in (a). The uncertainty in measuring the amplitude from the picture ranges from 2% to 5% typically (worse at lower frequency due to smaller amplitude). In addition there was an error of about 1% associated with identifying the frequency at the same location.

(f) Errors in temperature determination typically 1 m°K at 4.2°K and increased monotonically to about 10 m°K at 2.0°K were not important for our study and could be neglected for all practical purpose.

2.4 Results and Discussions

2.4.1 Static Electromagnetic Properties

The experimental results for the static electromagnetic properties are briefly summarized below only to the extent useful for our present purpose. A detailed account of this study has been published and can be found in the literature (2). The information of interest here includes the unloaded quality factor Q_0, and the electron loadings such as multipacting and field emission.

In Fig. 2.9 the measured low level resonator Q was plotted against frequency for two different superconducting surfaces. The

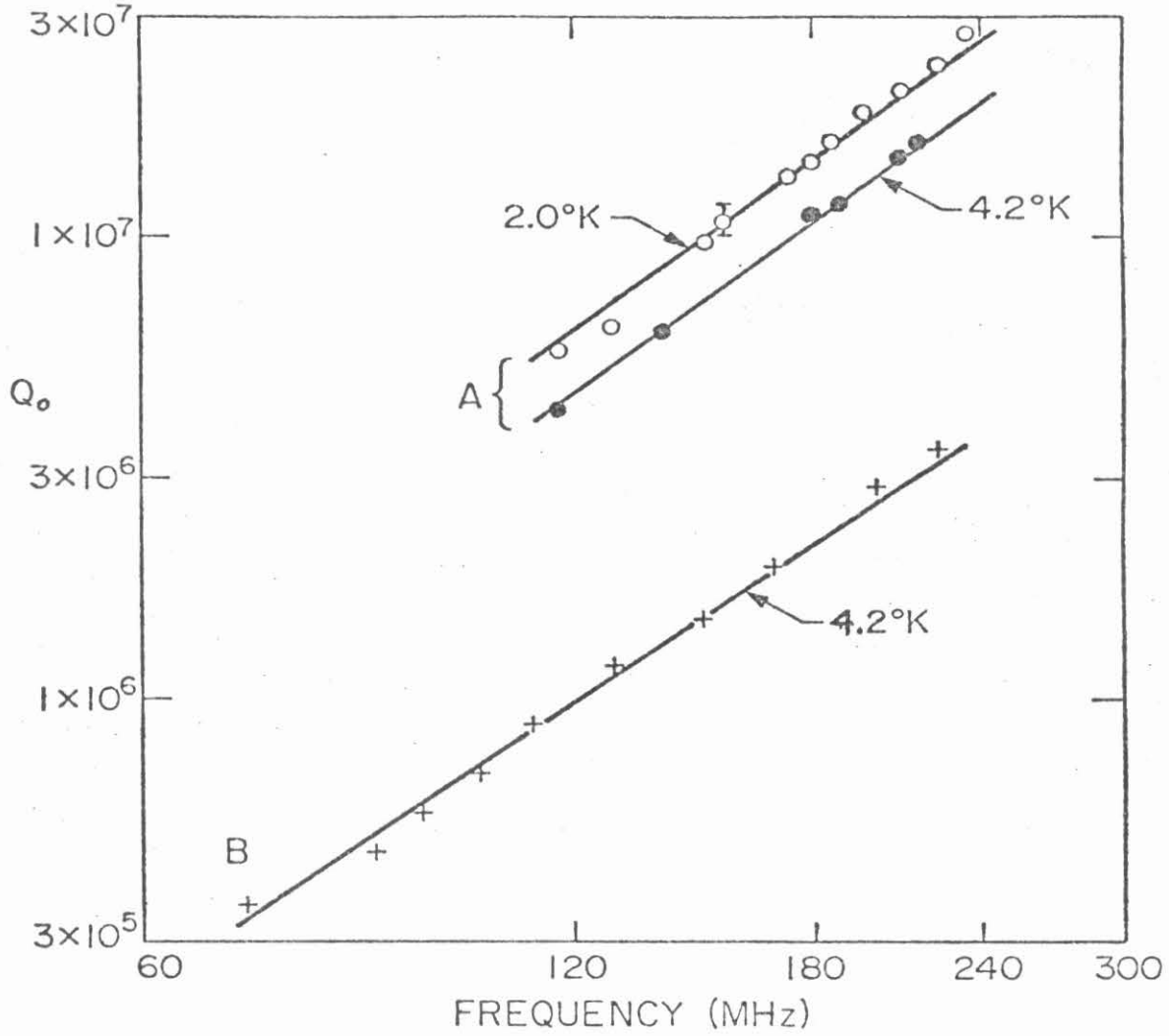

Fig. 2.9 Low level intrinsic quality factor Q of the superconducting reentrant resonator as a function of rf eigenfrequency. Curves A and B refer to two different electroplated surfaces. Typical temperature dependence of rf losses is shown in the two curves for surface A. The straight lines correspond to rf losses such that $Q \sim \omega^2$. This frequency dependence is consistent with the surface dielectric layer (lead oxide) induced losses in this resonator.

surface resistance corresponding to these unloaded Q values was ten times larger than by other independent measurements on similarly plated load surfaces where R_s typically was found to be $10^{-7}\Omega$/square at 200 MHz and 4.2°K (5). This disparity results from the dielectric losses in the surface oxide. Because of the strong capacitive loading of this type resonator, one might expect the resonator Q to be highly sensitive to any surface dielectric layer and limited by dielectric losses. The observed frequency dependence of the losses ($Q \sim \omega^n$, $n = 2.1 \pm 0.1$) and very weak temperature dependence support this view. We assume that this frequency dependence results from a thin layer of dielectric layer in the capacitive gap with frequency independent dielectric loss angle δ. The magnitude of the losses for the highest Q shown in Figure 2.9 would result from a surface dielectric film characterized by $(d \tan \delta)/k = 0.1$ Å where k is the dielectric constant of the oxide layer and d the layer thickness. Because accurate information of the properties of the dielectric film at these frequencies is very meager, an exact comparison with this number is not possible at present time. However if we use the value 10^{-3} radian for the loss angle at 100 - 200 MHz obtained from separate measurements on a lead plated helical resonator (6), and assume the dielectric constant is 26*, the lead oxide layer is then found to be about 1000 to 2000 A thick which is in agreement with known thickness of common lead oxide.

Multipacting -- a term for resonant reflection of electrons

---

* This is the dielectric constant for PbO at 200 MHz (7).

from the surfaces at well defined field levels -- was sometimes observed in these resonators. The multipacting persists when the yield of the secondary electrons produced from the primary ones bombarding the lead surface exceeds unity. Fig.2.10 shows the frequency dependence of one of the observed multipacting levels in our resonator. It can be shown that this observed frequency dependence is consistent with a spatially constant multipacting electronic orbit, located outside the capacitive gap in which the electron velocity increases linearly with rf frequency. There were several methods available to overcome the multipacting. Among them were: driving the cavity against these levels for an extended period of time until they went away; exciting more than two modes simultaneously; injecting short but high power pulses to overcome the levels; baking lead surface under vacuum, etc.. The reasons that multipacting might go away after these treatments are either that the condition of the surface had been drastically changed so that the secondary electron yield become less than unity, or that the electronic orbitals of the resonance absorption was disturbed and the multipacting is suppressed. It turned out a particular method might not be always successful for all the multipacting levels and an alternative one had to be used.

After the elimination of multipacting, the maximum electric field attainable was limited by field emission of electrons from the superconducting surface into the capacitive gap and occurred at about twelve times the highest level shown in Fig.2.10. For the resonators tested, field emission electron loading began typically at a surface field of 15 MV/m. A new lead plating technique as described in Sec.

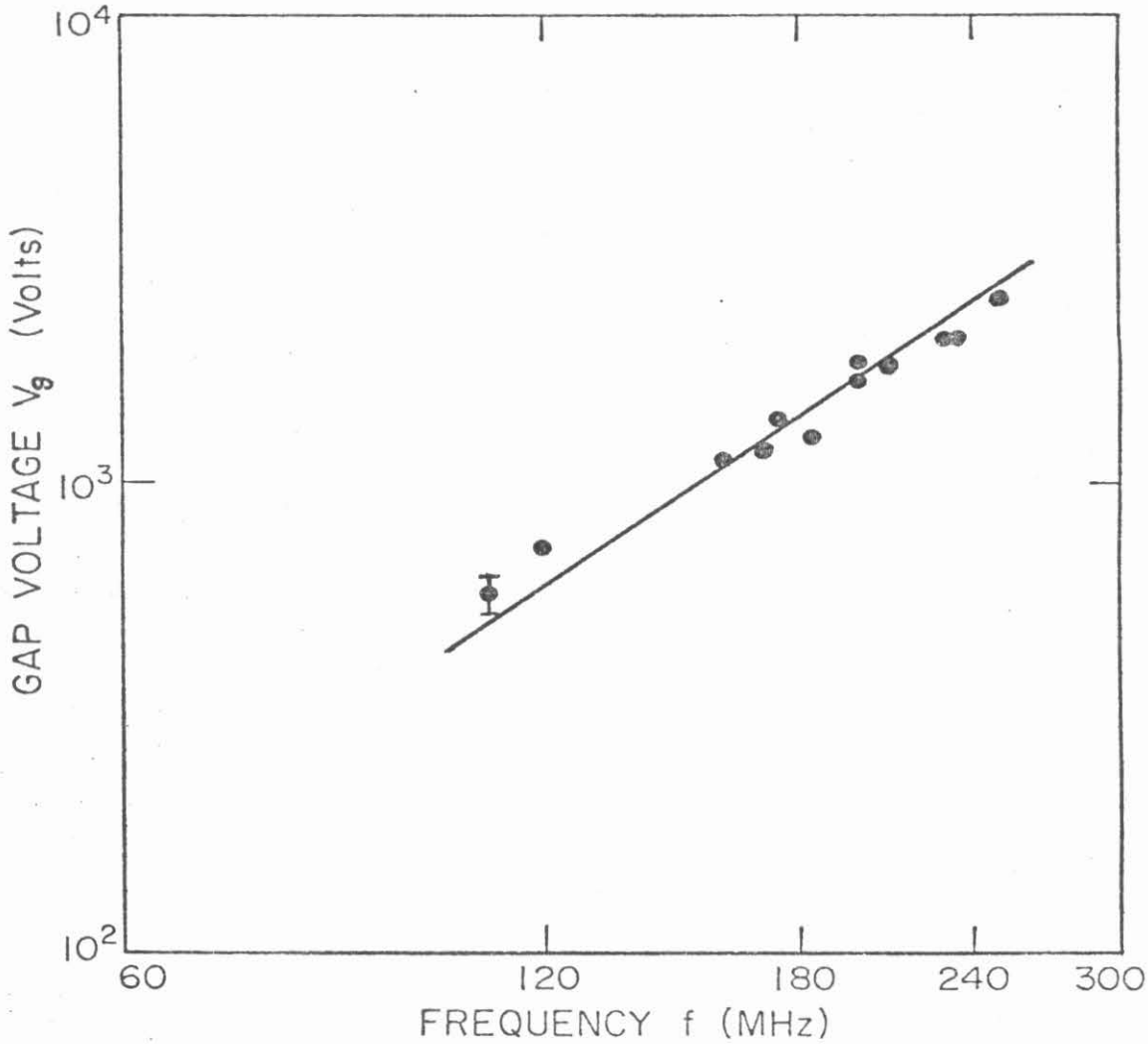

Fig. 2.10 Multipacting level as a function of rf frequency. This level is expressed in terms of the corresponding peak rf voltage across the capacitive gap when multipacting occurs. The solid line corresponds to a level having frequency square dependence.

2.3.2 was later developed which improved the surface quality considerably so that fields exceeding 25 MV/m were required to produce measurable electron loading. This field level corresponds to an rf energy content of 3×10^{-4} J. in the resonator.

The results obtained by deforming the top plate were compared to results from resonators whose eigenfrequences were changed by placing a metal spacer between the top plate and the housing (and no deformation). No evidence for additional losses in the deformed superconducting lead-plated resonator due to static strain in the top plate were found. Also the maximum strains under FM deformation approached the elastic limit of the copper substrate without noticeably affecting the rf properties of the superconducting surface.

2.4.2 Dynamic Electromagnetic Properties

For the dynamic electromagnetic properties, the time evolution of the energy content inside an electrically isolated resonator - subject to a mechanical frequency modulation - was of main interest. What was measured experimentally were pairs of time dependent quantities, the voltage and frequency (V(t), f(t)), with the instant of measurement as the evolving parameter. Many experimental runs have been performed but only the typical results are presented here to demonstrate the essential feature of this conversion scheme. Fig.2.11 shows such a typical photographed oscilloscope trace of the monitored voltage. The upper trace shows the exponential decay of the monitored voltage for a superconducting resonator of fixed resonant frequency. The lower one showed the corresponding voltage when the resonator was being

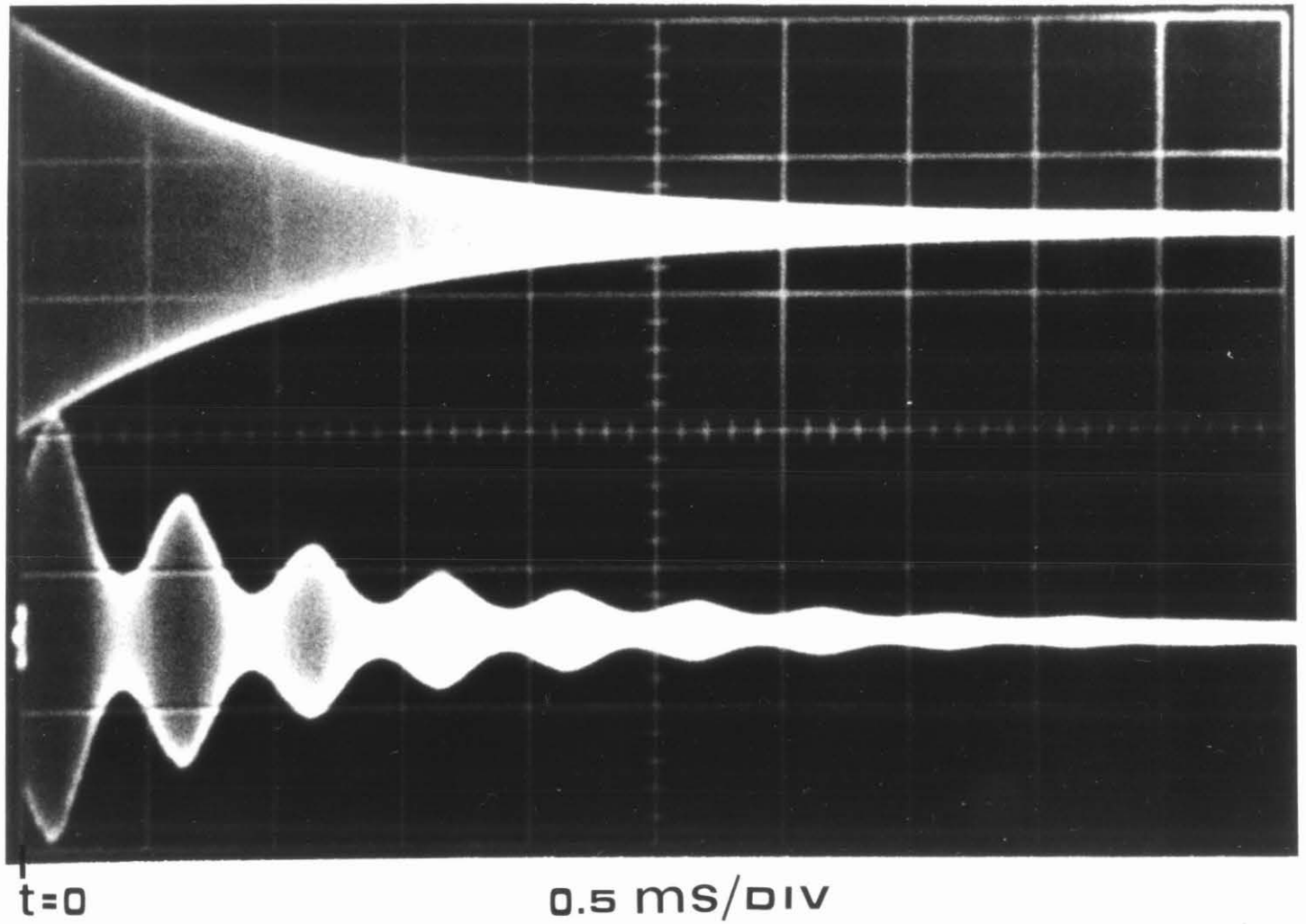

Fig. 2.11. Photographed oscilloscope traces of the time evolution of the stored electromagnetic field. The upper trace shows the exponential decay of the field for an unmodulated resonator and the lower one shows the modulated field of an FM resonator. At time t=0, the incident rf pulse energy is terminated. For large t, both traces show a small direct coupling between the incident and the monitored probes as well as an overexposure broadening.

frequency modulated. In both cases the injected energy terminated at time t = 0. The amplitude V(t) was measured from an expanded version of the lower trace and the frequency was identified by the zero beat generated with a local oscillator at the same instant as described in detail in Sec. 2.3.4 subsection (b).

Many runs were carried out with the injection point, the input power level, the input pulse width, and the modulation extent as variable parameters. Because the purpose of this experiment was to demonstrate this new energy conversion scheme via an adiabatically frequency modulated superconducting resonator no specific effort toward the optimization of the system was made (some design considerations are discussed in Sec. 2.5). Therefore, some of the studies are only qualitative in nature. For example, the coupling between the acoustic and the electromagnetic systems was neither studied in detail nor optimized. The only requirement was that the transducer produce sufficiently large modulation so that the behavior of the electromagnetic oscillation could be studied. This was partly justified because this modulation scheme would be eventually abandoned in favor of other better designs for practical devices. Other areas such as how to couple the rf energy into and out of the resonator at certain times and leave the resonator free from loading at other times still require extensive investigation. These are very complicated and real problems which are only studied theoretically to some extent later in this chapter. For our present experiment, a fixed rf input line was used to coupled the rf energy capacitively into the resonator. To

prevent the injection mechanism from loading the modulated resonator after the rf energy input ceased, the input line was extremely weakly coupled to the resonator over the modulation range for most of these studies. Due to this limitation, an exact quantitative evaluation of the energy coupled into the resonator could not be determined with certainty. Consequently results of varying input power levels and input pulse duration were observed only qualitatively. Despite that absolute measurements of the energy content were not possible with present arrangement, relative measurements nevertheless were able to yield useful information about the fundamental evolution of the electromagnetic oscillation within the resonator. In the subsequent discussion, we will take whatever amount of energy which is coupled into the resonator during the injection process as the total initial energy and examine its time evolution.

2.4.2(a). Typical Results with Small Frequency Modulations

Two typical results out of many experiments actually performed will be discussed here in view of our present experimental purpose to demonstrate this new conversion scheme. As an example, shown in Fig. 2.12(a) and (b) are the results for a single injection event. Part (a) shows the monitored voltage amplitude V(t) as a function of time and part (b) shows the determined oscillation frequency f(t) also as a function of time. The time t = 0 was taken at the instant when the input pulse was terminated. Small circles represent the experimental data, the solid lines are the analytic expressions discussed below. In this particular case, these expressions are respectively given by

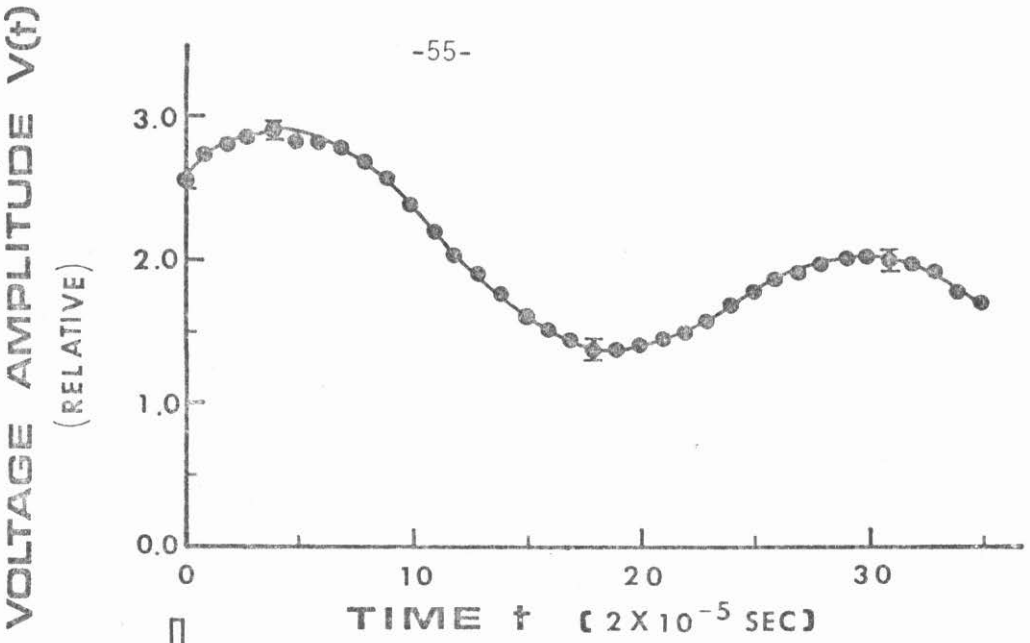

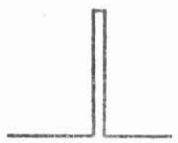

Fig. 2.12(a) Monitored voltage amplitude V(t) versus time. Solid circles are the experimental data which are fitted with an analytic curve given by Eq.(2.34) and shown as the solid line above. The input pulse is also shown to the left of this paragraph.

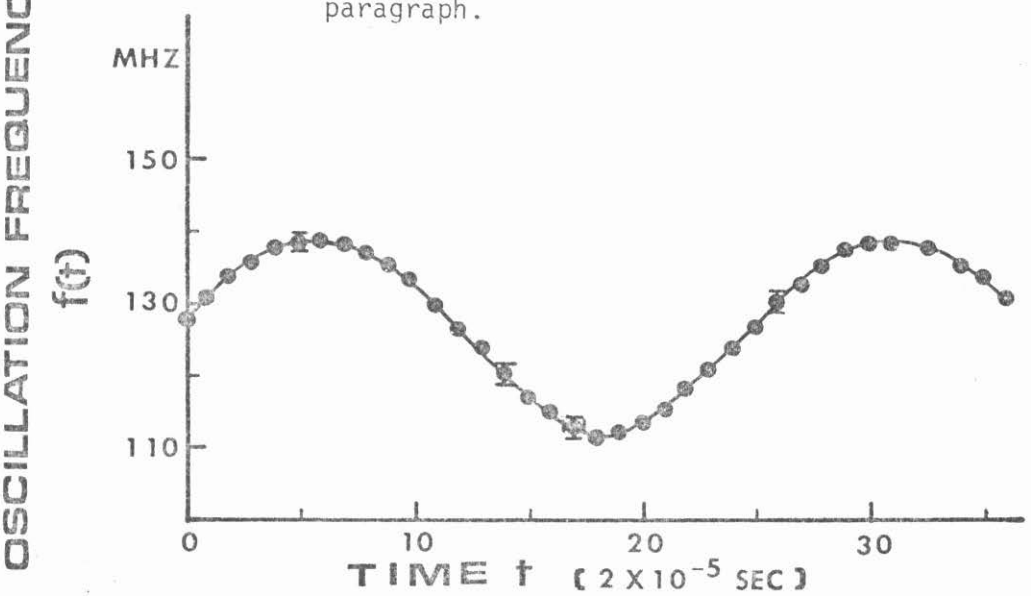

Fig. 2.12(b) Measured oscillation frequency f(t) versus time. Again solid circles are the experimental values while the solid curve is the analytic expression given by Eq.(2.33).

$$\frac{1}{f^2} = \frac{0.4357}{0.73 + 0.17\sin(\Omega t + \theta_1) - 0.005\cos(2\Omega t + \theta_2)} + 0.037 \qquad (2.33)$$

and

$$V(t) = 1.357\, e^{-t/t_o}\, (f(t))^{2.5} \qquad (2.34)$$

where f is in 100 MHz, t is in second, $\Omega = 7.08516\times10^{5}$ degree/sec, $\theta_1 = 10^{\circ}$, $\theta_2 = 25^{\circ}$, $t_o = 1.411\times10^{-3}$ sec.

Eq.(2.33) is obtained from Eq.(2.9) with a time dependent gap d(t). Since a small component at second harmonics is needed to fit the experimentally observed frequencies, the thin plate vibration is slightly nonlinear.

The 2.5 power dependence on the frequency of the voltage amplitude V(t) is suggested by the zeroth order relationship of Eq. (2.31). This comes about because $W(t) = \frac{1}{2}CV_g^2 = \frac{L}{2}\frac{V_g^2}{\omega^2}$. For the ideal case, the adiabatic theorem shows $W(t) \sim \omega(t)$, therefore

$$V_g(t) \sim \omega^{1.5}(t) \qquad \text{and} \qquad V(t) \sim \omega V_g \sim \omega^{2.5}(t)$$

The fact that V(t) can be fitted with this frequency dependence indicates the model used to calculate the energy content is consistent with the adiabatic theorem.

In Sec.2.4.1 it was shown for an unmodulated resonator the loss was characterized by the dielectric loss and the energy decay time τ_p was found to be proportional to $\omega^{1.1\pm0.1}$. Such frequency dependence was not taken into account to obtain Eq.(2.34). Instead, an averaged

voltage decay time t_o was found to fit the data reasonably well. The reason is due to small modulation (from 112 to 138 MHz) in this particular case.

An analytic evaluation of energy conversion via this technique can be obtained by substituting Eq.(2.34) into Eq.(2.29) and carrying out the indicated calculations. Since the monitoring probe is very weakly coupled to the resonator throughout the modulation, ωRC_o was found to be less than 10^{-3} and the limiting form of Eq.(2.29) is a good approximation in this case. In order to illustrate these results it is convenient to define new parameters. From Eq.(2.3) and the subsequent discussion, it is clear that the ratio of energy to frequency is a natural parameter for this system. Therefore, the evolution of this quantity will likely dominate. Consequently following the suggestion of Eq.(2.7) we define a quantity J(t) such that

$$J(t) \equiv \ln\left(\frac{W(t)}{f(t)}\Big/\frac{W(0)}{f(0)}\right) = \ln\left(\frac{V^2(t)}{f^5(t)}\Big/\frac{V^2(0)}{f^5(0)}\right) \qquad (2.35)$$

Using Eqs.(2.33) and (2.34), J(t) was evaluated at time interval of 2×10^{-5} second after t = 0 and plotted as solid circles shown in Fig. 2.13. Note that the crossed points also shown there are the results if the individual experimental datum for the measured voltage amplitude V(t), instead of Eq.(2.34), was used to calculate the same quantity J.

According to Eq.(2.7) J(t) should be equal to $-\int_o^t \frac{dt}{\tau_p}$, which is the total fractional energy loss up to that instant. If τ_p were assumed to be dielectric loss in nature as indicated by the static experiments, then $\tau_p \propto \omega^{1.1}$ with the proportional constant determined

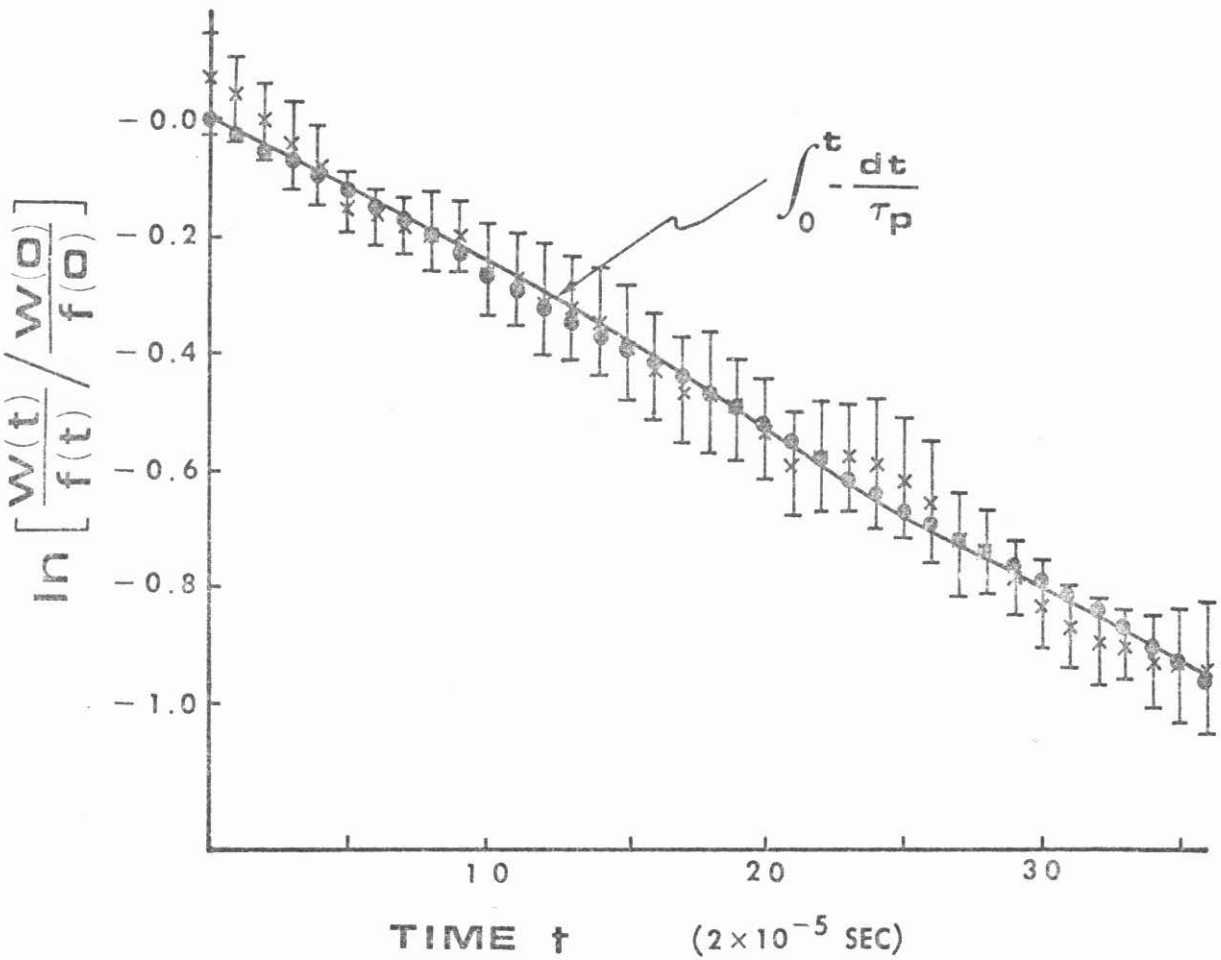

Fig. 2.13 The plot of $\ln(W(t)/f(t))$ versus time. The circles are deduced from the smoothed voltage amplitudes and frequencies as given by Eqs.(2.33) and (2.34) respectively. The crossed points show the data scattering if raw values of the measured voltage amplitude are used. The solid line is the integrated fractional energy loss assuming dielectric loss in the lead oxide layer dominates. The observed results agree well with this mechanism.

by the static data obtained before modulation was applied. The integral was subsequently carried out and plotted in Fig. 2.13 as the solid curve.

As can be seen from Fig.2.13, the data deduced from the analytic expressions for the measured voltage amplitude and the oscillation frequency agree quite well with the result based on the dielectric loss mechanism. The cross point data on the other hand show some deviations from the solid curve. These deviations do not appear completely random and are believed to be originated from the small systematic errors in correlating the measured amplitude and frequency at the same instant. Because of the high power dependence of J(t) on the voltage amplitude V(t) and the frequency f(t), small errors in V(t) and f(t) can cause a large uncertainty in J(t). For instance, even if the relative errors in V(t) and f(t) are as small as 2% and 0.3% respectively, the absolute uncertainty in the quantity J(t) itself is as large as ±0.043. For all experiments, these observed deviations are well within the uncertainties of the data points making the complete resolution of these deviations impossible with present experiments*. The nature of these deviations is of interest because according to Eq.(2.7) the slope for the curve of J(t) versus time should be always negative if the energy within the FM resonator is continuously

---

* The situation can be improved somewhat if both rf probes can be relocated to the bottom area of the resonator, and the capacitive coupling is replaced by an inductive coupling. The monitored voltage can then relate to the energy content directly because the effect of coupling change as frequency is varied is minimized. Present set up was originally designed for the electric field emission experiment and the improvement mentioned above was hard to implement without major changes in the dewar insert and the resonator structure.

dissipated. However, for some experiments these deviations tend to show zero or even positive slopes over part of the modulation cycle. If these deviations cannot be fully accounted for by the systematic errors, it must imply that additional energy generation processes are present to offset or even exceed the dissipation at these instants. Such generation processes are deemed very unlikely in our experiments; nevertheless they have not been completely ruled out either. The good agreement obtained by using the analytic expressions of amplitude and frequency is due to the results of averaging out the possible randomness among the measured amplitudes or the frequencies and much better correlations between these two quantities over the entire modulation cycle.

One important conclusion obtained from Fig.2.13 is that as far as the electromagnetic oscillation is concerned, its energy is indeed pumped up or drained down by the mechanical modulation mechanism so that the energy conversion is achieved as prescribed by the adiabatic theorem. It also demonstrates that a superconducting resonator is a necessary component for the success of this process. The agreement shown in Fig.2.13 indicates that all the energy loss during the modulation can be fully accounted for by the loss that occurs in the superconducting material and does not come from the electromechanical interaction itself. This implies that the electromechanical energy conversion itself is indeed highly efficient.

Fig.2.14 and Fig.2.15 are two aditional graphs for another injection event. The injection point was changed in this case along with slight increase in modulation range. Input power level was kept

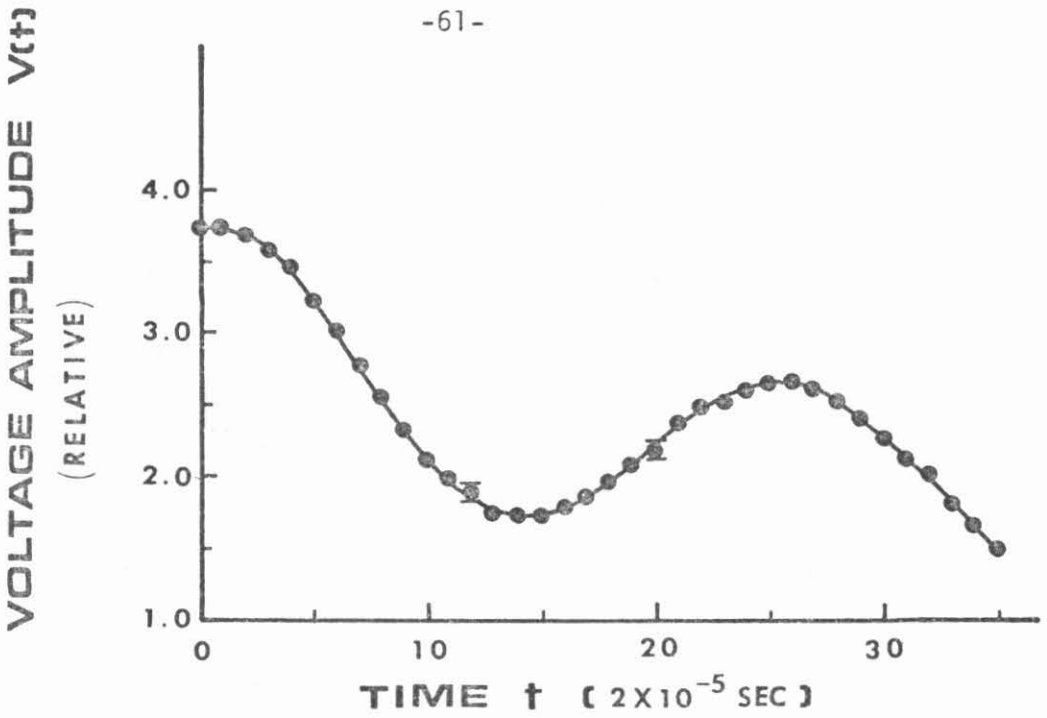

Fig. 2.14(a) Monitored voltage amplitude V(t) versus time for another injection event. Solid circles are the experimental data which are fitted with an analytic expression shown as the solid curve above.

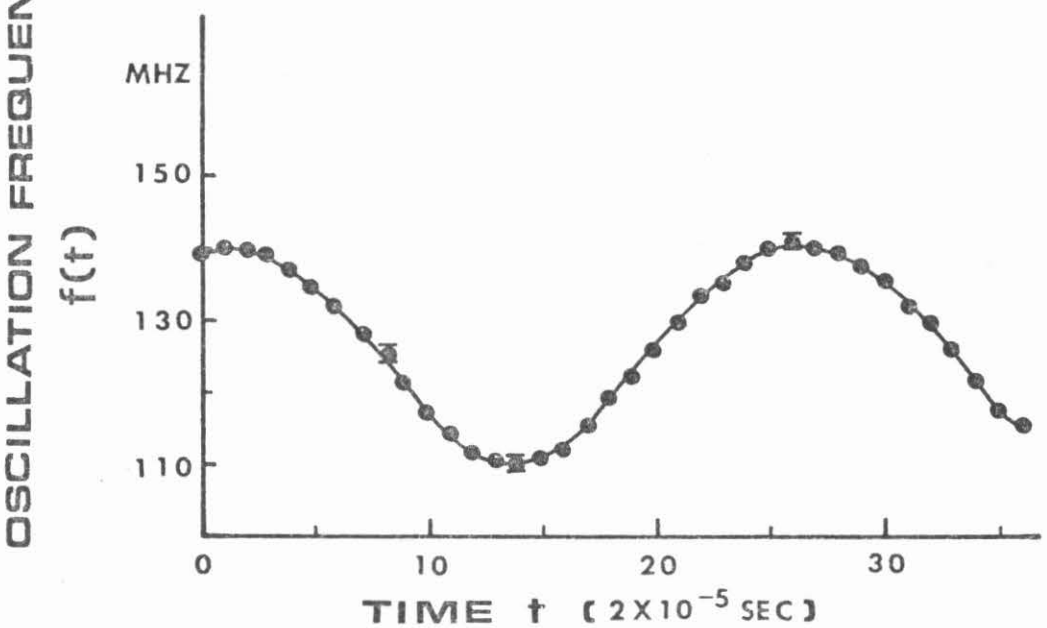

Fig. 2.14(b). Measured oscillation frequency f(t) versus time for the event of Fig.2.14(a). It is to be noted that the injection point in this case differs from the one shown in Fig.2.12(b).

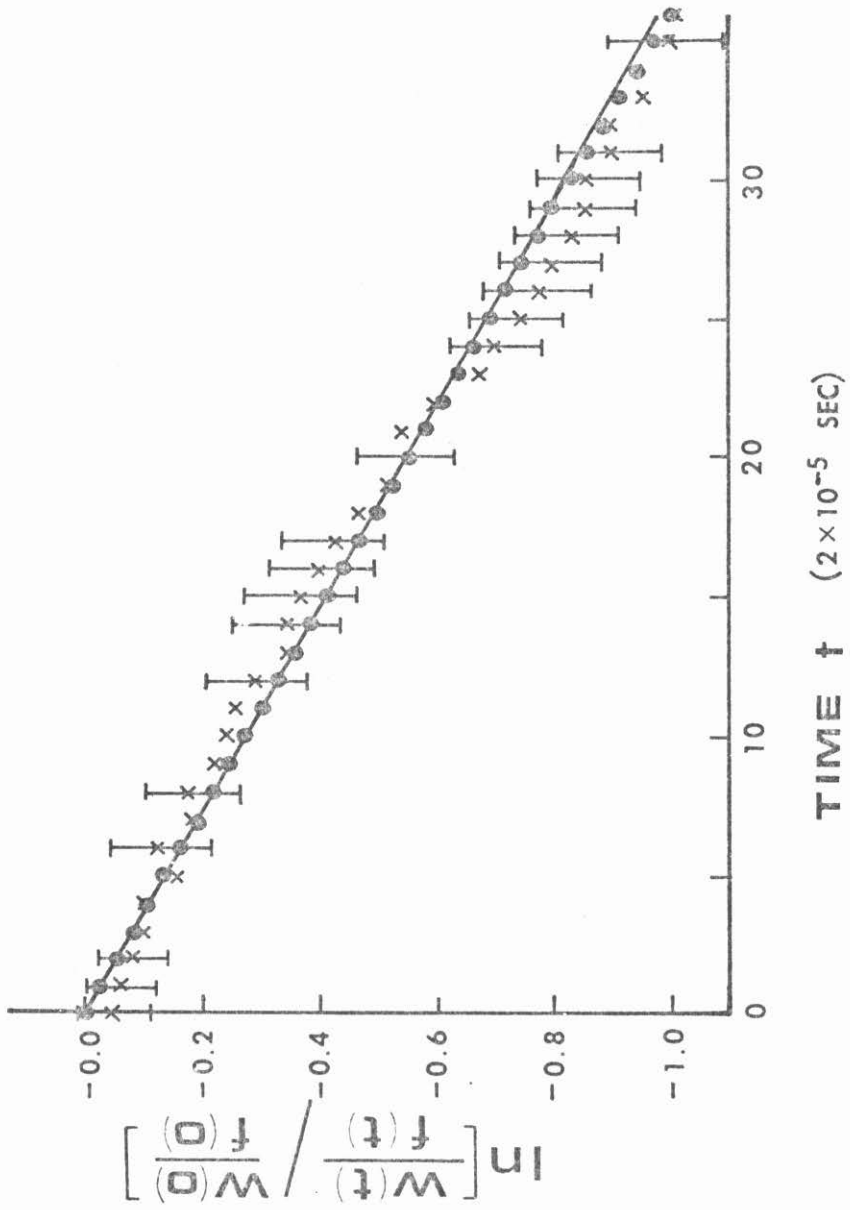

Fig. 2.15 The plot of $\ln(W(t)/f(t))$ versus time for the event shown in Fig. 2.14. The deduced experimental results again agree well with the result (shown as the solid curve) if the dielectric loss is assumed to dominate. Refer to the text for detailed explanation.

approximately the same as before. The method of data deduction, and the meaning of each symbol remain the same. Clearly, the characteristics of these graphs are very similar to the previous ones indicating that the conversion process takes place as expected regardless of the injection timing.

2.4.2(b) Typical Results with Larger Frequency Modulations

In order to see any effect when the modulation range was much larger, the transducer was driven to larger amplitudes. Several difficulties arose:

(1) Because the thin plate vibrations became quite nonlinear when the vibrational amplitude was large, vibrational instability and detuning effects were observed. Arcing between the two transducer plates finally limited the maximum allowable modulation; ranging from 95 MHz to 155 MHz.(2) As the modulation was increased the coupling capacitance C_o itself appeared to become time dependent over part of the cycle, unlike the small modulation case. For instance, in the lowest frequency range, the coupling became so weak that it was essentially decoupled. In order to observe whe whole history of energy evolution, the coupling was increased so that the entire voltage V(t) could be displayed on the oscilloscope throughout the whole modulation period. However this introduced unavoidable coupling loading on the resonator over about half a modulation cycle.

As a qualitative illustration, Fig. 2.16(a) and (b) again show the measured voltage amplitude V(t) and oscillation frequency f(t) for an injection event with a larger frequency modulation (from 98 to 152 MHz). As in previous figures, the circles represent the experimental

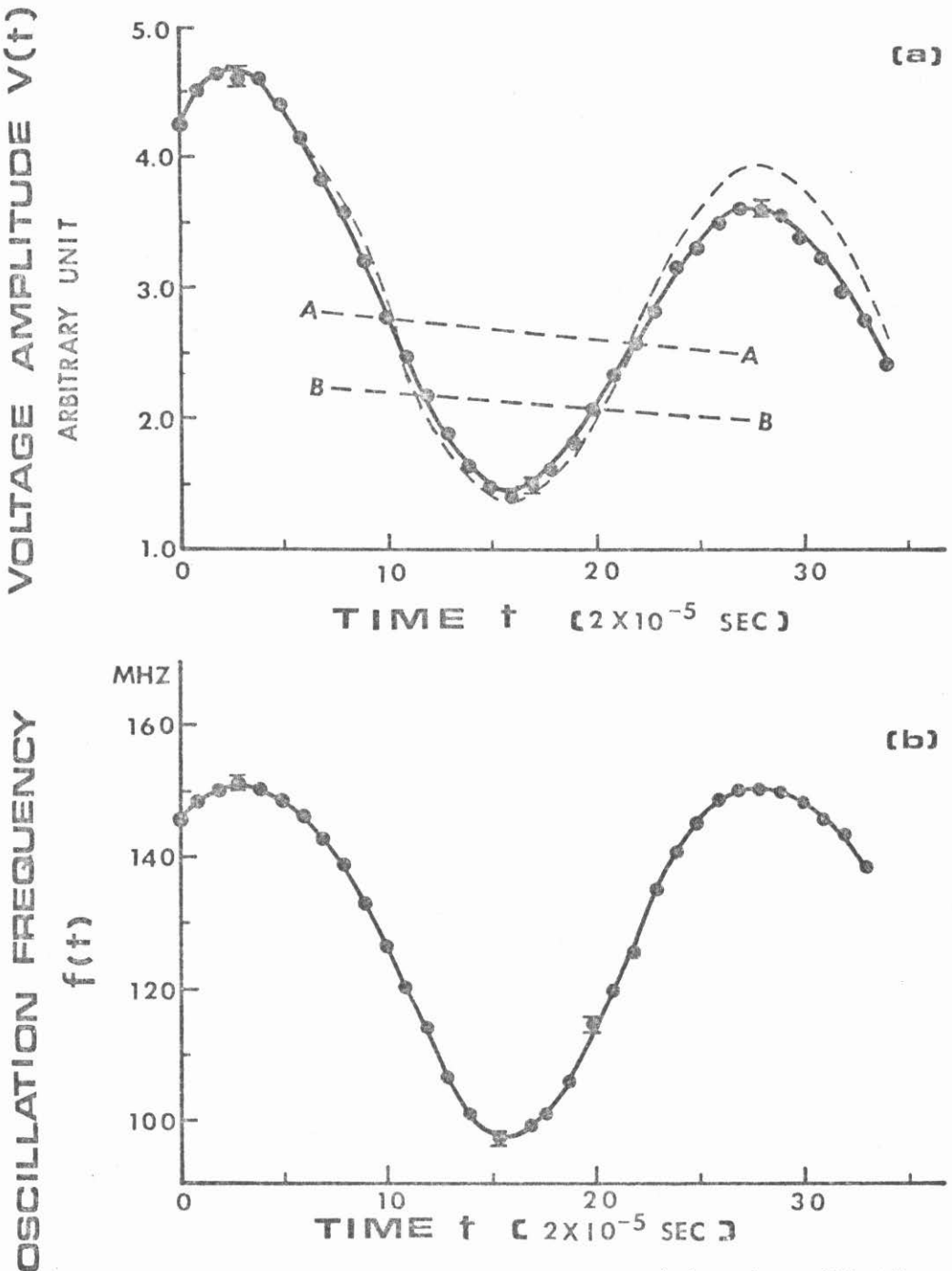

Fig. 2.16 Measured voltage amplitude V(t) and oscillation frequency f(t) for an injection event with a large frequency modulation. All the solid circles represent experimental data. The detailed explanations of the solid and dashed lines are given in the text on p.63 and p.65.

data and the solid lines represent the analytical expressions used to fit them. For this example, the expressions are given respectively by

$$\frac{1}{f^2(t)} = \frac{0.4357}{0.765 + 0.325 \sin(\Omega t + \theta_1) + 0.01 \sin(2\Omega t + \theta_2)} + 0.037 \qquad (2.37)$$

and

$$V_1(t) = 1.715\, e^{-t/t_{01}} (f(t))^{2.5} \quad \text{for } f(t) > 1.25$$

$$V_2(t) = 1.70\, e^{-t/t_{02}} (f(t))^{2.5} \quad \text{for } f(t) < 1.15 \qquad (2.38)$$

where f(t) is in 100 MHz,

V(t) is in an arbitray unit

$\Omega = 7.185 \times 10^3$ degrees/sec

$\theta_1 = 43.1^\circ$

$\theta_2 = 100^\circ$

$t_{01} = 1.99 \times 10^{-3}$ sec

$t_{02} = 2.80 \times 10^{-3}$ sec.

Again the frequency and the measured voltages were fitted with the same functional forms as in the small modulation cases. The only difference is that it is no longer possible to fit the measured voltage well with only one averaged decay time over the entire range. Above dotted line AA, the experimental data can be described by $V_1(t)$ and below line BB by $V_2(t)$. The dotted curves are the extensions of

$V_1(t)$ and $V_2(t)$ into respective regions where they are not valid.

For frequency range $1.15 < f(t) < 1.25$, the curves were drawn so that they made a smooth transition from one region to the other as shown in Fig.2.16(a). That two distinctive "averaged voltage decay time" t_{01} and t_{02} are needed in order to fit the monitored voltage reasonably well indicates that there exists additional losses which are significant in a certain frequency range but becomes unimportant in the others. In fact, since $t_{01} < t_{02}$ we can conclude that the dielectric loss is not responsible for the entire dissipation because it would otherwise require $t_{01} > t_{02}$. This is consistent with the experimental observations that appreciable coupling loading was found for most of the frequency range when the coupling was increased. To account for this effect quantitatively, accurate descriptions of how the coupling strength and the coupling loss change with the time are indispensable. These were difficult to obtain especially for frequencies less than 110 MHz in our present experiment because of very small observable signals. Furthermore to fit the monitored voltage with only two averaged decay times will overlook the significance of frequency dependent dissipations which may be observable for larger modulations. These effects tend to make the results obtained with simple approximations less reliable and possibly with systematic errors. Because this additional coupling loss is not intrinsic to the energy conversion process and can be minimized by other means (see footnote on P.59), a quantitative agreement was not pursued further.

Despite the difficulties encountered with the present experi-

ments, this study nevertheless is the first attempt ever made to measure the electromagnetic energy inside a resonator which is subject to a large frequency modulation. This type of measurement could not be done previously with normal resonators and therefore the significance and the potential for this new mode of electromechanical energy conversion have never been appreciated. Present experiments have shown that a moving superconducting boundary can provide a very low loss interface across which significant direct exchange between the electromagnetic and the mechanical energy can take place. This new mode of energy conversion is further considered for practical applications in the next section.

2.5 Electromechanical Energy Conversion Devices Using FM Superconducting Resonators

The experimental results of Sec.2.3 and Sec.2.4 demonstrate that an adiabatic energy conversion can be obtained when superconductors are used as an interface between a high frequency electromagnetic oscillation and a mechanical modulation mechanism. This conversion process is characterized by a direct energy transformation between high frequency electromagnetic energy and mechanical energy, with high conversion efficiency. These characteristics are further discussed below after a brief review of conventional devices in Sec. 2.5.1.

2.5.1 Brief Discussion of Conventional Electromechanical Devices for Energy Conversion

Conventional electromechanical energy conversion at moderate to

high power levels has been accomplished by the interchange of energy between an electrical system and a mechanical system through the medium of a magnetic field. The mechanisms responsible for the conversion are two basic electromagnetic laws, namely, the Lorentz force law and Faraday's induction law. The Lorentz force law governs the motions of charge carriers in the electromagnetic fields, while the Faraday's induction law governs the phenomena associated with the time changing magnetic flux. For conventional rotating machines, an electrical current carrying field winding or a mechanically driven rotor in the presence of a static magnetic field provides the actual generating or motoring function. The most prominent feature characterizing these machines is that a direct or a low frequency alternating current (typically 60 Hz) is involved, that is, the electrical energy supplied to or generated from them is either at zero frequency (d.c) or at the very low mechanical frequency used in these machines.

Both electric motor and generator have undergone extensive research and improvement over the past century or so, and satisfactory efficiency has been achieved. For example, in an electrical generator of moderate to high output rating, the losses in the stator core, stator copper, rotor copper and rotation itself can be minimized to give an efficiency of up to 99%. Recently, superconductors have been incorporated into the conventional machines to raise the magnetic flux density and current carrying ability. As a result, superconducting rotating machines of superior performance, small size, light weight and higher power density become possible. Despite this utilization of superconductors, the energy transformation still takes place at

zero or low mechanical frequency. This characteristic contrasts greatly to what will be discussed in the next section at least as far as the fundamental concept is concerned. There, a direct electromechanical energy conversion scheme at microwave frequency is explored.

2.5.2 Characteristics of Electromechanical Energy Conversion Devices Using Superconducting FM Resonators

The new technique for electromechanical energy conversion to be discussed here involves the "compression and expansion" of electromagnetic fields. This class of machine operates somewhat analogous to the conventional engines by going through compression and/or expansion phases. However, the working medium here is the "photon gas" associated with the electromagnetic fields.*(8)

For the upconversion aspect of the process, microwave energy is injected into a resonator at some initial frequency f_o and the resonator is subsequently isolated from any further microwave energy input. Immediately afterwards, the configuration of the resonator is adiabatically changed by a mechanical system so that the resonant frequency is raised to a larger final value f_1. The nature of this process has been discussed in detail in the previous section. It is similar to the adiabatic compression of a thermodynamic system. In both cases the number of the particles of the system (i.e., photon and molecules respectively) is conserved.** The compression process

---

* It is possible to study the conversion mechanism using traditional energy-momentum formulism with field components as variables. However, the photon picture is by far the most intuitive approach and yields most of the essential results without actually solving the complicated problem.

** Here we are dealing with ideal systems only, the effect of dissipation is considered later.

results in higher system frequency for the former and higher system temperature for the latter. Since the photon energy is a function of frequency only, higher photon frequency also implies higher total photon energy. This increase in energy comes from the frequency shift (the Doppler effect) when the photons bounce back from an oncoming moving boundary coherently. For each bounce, they gain an infinitesimal amount of momentum and a corresponding amount of energy. Because the electromagnetic excitation inside the resonator persists indefinitely in the adiabatic limit (see Sec.2.2) the infinitesimal energy increases can accumulate over a long period of time resulting in a macroscopic energy gain. This macroscopic energy gain comes from the work done by the moving boundary against the force exerted on the surface due to the momentum exchange with the bounced photons. Obviously the energy is converted directly from mechanical form into high frequency electromagnetic form.

For the motor aspect, a reverse process takes place; photons of frequency f_1 bounce back from an outgoing moving boundary and undergo a Doppler shift toward lower frequency f_o similar to the adiabatic expansion of thermodynamic system. The effect of accumulating such events continuously is that a macroscopic quantity of work is done on the boundary by the photons and a large cumulative reduction in photon frequency occurs at the same time. As an example, in Fig. 2.17, a highly schematic drawing is used to illustrate typical operation of this type of machine. Shown there is a cross sectional view of a microwave cylindrical cavity discussed at the beginning of this chapter. The resonant frequency of its TE_{111} mode is determined by

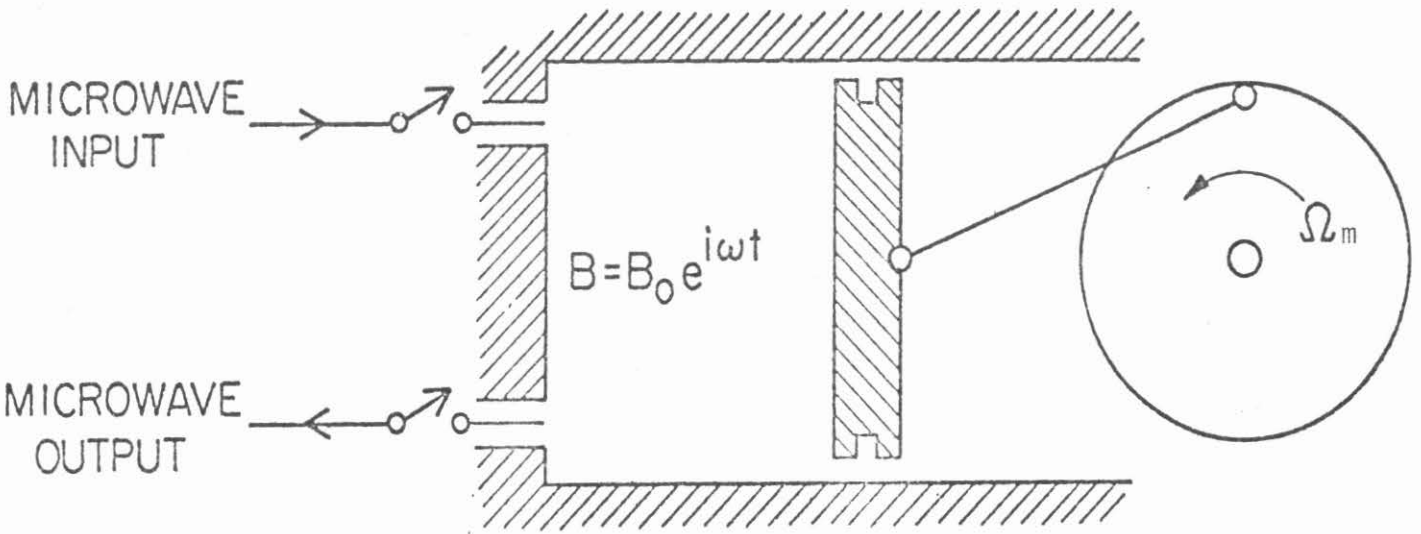

Fig. 2.17 Schematic diagram for a conceptual electromechanical energy conversion device operating in the TE_{111} mode of a cylindrical microwave resonator. The "piston" is driven by a mechanical device of angular frequency Ω_m. The microwave input and output switches are also symbolically shown.

the position of the movable piston which is assumed to be driven by or able to drive a mechanical device in such a way that the operation is always in the adiabatic limit. As an up-converter, microwave energy is injected through the input valve when the resonant frequency of the TE_{111} mode is at its minimum value. Once the mode is excited, the input valve is closed. The microwave energy inside is then pumped to a higher value at higher frequency when the piston is driven inward by mechanical means. As soon as the frequency reaches the desired value, an output valve is then opened so that energy can be coupled out of the resonator. As a motor, the previous procedure is reversed, i.e., the energy is initially injected at the highest frequency from which some portion of energy is available as mechanical work when the piston displaces outward under the action of the radiation pressure. The remaining electromagnetic energy at very low frequency becomes the "exhaust" of this process.

In order to accomplish the proposed conversion practically, three conditions must be satisfied:

(1) The theory of operation is based on the results of the adiabatic theorem, therefore, the adiabatic condition must be satisfied to begin with. That is, the modulation rate be much slower than the rate change of the electromagnetic oscillation itself. For cyclic operation it is equivalent to require the frequency of the mechanical modulation F be much smaller than the microwave frequency f. This condition is impossible to violate for a microwave system with mechanical modulation because material consideration limits the practical linear velocity for a rotating machine to about 300 m/s (i.e., rotational

speed of 6×10^4 RPM for a characteristic radius of 5 cm).

(2) Previous discussion of the operation also assumes a lossless system. Since any real resonator possesses various forms of losses, the results for ideal system are approximately true only if these losses are very small; specifically, the energy loss over a characteristic modulation time should be insignificant compared to the total energy. This condition excludes the possibility of using normal resonators because the energy inside would have decayed in a matter of a few microseconds,while the fastest mechanical modulation time achievable is of the order of 0.1 ms only. Clearly devices made use of normal conductors would never be operative. Thanks to the advanced material processing, superconductors are now available by which this condition can be practically satisfied. Superconducting resonators of one second or longer power decay time are obtainable at microwave frequencies nowadays. Later it will be shown that the power decay time affects the eventual conversion efficiency directly. It goes without saying, the unique properties of superconductors are essential for the success of this kind energy conversion.

(3) So far we have been assuming that a particular mode when excited will follow the eigenmode (local eigenmode*) corresponding to the instantaneous boundary which is adiabatically modulated. This is correct as long as no degeneracy occurs over the whole modulation range. That is, the eigen frequencies of two eigenmodes of the

---

*Local eigenmode is the eigenmode of the system whose boundaries are instantly frozen at that instant. In the adiabatic limit, the boundaries are quasi-statically changed, the local eigenmode is approximately equal to the true solution.

resonator must be sufficiently separated in frequency that the frequency of the initial mode will not be tuned to cross that of the other within the tuning range. Otherwise mode coupling will occur and the energy concentrated in the initial mode will be redistributed between these two modes. As far as the initial mode is concerned, mode coupling can constitute a substantial energy loss mechanism when function of a motor or an upconverter is desired. The situation for mode crossing is very similar to that of two coupled non-degenerate oscillators whose decoupled frequencies cross each other. The latter is treated in detail in Chapter III. With slight modification, the conclusion can be applied directly to the problem of mode crossing raised here.

The efficiency of the power conversion is discussed below. In Appendix A, it has been shown that the microwave energy W(t) inside an adiabatically frequency modulated resonator is governed by

$$\frac{dW(t)}{dt} = - \frac{W(t)}{\tau_p} + \frac{1}{f(t)} \frac{df(t)}{dt} \qquad (2.39)$$

where τ_p is the power decay time.

Integrate Eq.(2.39) from t_o to t_1 we have

$$\ln \left(\frac{W(t_1)}{f(t_1)} \Big/ \frac{W(t_o)}{f(t_o)} \right) = - \int_{t_o}^{t_1} \frac{dt}{\tau_p} \qquad (2.40)$$

If $t_1 - t_o$ is the characteristic modulation time τ_m, and $\langle \tau_p \rangle$ is the mean power decay time during that period of time, Eq.(2.40) can be

written as

$$\frac{W(t_1)}{W(t_o)} \cdot \frac{f(t_o)}{f(t_1)} = \exp\left(-\frac{\tau_m}{\langle\tau_p\rangle}\right) \tag{2.41}$$

Since it is of practical importance only if $\tau_m \ll \tau_p$

$$\frac{W(t_1)}{W(t_o)} \simeq \frac{f(t_1)}{f(t_o)} \cdot \left(1 - \frac{\tau_m}{\langle\tau_p\rangle}\right) \tag{2.42}$$

We define the efficiency of the up-conversion* η as the ratio of the final output energy available to the total input energy, i.e.,

$$\eta = \frac{W(t_1)}{W(t_o) + \text{Mechanical Work}} \tag{2.43}$$

$$\text{Since mechanical work} = W(t_1) - W(t_o) + \text{Dissipation} \tag{2.44}$$

$$\eta = \frac{W(t_1)}{W(t_1) + \text{Dissipation}} \tag{2.45}$$

Rewrite Eq.(2.42) as

$$W(t_o)\left(\frac{f(t_1)}{f(t_o)} - 1\right) = W(t_1) - W(t_o) + W(t_o)\cdot\frac{f(t_1)}{f(t_o)} \cdot \frac{\tau_m}{\langle\tau_p\rangle} \tag{2.46}$$

---

* The efficiency for motoring conversion can be similarly defined.

where the left hand side is the total external energy added (i.e., mechanical work). Compare Eqs.(2.44) and (2.46), the dissipation is identified as

$$W(t_o)\,\frac{f(t_1)}{f(t_o)}\cdot\frac{\tau_m}{<\tau_p>}$$

Substitute it to Eq.(2.45) and use Eq.(2.42), we have

$$\eta \simeq \frac{1}{1+\left(\frac{W(t_o)}{W(t_1)}\cdot\frac{f(t_1)}{f(t_o)}\right)\frac{\tau_m}{<\tau_p>}}$$

$$\simeq \frac{1}{1+\left(1+\frac{\tau_m}{<\tau_p>}\right)\frac{\tau_m}{<\tau_p>}}$$

$$\simeq 1-\frac{\tau_m}{<\tau_p>} \qquad (2.47)$$

The term $\frac{\tau_m}{<\tau_p>}$ represents the averaged fraction of microwave energy lost during the modulation and Eq.(2.47) appears intuitively true. However the overall efficiency for a low temperature machine must also account for refrigeration. From thermodynamic and practical consideration, each watt dissipated at low temperature ($\sim$4.2°K) requires approximately 1000 watts of room temperature refrigeration power to extract it, therefore, Eq.(2.47) should be modified with the dissipation part multiplied by this proportionality, i.e.,

$$\eta = \frac{W(t_1)}{W(t_1) + 10^3 \cdot \text{Dissipation}} \tag{2.48}$$

Following the same derivation again with a more stringent assumption $10^3 \cdot \frac{\tau_m}{\langle \tau_p \rangle} << 1$, we arrive at

$$\eta \simeq 1 - 10^3 \cdot \frac{\tau_m}{\langle \tau_p \rangle} \tag{2.49}$$

Eq.(2.49) shows that in order to improve the conversion efficiency, the modulation time τ_m should be decreased and the average power decay time $\langle \tau_p \rangle$ increased as much as practically allowed. Though improvement in refrigeration efficiency will also improve the overall efficiency, we will assume the number used here is a conservative estimation and is regarded as fixed. Assuming that a one second power decay time τ_p is achievable with a real device along with $\tau_m \sim 10^{-4}$ sec, which seems feasible with a superconducting turbine, Eq.(2.49) implies an overall efficiency including refrigeration of about 90%. When the device is used as a motor, this overall thermodynamic efficiency is very important. However for certain applications, such as upconversion and switching applications, the microwave energy is the desired quantity and as far as the microwave energy itself is concerned, it may be that the conversion efficiency given by Eq.(2.47) is enough. In these cases the conversion efficiency is close to 100%.

The output power available from this type of device is considered next. Since we will not deal with a specific design, a

general estimation is made. The averaged output power is approximately obtained by calculating the maximum electromagnetic energy that can be stored in the resonator W_{max} divided by the time it takes to convert it into mechanical energy. This time is expected to be of the order of modulation time τ_m. Assume it is exactly τ_m, then the maximum output power is given by

$$P_{out} \simeq \frac{W_{max}}{\tau_m} \qquad (2.50)$$

The maximum energy density that can be stored in a superconducting resonator is limited either by the critical rf magnetic field H_c^{rf} of the superconducting material or by the electron emission process due to high surface electrical field. The critical rf magnetic field is an intrinsic property of a superconductor. At present, the maximum rf field which has been achieved in superconducting resonators is approximately 1500 Gauss (0.15 T). Taking 0.1 T as a reasonable estimation, the maximum energy density $\frac{B_c^{rf\,2}}{2\mu_o}$ is about 5×10^3 Joules/m^3. On the other hand if the limitation is due to electron emission, the maximum energy density is given by $\frac{\varepsilon E_{pk}^2}{2}$ where E_{pk} is the peak surface electrical field before electron emission sets in and strongly depends on the surface conditions. For superconducting lead surface this can be as high as 25 MV/m (up to 70 MV/m has been obtained on other surfaces). Taking 25 MV/m as a reasonably achievable field, the maximum energy density would be about 2.8×10^3 Joules/m^3.

In any case, the maximum energy density seems to be of the order of a few kilojoules per cubic meter. Accordingly the limiting

output power density is of the order of 10 MW/m^3 (assuming $\tau_m \sim 10^{-4}$ sec). For a resonator of 10^3 cm^3 active volume, the limiting output power is of the order of 10 kilowatts. (For conventional rotating machine with ferromagnetic core, the power density is limited to about 10^3 MW/m^3.)

2.5.3 Some Design Considerations

In addition to the limitations inherent with this conversion scheme, there are other practical considerations that should be taken into account. Again because a specific design is not available now, three major considerations will be discussed in general terms.

(1) As a useful device, the active electromagnetic volume inside the resonator should be maximized since the eventual output power available is equal to the power density times this active volume. The reentrant cavity used in this experiment has proved useful in demonstrating the principle, but seriously limited in practical application. The reason is that the useful volume for the energy storage is provided only by the tiny volume between the top plate and the reentrant post ($4\text{-}8\times10^{-8} m^3$). This limits the maximum energy which can be stored to about 10^{-4} J and available power to 100 mW. To make a practical device, the useful volume should be increased so that total energy stored can be increased while keeping the dissipation to a minimal level. One way of achieving this is to design a resonator so that the average field level is approximately the same throughout its geometric volume (obviously the reentrant cavity does not meet this requirement). This condition seems rather difficult to satisfy general-

ly however. Extensive studies of the possible resonator structure and mode configuration are still needed.

(2) Often a device capable of cyclic operation is a desired feature because it can provide a quasi-continuous power flow. A rotary configuration appears to be attractive in this regard, because of the vast knowledge and experience gained from designing conventional rotating machines. In addition it is possible to design a rotating structure so that it possesses certain rotational symmetry, say, an n-fold symmetry. If this device rotates with a period T_1 the resonant frequency will be modulated from high frequency (f_1) to low frequency (f_2), n/T_1 cycles per second. Each time this occurs a fraction $(\frac{f_1 - f_2}{f_1})$ of the energy is converted to mechanical energy and the total mechanical power generated will be proportional to $E(\frac{f_1-f_2}{f_1})\frac{n}{T}$, where E is the energy content at frequency f_1. For this case it is advantageous to maximize the product of n and E to yield maximum output power. For example, by making n large may require a reduction in the resonator volume. However if average field level can be raised at the same time, the result could be a net increase in the output power. Clearly, optimization of the resonator structure is one of the major engineering problems.

(3) For a successful energy conversion device, electromagnetic energy must be able to couple into or out of a variable frequency resonator efficiently. This coupling process (i.e., the input and output switching shown in Fig. 2.17) possesses several unique requirements: at certain instants of time, the coupling must be strong enough so the injection or extraction of electromagnetic energy is very effective. At all

other times, the coupling should remain so weak as not to destroy the high Q of a superconducting resonator. In addition, a large amount of electromagnetic energy should be able to be coupled into or out of the resonator with little dissipation at specific instants but of quite different frequencies. To satisfy these difficult requirements simultaneously is further complicated by the fact that both the frequency and the mode configuration are time dependent. As a result, conventional technique of optimizing the coupling by impedance matching is inappropriate because impedance itself changes with time. Fortunately a scheme involving electrically coupled superconducting FM resonators appears able to overcome these nearly impossible requirements. Properties of coupled FM resonator systems are studied later in Chapter III.

In summary, this scheme of electromechanical energy conversion using superconducting resonators is quite complex. No previous experimental work has been done along this direction. Though recently there have been some theoretical studies exploring the capability of this scheme, their conclusions remain largely speculative. It is clear from the discussion above, all the aspects of the devices must be taken into account simultaneously, even though some of them are seemingly competing factors. Throughout this study various assumptions have been made to simplify the analysis. Even if these turn out to be completely valid and the individual aspects of performance have been demonstrated, there still remains the question of whether the device will work to the expected specification when every part is put together. The ultimate answer seems to lie upon a prototype machine of practical rating.

2.6 Brief Comparison with Conventional Parametric Amplifiers

In a broader sense, FM resonator is also a parametric device because the resonator "parameter" (i.e., the boundary in this case) is varied. However the operation of FM resonators discussed here is somewhat different from that of a conventional parametric amplifier; a device well understood by electrical engineers (9). An ordinary non-degenerate parametric amplifier has three channels: namely the signal, the pump and the idler, coupled together. A typical operation involves supplying a pumping signal through the pump channel so that with an incoming signal fed into the signal channel, an output signal is available. The nature of this output depends on the special relationships among the pump frequency f_p, the signal frequency f_s and the idler frequency f_i. These three frequencies must be related in such a way that $\pm lf_p \pm mf_2 \pm nf_s = 0$ where l, m, and n are positive integers. The idler channel is needed to insure the proper operation of the device. For one particular application which resembles the upconverter discussed here a fourth frequency exists at the output port such that $f_4 = f_p + f_s$. Under this condition an input signal at frequency f_s can be up-converted to provide an output at frequency $f_p + f_s$ with the conversion gain equal to the frequency ratio f_4/f_s.

Two main differences between this kind of parametric device and our FM resonators are noted. For a conventional parametric amplifier, the pumping frequency, f_p, is related to the signal frequency, f_s, in a nontrivial way. Furthermore the integers that relate these frequencies are usually so small that all the frequencies are essentially of the same order of magnitude. Under this condition the operation appears

to depend very critically on the relative phase between the pumping and the input signal. However this usually can be taken care of by the idler channel which will be automatically set up in the proper phase as a result of the pumping action. The trade-off here is that the pumping has to provide the energy to both the signal and the idler channel to insure the proper operation. As far as the signal channel is concerned, the maximum efficiency of the conversion is thus limited by the requirement which is essential to the operation itself. For the parametric conversion with FM resonators, there is no restriction imposed on the mechanical pumping with respect to the signal as long as the pumping rate is sufficiently slow. Consequently, the relative phase between the signal and the pumping is not an important parameter, and no counterpart of the idler channel is needed here. In principle all the pumping energy can be converted into the signal energy in this case resulting in a highly efficient conversion. Also conventional parametric amplifiers are mainly used as low noise signal amplifiers and the signal power level involved is usually much less than one Watt. On the other hand our FM resonator is a high power device.When used as an upconverter it has a potential of producing high power microwave at frequency up to k band.

2.7 Conclusions

In this chapter the new electromechanical energy conversion scheme based on the adiabatic principle was demonstrated experimentally using a frequency modulated superconducting resonator. The results showed that a moving superconducting boundary is able to provide a low loss and quite effective interface between mechanical and electro-

magnetic energy. This is brought about because of the unique properties of superconductors. The phase of the electromagnetic oscillation inside a superconducting resonator is maintained over a long period of time during which small Doppler effect can accumulate coherently resulting in an amplified effect of 10^9 to 10^{10} times larger. The outcome is that a fundamentally very weak electromechanical effect is transformed into a high power process. With existing superconducting technologies, the electromechanical generation of CW microwave energy in the power density range of 10^6 - 10^7 W/m^3 seems feasible with overall efficiency including refrigeration exceeding 80%.

Present microwave sources are able to deliver 100 KW or more CW microwave energy at frequencies extending from 350 MHz to X band with efficiencies ranging approximately from 30% to 80% (10). Such high power sources are virtually nonexistent however for frequencies beyond X band. Present devices operated in that range can only provide output power of much less than 1 KW. The superconducting frequency modulated resonator discussed here appears quite promising as a potential high power source for that frequency range. By operating it as an upconverter a large amount of microwave energy at S or X band is coupled into a superconducting FM resonator which is subsequently mechanically modulated so that both the frequency and the energy can be increased by a factor of 2 or 3 as prescribed by the adiabatic theorem. The existing superconductivity technology indicates that microwave energy at frequency below X band can be stored in a superconducting resonator with energy density of about one kilojoules/m^3 and can provide a CW output power density up to 10 KW/$10^3 cm^3$. If the

superconducting properties do not change significantly when the frequency is tuned from a few GHz to 10 - 30 GHz, this upconversion process should be able to provide an output power density of the order of 20 - 30 KW/$10^3 cm^3$ at 10 - 30 GHz.

Another unique and promising application of superconducting FM resonators is that they can be used as inline transducers to achieve transformation between mechanical and high frequency electromagnetic energy within a power transmission and distribution system whose primary "fuel" is in the form of microwave energy. Such energy transfer based on microwave power transmission has been shown to be feasible and appears to be quite efficient even with room temperature components made of copper. However because all the rotating machines can be operated only with very low frequency electrical energy, the transmitted microwave power has to be rectified before being converted to do mechanical work. Obviously successful electromechanical energy conversion using superconducting FM resonators would only make this mode of power transmission more viable in the future.

References

1. L. Brillouin, Les Tenseurs p.183 (New York, 1946).
2. J.R.Delayen, H.C.Yen, G.J.Dick, K.W.Shepard and J.E.Mercereau, IEEE Trans MAG-11, 408-410 (1975).
   Also J.R.Delayen, Ph.D.thesis, California Institute of Technology (1978).
3. G.J.Dick, J.R.Delayen, and H.C.Yen, 1977 Particle Accelerator Conference, Chicago. To be published in Proc. IEEE 1977.
4. A.Blanchard, Phase-locked Loops (John Wiley & Sons, 1976).
5. T.Yogi, Ph.D. Thesis, California Institute of Technology (1977).
6. J.Dick, Preprint. J. Appl. Phys. 42, 106(1971).
7. CRC Handbook of Chemistry and Physics, 52nd Edition.
8. J.Dick, IEEE Trans MAG-11, 441-442 (1975).
9. S.N.Levine and R.R.Kurzrok, Selected Papers on Semiconductor Microwave Electronics (Dover Publications Inc., New York, 1964).
10. E.C.Okress, Microwave Power Engineering (Academic Press, New York, 1968).

CHAPTER III

COUPLED FM RESONATOR SYSTEMS AND THEIR APPLICATIONS TO MICROWAVE ENERGY SWITCHING AND HIGH POWER MICROWAVE PULSE GENERATION

3.1 Introduction

In Chapter II, we set out to investigate the properties of a single adiabatically frequency modulated (FM) superconducting resonator and its potential applications. However during the course of that study, the behavior of coupled FM resonator systems was suggested to play an essential role in determining the practical configuration of the energy input and output switches for the superconducting devices as discussed in Sec.2.5.3. There the treatment of coupled resonant systems was postponed to this chapter not only for the sake of clarity and continuity but also for their own potential applications. In Sec. 3.2 qualitative analyses of coupled resonant systems will be presented using two coupled resonant circuits as an example. The results are discussed in somewhat detail for the case where the frequency variations are linear in time. Later these results are compared to those obtained by an analog computer simulation. In Sec. 3.3 an analytic approximation method is developed to provide some useful expressions valid for smooth frequency variations, so that the nature of the coupling process can be semiquantitatively investigated and their potentials assessed. In Sec. 3.4 applications of coupled resonator systems as microwave energy switching devices and high power pulse generators are proposed and their characteristics discussed.

3.2 Qualitative Analyses of Coupled Resonant Systems

The behavior of two weakly coupled resonant systems (resonators) which have equal fixed resonant frequencies when decoupled is extensively studied in elementary physics and will be briefly summarized below to provide a common language for discussing a coupled system.

Before these two resonators are coupled together, there exist two degenerate eigenmodes of the total system* (which consists of the two decoupled resonators) corresponding to the states resulting from exciting each single resonator. Being an eigenmode of the system, this state will persist in time indefinitely if no dissipation is present. If both resonators are excited simultaneously both eigenmodes are excited. However each resonator will oscillate independent of the other because of the absence of the coupling. In this case, neither the absolute phase of the individual oscillation is of real physical significance nor their relative phase is of any importance in characterizing the system behavior. Obviously this relative phase between these two individual oscillations is also the relative phase between the two eigenmodes.

As soon as the coupling between them is turned on, no matter how weak it is, the situation has fundamentally changed. Two new eigenmodes which are no longer degenerate emerge for the coupled system. The state with only one resonator excited no longer corresponds to an eigenmode of the coupled system. Instead, it is a combination of both new eigenmodes. The beating phenomenon which shows itself in the energy oscillating back and forth between these two resonators

---

* For simplicity, let us assume each subsystem has one eigenmode only. This assumption does not affect our conclusions.

is a direct result of the interference between these two new eigenmodes. Furthermore, the phase information of the individual oscillation can be transmitted through the coupling so that the accumulated relative phase of these two eigenmodes is an important parameter in characterizing the spatial and temporal energy distribution within the coupled system.

A similar language can be used to describe the behavior of a system composed of coupled frequency modulated resonators*. This task is made somewhat easier and clearer if two ideal resonant LC circuits weakly coupled together is used as a model system. For simplicity but without losing generality, we shall assume only one of the circuits has a variable resonant frequency. Furthermore, the inductance is made fixed and equal to each other for both circuits so that only the capacitor of circuit a (C_a) is variable as shown in Figure 3.1. When they are decoupled, circuit a and b are independent of each other; in particular the eigenmode and eigenfrequency Ω_a of resonant circuit a can be continuously tuned across the eigenfrequency Ω_b of circuit b by varying capacity C_a without causing any interaction. However, if these two circuits are coupled, no matter how weak the coupling strength is, an entirely different set of eigenmodes for the coupled system is generated. In Fig.3.2, the new eigenfrequencies Ω_A, Ω_B are plotted as a function of $C_a^{-1/2}$. For any value of the variable capacitance C_a, two eigenmodes exist; one at higher frequency than the other. In general, the frequency of each mode depends on C_a as

---

* Frequency modulation of our interest satisfies the adiabatic condition.

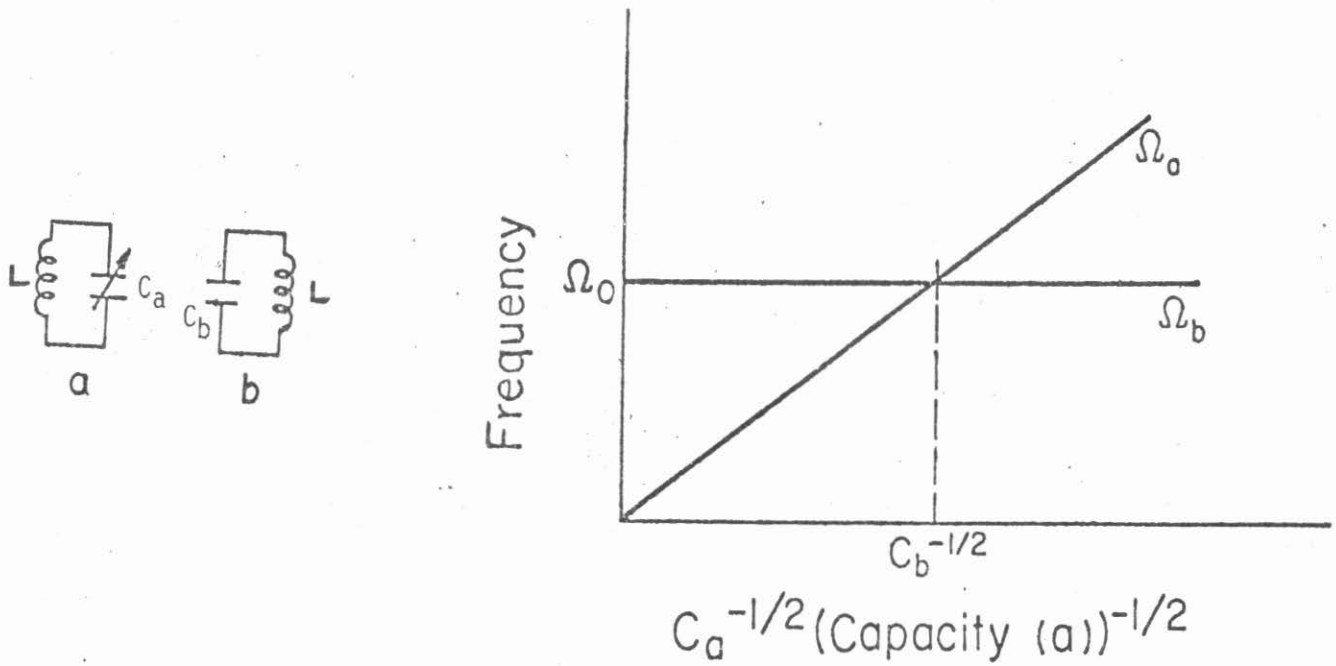

Fig. 3.1 The left hand side shows a system consisting of two decoupled resonant circuits one of which is tunable. The right hand side shows the eigenfrequencies of this system as a function of the variable capacitance of circuit a. Since there is no coupling between these two circuits, the resonant frequency of circuit a can be tuned to cross that of circuit b without causing any interaction.

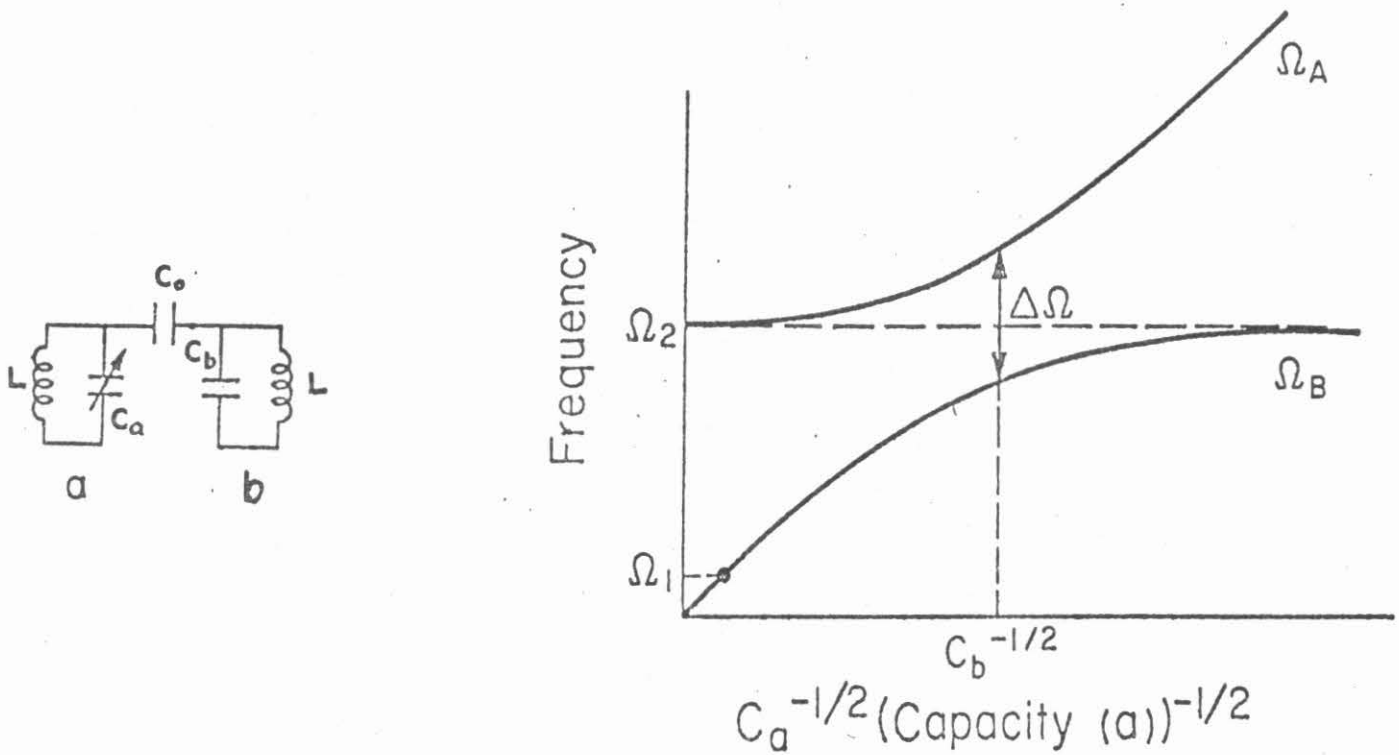

Fig. 3.2 The left hand side shows a system consisting of two coupled resonant circuits one of which is tunable. The right hand side shows the eigenfrequencies of this coupled system as a function of the variable capacitance of circuit a. Notice that the behavior of these two eigenfrequencies is quite different from the previous ones shown in Fig. 3.1. The field configurations for each eigenmode also look differently when C_a is varied from $C_a >> C_b$ to $C_a << C_b$. This feature forms the basis for our switching principle.

does the field configuration of the mode.*

If C_a is adjusted so that the resonant frequency of circuit a when isolated (Ω_a) is much less than that of circuit b when isolated (Ω_b), the low frequency eigenmode of the coupled system (i.e., with eigenfrequency Ω_b) is then characterized by a concentration of the field and therefore the energy in circuit a. This comes about from the fact that at this extreme the effective coupling between these two resonators is considerably weakened by the great disparity in the resonant frequencies despite the constant presence of the small coupling capacitor C_o. Physically, the low frequency eigenmode of the system essentially looks like having resonator a excited only. Conversely when C_a is such that Ω_a is much larger than Ω_b, the low frequency eigenmode is characterized by a concentration of the fields in circuit b. Similar statement regarding the relative energy distribution also follows for the high frequency eigenmode of the coupled system. Consequently, C_a can be considered as a parameter which determines the spacial field configuration and the energy distribution within the system. Obviously, we can take advantages of this unusual characteristic to effect an energy transfer from one resonator to the other if we can manipulate the variable capacitance c_a by external means.

To illustrate this "switching" process, we shall make use of

---

* Strictly speaking, when C_a is changing in time, no true system eigenmodes exist in the ordinary sense because the system itself is time dependent. However when C_a varies adiabatically slowly, it is found useful to apply the eigenmode concept to this situation where eigenmodes are understood to be local eigenmodes. A local eigenmode is the eigenmode one would get if the instantaneous system parameters were fixed at that instant. In the adiabatic limit, the local eigenmode is expected to be a good approximation to the true situation.

the curves showing the functional dependence of the system eigenfrequencies Ω_A and Ω_B on the variable capacity C_a as shown in Fig.3.2. Initially, C_a is adjusted so that $\Omega_B = \Omega_1$ and the system is excited in its lower frequency eigenmode. Physically, this essentially corresponds to exciting resonator a only. The system is then "tuned" via capacitor C_a to a higher frequency say Ω_2. If the tuning is carried out slowly, the eigenfrequency will follow the curve labeled Ω_B as C_a is decreased from its initial value (i.e., from $\Omega_a << \Omega_b$ to $\Omega_a >> \Omega_b$). However the excitation of the lower frequency eigenmode at frequency Ω_2 represents predominantly the excitation of resonator b only. That is, through the process of "adiabatic tuning", the energy has been switched from resonator a to resonator b. The reason that the energy can be switched is because in the adiabatic limit, the energy that we start with when the lower frequency eigenmode is excited will remain almost completely confined to this same mode as the variable capacitor C_a is continuously changed throughout the tuning process. But the field configuration of this mode looks quite different when the capacity C_a is varied from one extreme to the other.

It will be shown in Sec.3.3 that the switching action is a result of accumulation of relative phase between the coupled oscillations in each resonator and the variation of the effective coupling strength. The scheme used here involves tuning one of the resonators so that its resonant frequency when decoupled can be tuned to cross the fixed resonant frequency of the other resonator. Because the effective coupling strength between these two weakly coupled resonators depends on the difference between two decoupled resonant frequencies

in addition to the constant coupling element, it can not remain constant in our case. For example initially the coupling is very weak because of large difference in decoupled resonant frequencies. As the variable frequency Ω_a approaches the fixed frequency Ω_b, the effective coupling becomes much stronger. After the frequency crossing, the difference once again becomes large and the coupling becomes weak. This "decoupling" feature inherent in this process is important because it is responsible for the unidirectional energy switching from one resonator to the other. Furthermore, it turns out that the exact amount of the accumulated relative phase is not critical at all to accomplish a substantial switching so long as the frequency change is very slow when the two decoupled resonant frequencies are about equal to each other. This point will be discussed and demonstrated semiquantitatively later in this and the next sections.

In summary, the energy switching scheme discussed here is characterized by a variable effective coupling strength and unidirectional energy transfer. It involves only one eigenmode of the coupled system throughout the whole switching process (in the adiabatic limit). It is interesting to notice the fundamental differences between this circumstance and that which results when only one of the two coupled fixed resonators is excited (not an eigenmode). There the excitation energy is transfered to the other resonator through the coupling mechanism as time goes by. After a definite time T, the transfer is complete and the energy in the original resonator is emptied. However after another period of time T, the whole energy will return to the original resonator. The energy flows back and forth between these two

resonators, producing the "beat" phenomenon. Clearly in order to achieve unidirectional energy transfer, at the proper instants, the transferred energy should be exhausted to an external load, or the resonators be decoupled suddenly. If the couple system is left alone after one of resonators is excited, all the consequent behaviors of the system are the result of having a constant coupling of fixed strength. As a result the characteristics of the eigenmodes of the coupled system are already fixed once the coupling is turned on and do not change in time. With one resonator excited only, the state involves exciting both eigenmodes. The interference effect between them results in this bidirectional energy transfer. For the scheme studied here, a modulation mechanism is provided so that the effective coupling strength can be varied by the frequency tuning. A unidirectional energy transfer thus becomes possible.

Since external means are used for tuning one of the resonators, the coupled FM resonator system is not a closed system. In the course of tuning compression and/or expansion of the"photon gas" as discussed in Chapter II also occurs. The amount of energy which is switched thus depends not only on the initial energy distribution but also on the way the system parameters are varied. For instance, in the example given above, we start with all the energy stored in circuit a when Ω_a is much smaller than Ω_b. As Ω_a is increased toward Ω_b, the system energy in the electromagnetic form is increased according to the adiabatic theorem until appreciable energy transfer takes place when $\Omega_a \simeq \Omega_b$. After substantial energy has been transferred to resonator b, the energy remains there without changing the amplitude

or the oscillating frequency in time, because resonator b is a fixed frequency resonator. In this example, the modulation is not turned off after the transfer, therefore compression and/or expansion of the residual energy in resonator a is still taking place. But with very efficient transfer, the residual energy in resonator a is quite small and this effect can be neglected.

In Sec.2.5.3 one of the practical considerations for a superconducting electromechanical energy conversion device calls for a special kind of microwave energy input-output switch. In view of the decoupling feature, the simple configuration and the fact that high switching efficiency does not critically depend on the exact relative phase, this scheme of using coupled FM resonators to effect energy transfer seems to be an ideal solution. The prospect for this application is being further examined at present.

This switching principle has been recognized for sometime in connection with the adiabatic crossing of energy levels in quantum mechanics (1). About twenty years ago, a similar scheme involving a spatial variation of wave propagation coefficients was proposed to build broad band microwave directional couplers (2). Because of the large coupling length required, this scheme was regarded as impractical at that time and gradually forgotten. Recently there is a reviving interest in using this same scheme to build optical directional coupler because of much shorter wavelength involved, therefore much shorter coupling length required (3). Although the principles and the results for the scheme using spatially varying wave propagation coefficients and that using time varying frequencies are almost

identical, there exist slight physical differences due to the nature of the spatial and temporal variables. As we know, the total energy of a time invariant isolated system is conserved, therefore, for the scheme with only spatial variation, the total energy is constant. The switching process only redistributes the energy among various coupled channels. This contrasts to the time variant scheme, where electromagnetic energy can be added, or extracted during the switching process, that is, energy conversion also takes place at the same time. It also appears the former scheme is more suitable for a propagating mode while the latter for a standing mode due to the nature of the independent variable.

As mentioned before, the energy switching is accomplished by maintaining almost all the energy in one of the system eigenmodes thoughout the tuning process. In order to achieve a high degree of confinement and thus high efficiency for the switching, the rate of tuning must be generally slow, especially when two eigenfrequencies of the coupled system are very close to each other, i.e., when the separation is minimal (which occurs at $C_a \simeq C_b$) as shown in Fig.3.2. A very rapid tuning through this region can cause the excitation of the other eigenmodes. The energy originally confined in the desired eigenmode will then be substantially diverted to other modes and effectively destroy the highly efficient unidirectional energy transfer from one location to the other (non-adiabatic crossing).

For an infinite system (i.e., time can vary from $-\infty$ to $+\infty$), if frequency Ω_a varies linearly in time and the coupling coefficients

between two resonators are kept constant*, the behavior of the coupled system can be solved exactly in terms of functions known as parabolic cylinder functions(3). Furthermore, the calculation shows a theoretical limit for energy switching given by the following equation:

$$\eta = 1 - \exp\left(-\left(\frac{\pi}{2}\right)\cdot\frac{(\Delta\Omega)^2}{\left(\frac{d\Omega}{dt}\right)} \right) \qquad (3.1)$$

where the efficiency η is defined as the final energy ended up in resonator b divided by the total initial energy in resonator a. $\Delta\Omega$ is the minimum separation of the two eigenfrequencies of the coupled system, and $\frac{d\Omega}{dt}$ is the constant rate change of Ω_a.

Equation (3.1) cannot give completely accurate account for the switching efficiency for our scheme because it is a result based on an infinite system assumption while any real system must always be finite. Furthermore the total energy in our scheme is not conserved, making the definition of switching efficiency somewhat ambiguous. An analog computer simulation was carried out to study the effects due to these two factors. The model system used for this simulation is two coupled pendula, one with a variable period. The equations of motion governing pendulum oscillation are given below to the first

---

* The constants are such that the total energy is conserved. Strictly speaking this is possible only for time invariant system. For time variant system such as the scheme discussed here, the transfer actually takes place essentially in the vicinity of minimal eigenfrequency separation during which the effect of compression or expansion of the energy is small and the total energy is approximately constant.

order of slowness in frequency variation:*

$$\ddot{Y}_a + \omega_a^2(t)Y_a = h^2(Y_b - Y_a)$$

$$\ddot{Y}_b + \omega_b^2 Y_b = h^2(Y_a - Y_b) \qquad (3.2)$$

where Y_a and Y_b are the oscillation amplitudes; $\omega_a(t)$ varies linearly in time; h is a coupling coefficient and is related to the minimum splitting of the eigenmodes ($\Delta\Omega$).

Define

$$\omega_a(t) = P(t)\omega_b$$

$$h = q\,\omega_b \equiv \sqrt{\omega_b(\Delta\Omega)}$$

$$\omega_b t = Z$$

and assume Y_a and Y_b are already normalized. Eq.(3.2) can be rewritten in a dimensionless form as follows:

$$\frac{d^2Y_a}{dZ^2} + P^2(t)Y_a = q^2(Y_b - Y_a)$$

$$\frac{d^2Y_b}{dZ^2} + Y_b = q^2(Y_a - Y_b) \qquad (3.3)$$

---

* The slowness is measured by the quantity $s_\omega = \left|\frac{1}{\omega^2}\frac{d\omega}{dt}\right|$

Simulation was carried out using Eq.(3.3) with results applicable to any frequency range when properly scaled.

A typical simulated result is shown in Fig.3.3. There the energy stored in each pendulum is plotted versus time. At $t = t_o$, both decoupled frequencies were made equal. Initially only pendulum a was excited as indicated by the finite amplitude of energy E_a at $t = 0$. For $t < t_o$, the compression of the energy was observed as expected. When $t \sim t_o$, appreciable exchange of energy took place. At $t = t_o$, the energy was equally divided between them and half transfer had been accomplished. As t was increased further so that $t >> t_o$, the switching was essentially complete. The detail oscillatory structure of the energy curves are due to the frequency difference between the two pendula. The asymmetry of the oscillatory structure before and after the crossing as shown in Fig.3.3 is due to the finite time interval from $t = 0$ to $t = t_o$. If the tuning rate is reduced toward zero, this interval becomes longer and approaches infinity. In this limit, the oscillatory structure will look symmetrical with respect to the crossing point.

Fig.3.3 also confirms that the switching essentially takes place in the vicinity of $t = t_o$ only. During that short span of time, the total system energy is approximately constant.

In this illustration, the residual energy remaining in pendulum a was quite small, therefore, even if we did not turn off the frequency modulation for $t >> t_o$, the increase in energy was negligible. Under this condition, a working definition for switching efficiency can be

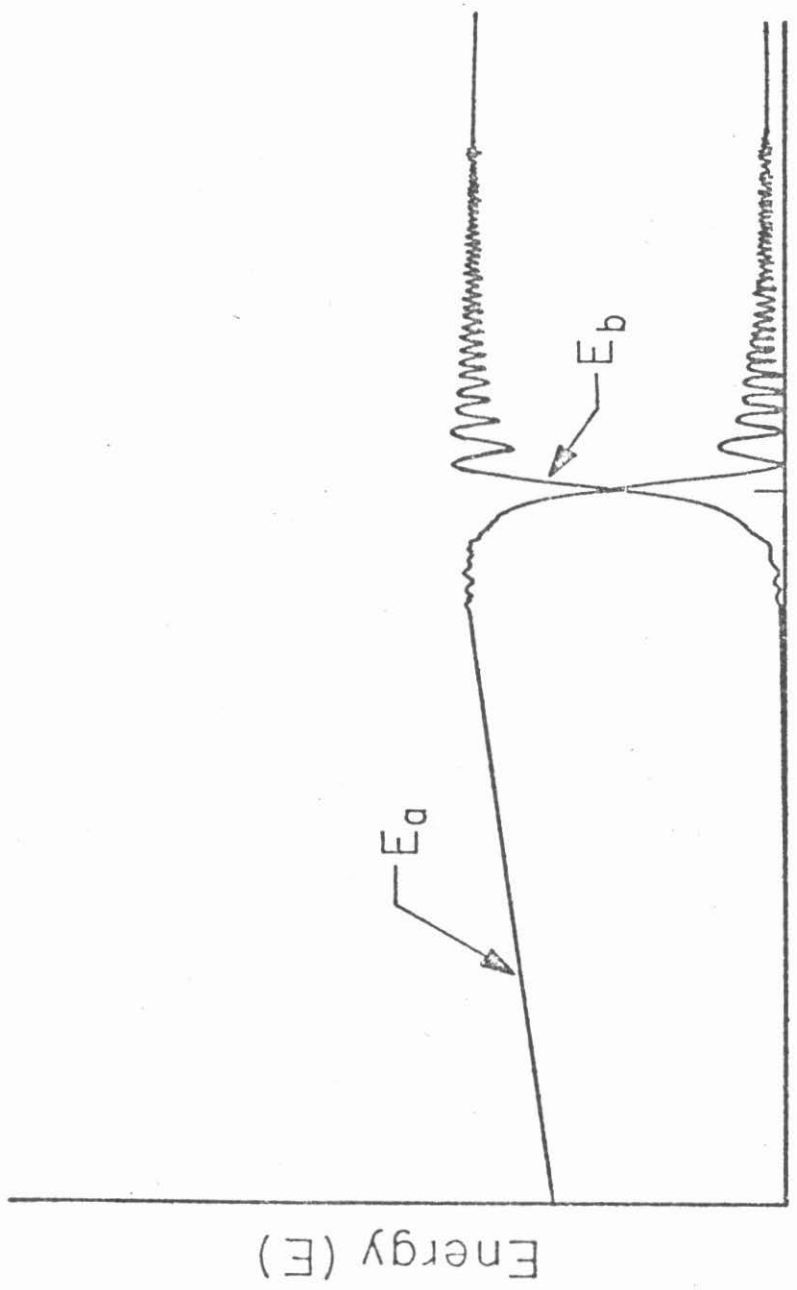

Fig. 3.3 A typical computer simulated result for two coupled pendula. The energy stored in the two pendula are plotted against time. At t = 0 all the energy concentrates in pendulum (a). The oscillation frequency of pendulum (a) is varied linearly with time and one observes a transfer of energy from pendulum (a) to (b).

given as follows:

$$\eta' = \frac{E_b}{E_a + E_b}$$

when $t >> t_o$.

In this simulation study, the rate of frequency change $d\Omega/dt$ and coupling strength $\Delta\Omega$ were varied to study the systematic behavior. A plot of the efficiency η' versus the ratio $(d\Omega/dt)/(\Delta\Omega)^2$ is shown in Fig. 3.4. Again $d\Omega/dt$ is the constant rate of change, and $\Delta\Omega$ is the minimum eigenfrequency separation.

The crossed points are the simulated results and the solid line is the analytic expression given by

$$\eta' = 1 - \exp\left(-\frac{3}{2}\frac{(\Delta\Omega)^2}{(\frac{d\Omega}{dt})}\right) \qquad (3.4)$$

As can be seen. Eq.(3.4) fits the simulated results extremely well. It is interesting to note that Eq.(3.1) and Eq.(3.4) are almost identical except the coefficients of the exponent are slightly different (i.e., $\pi/2$ and $3/2$ respectively). This indicates a finite system has a somewhat smaller switching efficiency than an infinite one.

Fig. 3.4 shows that high switching efficiencies are achievable with a combination of moderate coupling and crossing rate. In the example of Fig. 3.3, the coupling strength and FM rate have been chosen to give an energy transfer efficiency of about 95%.

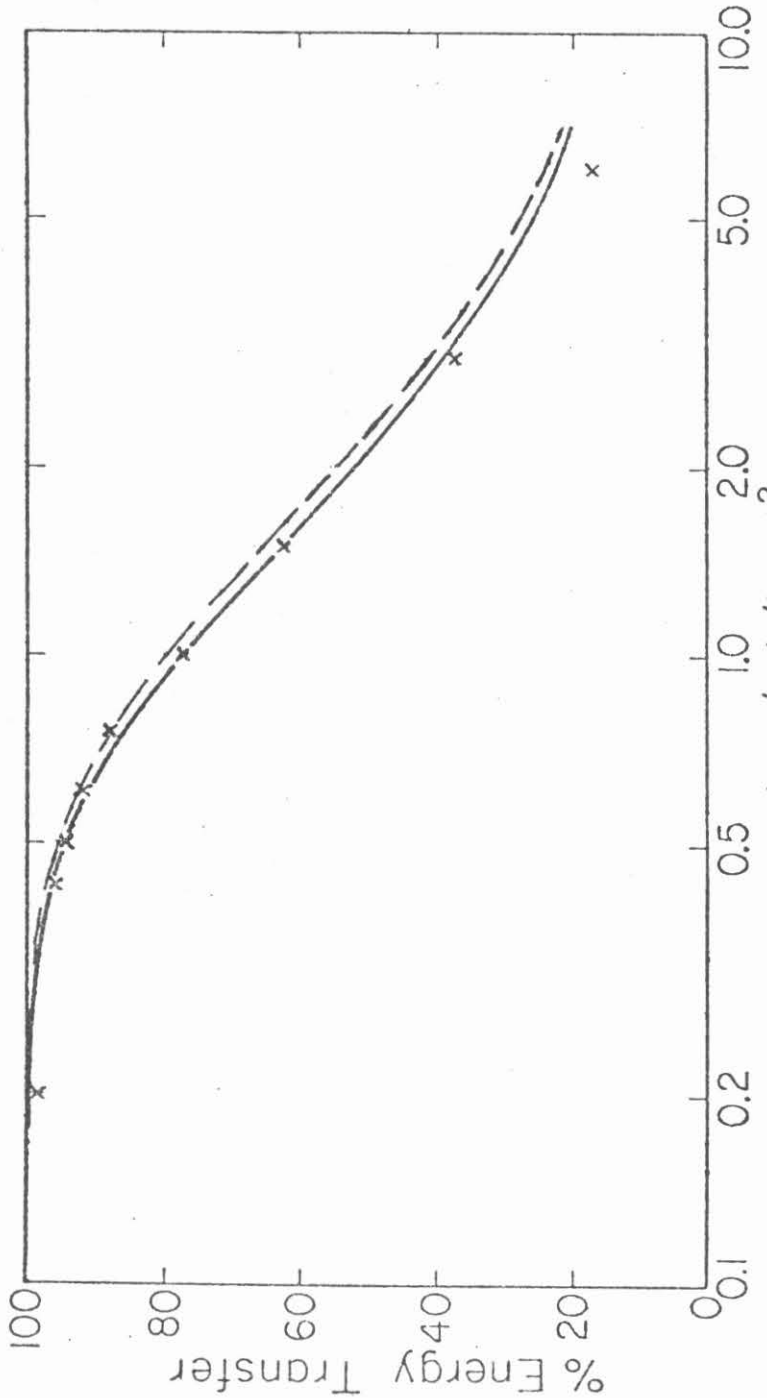

Fig. 3.4 Energy transfer efficiency versus $(d\Omega/dt)/(\Delta\Omega)^2$. The crossed points are the computer simulated results. Eq.(3.4) is plotted as the solid curve while Eq.(3.1) as the dashed curve. The difference between these two curves is due to finite time span assumed in the simulation.

The reversibility of this process has also been confirmed by the analog computer simulation. In this case, only the pendulum b was set to oscillate initially. After the adiabatic crossing, substantial portion of this energy was transferred to pendulum a. Because pendulum a was subject to the external modulation continuously, the energy was also continuously increased after transfer. This made the definition of switching efficiency ambiguous in this case.

Up to now, ideal resonators have been assumed through our analyses. For practical applications, the finite energy decay time has always to be considered. This matter will be taken up in Sec.3.4 when the application as a microwave energy switch is considered.

3.3 Semiquantitative Study of Coupled Resonant Systems

Even though under certain conditions, it is possible to obtain exact solutions for the linear frequency modulation case (1,3), the solutions remain largely unusable due to lack of the representation in elementary functions for the parabolic cylinder functions of arbitrary arguments. Numerical tables for these functions are not presently available either. Thus the system behavior near the frequency crossing has not yet been well studied. The situation becomes even worse if an arbitrary smooth frequency modulation is desired because the exact solutions may never exist at all. In order to overcome this difficulty, a matrix formulism is presented to obtain semiquantitative results without actually solving the complex coupled differential equations if certain conditions can be satisfied*. This

---

* This approach has been used before by Waldron to solve coupled mode

(To be continued)

formulism provides us a way to study the nature of the frequency crossing and is general enough to be applicable to almost all smooth frequency variations.

We start with a pair of coupled differential equations describing the complex amplitudes of oscillation for both resonators as a function of time.*

$$\frac{da_1}{dt} = j\omega_1 a_1 + c_{12} a_2$$

$$\frac{da_2}{dt} = j\omega_2 a_2 + c_{21} a_1 \qquad (3.5)$$

where a_1, a_2 are the amplitudes in the coupled mode formulism(5), and are related to the stored energies in the resonators 1 and 2 according to $E_1 = |a_1|^2$ and $E_2 = |a_2|^2$ respectively. In general the angular frequencies ω_1, ω_2 and coupling coefficients c_{12}, c_{21} are

---

(continued from previous page)
problems (4). However his solutions are erroneous because of several inconsistencies and mistakes in his derivation. In Appendix C, this method is applied to a time dependent system which is of our interest and solutions obtained there are then used in this section for further discussion.

* Eq.(3.2) is a set of coupled second order differential equations while Eq.(3.5) is of first order. There is no inconsistency between them because the variables in Eq.(3.2) are real while those of Eq. (3.5) are complex. For instance, the complex amplitude a_1 has a real part which is proportional to the real amplitude of resonator 1 and an imaginary part which is proportional to the first derivative of this real amplitude. Eq.(3.2) follows immediately when Eq.(3.5) is separated into real and imaginary parts.

complex and time dependent. For a dissipationless system ω_1 and ω_2 become real. $j = \sqrt{-1}$.

For a small change in time δt, the amplitudes at time $t + \delta t$ are related to those at time t according to Eq.(3.5) as follows:

$$\begin{pmatrix} a_1(t+\delta t) \\ a_2(t+\delta t) \end{pmatrix} = \begin{pmatrix} 1+j\omega_1\delta t & c_{12}\delta t \\ c_{21}\delta t & 1+j\omega_2\delta t \end{pmatrix} \begin{pmatrix} a_1(t) \\ a_2(t) \end{pmatrix} \qquad (3.6)$$

Our task is to find a matrix which will relate the amplitudes at time $t + t_o$ to those at time t, where t_o is a finite time span. Let us imagine the time interval t_o is divided into a large number n of elementary time subintervals δt so that in the limit $\delta t \to 0$, $n \to \infty$, $n\delta t \to t_o$. If we define a matrix A such that

$$A = \begin{pmatrix} 1 + j\omega_1\delta t & c_{12}\delta t \\ c_{21}\delta t & 1 + j\omega_2\delta t \end{pmatrix} \qquad (3.7)$$

It follows for finite time interval t_o

$$\begin{pmatrix} a_1(t+t_o) \\ a_2(t+t_o) \end{pmatrix} = \underset{\substack{\delta t\to 0, n\to\infty \\ n\delta t\to t_o}}{\text{Limit}} \prod_{p=1}^{n} A_p \begin{pmatrix} a_1(t) \\ a_2(t) \end{pmatrix} \qquad (3.8)$$

where A_p is the matrix A appropriate for the pth time element δt. The problem is exactly solved if we can express the term in the parentheses in terms of the known time variations of the frequencies

and the coupling coefficients. This is difficult to achieve for almost all real situations and approximations are needed. In Appendix C, the calculation of Eq.(3.8) is carried out further. It was found in the adiabatic limit (i.e., ω_1, ω_2, c_{12} and c_{21} are adiabatically varied. See Eqs.(2.4) and (C.16).)

$$\begin{pmatrix} a_1(t+t_o) \\ a_2(t+t_o) \end{pmatrix} = F \cdot T \begin{pmatrix} a_1(t) \\ a_2(t) \end{pmatrix} \tag{3.9}$$

where

$$F = \exp\left(j \int_t^{t+t_o} \left(\frac{\omega_1 + \omega_2}{2} \right) dt \right) \tag{3.10}$$

$$T = P^{-1}(t+t_o) \begin{pmatrix} e^{jJ} & 0 \\ 0 & e^{-jJ} \end{pmatrix} P(t) \tag{3.11}$$

$$J = \int_t^{t+t_o} \sqrt{\left(\frac{\omega_1 - \omega_2}{2} \right)^2 - c_{12}c_{21}}\, dt \tag{3.12}$$

$$P = \frac{1}{\sqrt{Y^2 - c_{12}c_{21}}} \begin{pmatrix} Y & -jc_{12} \\ jc_{21} & Y \end{pmatrix} \tag{3.13}$$

$$Y = \frac{(\omega_1 - \omega_2)}{2} + \sqrt{\left(\frac{\omega_1 - \omega_2}{2} \right)^2 - c_{12}c_{21}} \tag{3.14}$$

Once the time dependence of ω_1, ω_2, c_{12} and c_{21} are known, matrix P

and integrals J and F can be evaluated. The problem is then approximately solved.

The factor F is common to both amplitudes and represents a common phase progression. If we make a coordinate transformation so that the new coordinate system rotates at the angular rate of $(\omega_1 + \omega_2)/2$ relative to the original one, this common factor will disappear in the transformed equation. Obviously, it is of no physical consequence. For example, when calculating the energies in each resonator, this factor will drop out.

The quantity 2J represents the total accumulated phase difference between the two eigenmodes over the period of time t_o. This relative phase includes the contributions from the accumulated relative phase between the two individual oscillations as well as the coupling as can be seen from Eq.(3.12). If we turn off the coupling, 2J becomes the relative phase between the two individual oscillations as expected. From Eq.(3.9), the switching is determined by the T matrix in which the effect of the accumulated relative phase appears in the phase factor J only.

Substituting Eq.(3.13) and Eq.(3.14) into Eq.(3.11) and carrying out the matrix multiplication we obtain

$$T = \frac{1}{N} \begin{pmatrix} Y(t+t_o)Y(t)e^{jJ} - c_{12}(t+t_o)c_{21}(t)e^{-jJ} & \\ -j(c_{21}(t+t_o)Y(t)e^{jJ} - c_{21}(t)Y(t+t_o)e^{-jJ}) & \end{pmatrix}$$

$$(-j)\left(c_{12}(t)Y(t+t_o)e^{jJ} - c_{12}(t+t_o)Y(t)e^{-jJ} \right) \Bigg)$$

$$- c_{12}(t)c_{21}(t+t_o)e^{jJ} + Y(t)Y(t+t_o)e^{-jJ} \Bigg)$$

(3.15)

where $N = \sqrt{(Y^2(t)-c_{12}(t)c_{21}(t))\ (Y^2(t+t_o)-c_{12}(t+t_o)c_{21}(t+t_o))}$

(3.16)

We shall apply this formulism to a weakly coupled system where decoupled resonator frequencies cross each other linearly and quadratically. The crossing is assumed to be adiabatic(see Eq.(c.16)). The coupling coefficients are chosen so that $c_{12} = -c_{21} = c$ for simplicity, where c is a positive real constant. The relative sign between c_{12} and c_{21} is chosen to conserve the total energy which is approximately true in our case.

In addition, at initial time $t = -t_1$ ($t_1 > 0$) when the resonators are essentially decoupled, all the energy is assumed to be concentrated in resonator 2, i.e., we assume

$$\begin{pmatrix} a_1(-t_1) \\ a_2(-t_1) \end{pmatrix} \simeq \begin{pmatrix} 0 \\ 1 \end{pmatrix} \qquad (3.17)$$

(I) Linear Crossing

The decoupled frequencies are assumed to cross at t = 0 and

are given by

$$\omega_1 = \omega_o + r_1 t$$

$$\omega_2 = \omega_o - r_2 t \tag{3.18}$$

where $r_i = \frac{d\omega_i}{dt} << \omega_i^2 \qquad (i = 1,2)$

For time $t > 0$, we have

$$\begin{pmatrix} a_1(t) \\ a_2(t) \end{pmatrix} = \frac{F}{N} \begin{pmatrix} (-j)\ (c_{12}(-t_1)Y(t)e^{jJ} - c_{12}(t)Y(-t_1)e^{-jJ}) \\ - c_{12}(-t_1)c_{21}(t)e^{jJ} + Y(-t_1)Y(t)e^{-jJ} \end{pmatrix} \tag{3.19}$$

$$\begin{pmatrix} E_1(t) \\ E_2(t) \end{pmatrix} = \frac{1}{N^2} \begin{pmatrix} c^2(Y^2(t)+Y^2(-t_1)-2Y(t)Y(-t_1)\cos 2J) \\ Y^2(t)Y^2(-t_1)+c^4+2c^2Y(t)Y(-t_1)\cos 2J \end{pmatrix} \tag{3.20}$$

where $N^2 = (Y^2(t) + c^2)\ (Y^2(-t_1) + c^2)$

$$J = \int_{-t_1}^{t} \sqrt{\left(\frac{\omega_1 - \omega_2}{2}\right)^2 + c^2}\ dt$$

Suppose at $t = -t_1$, $\omega_1 << \omega_2$ and at time $t\ (\simeq t_1)$ $\omega_1 >> \omega_2$. Also assume $|\alpha| = |\omega_1 - \omega_2| >> c$ at both extremes, i.e., when we are

somewhat away from the crossing point and the coupling coefficient c is small, it follows:

$$Y(-t_1) \simeq c^2/\,|\alpha(-t_1)|$$

$$Y(t) \simeq \alpha(t) + c^2/\,|\alpha(t)| \qquad (3.21)$$

$$Y(t)Y(-t_1) \simeq c^2\,\frac{\alpha(t)}{|\alpha(-t_1)|} \simeq c^2 \qquad \text{if } t \simeq t_1$$

Therefore

$$\begin{pmatrix} E_1(t) \\ E_2(t) \end{pmatrix} \simeq \frac{1}{(\alpha^2(t)+4c^2)} \begin{pmatrix} \alpha^2(t)+2c^2(1-\cos 2J) \\ 2c^2(1+\cos 2J) \end{pmatrix} \qquad (3.22)$$

$$\simeq \begin{pmatrix} 1 \\ 0 \end{pmatrix}$$

where $\alpha(t) >> c$.

Equation (3.22) confirms the assertion that the transfer is always almost complete regardless of the exact value of the accumulated relative phase 2J, as long as the adiabatic conditions are satisfied. This feature makes this switching scheme very useful because it can be easily implemented without having to know the exact relative phase.

However it is still possible to have a complete transfer at some specific instants when the proper amount of the relative phase has been accumulated. This can be shown at least in principle by

setting Eq.(3.20) equal to $\begin{pmatrix} 1 \\ 0 \end{pmatrix}$, and solving the resultant matrix equation to obtain the required coupling and the instants when the complete transfer have taken place. In reality, this is a difficult task because coupled integral equations are involved. Nevertheless, this feature can be observed from the computer simulated result shown in Fig.3.3. There in the oscillatory region after the frequency crossing, there are several instants when the energy inside the resonator a becomes zero indicating a complete transfer has taken place*. Because this mode of complete transfer depends very sensitively on the exact amount of phase and correct coupling, it is deemed as less practical than the one we have proposed.

(II) Quadratic Crossing

Since we are interested in the capability of sinusoidal cyclic operation, the study of the quadratic crossing of two decoupled eigenfrequencies between a sinusoidal frequency variation and a constant frequency is appropriate. The two decoupled frequencies are given by the following expressions:

$$\omega_1 = \omega_o$$

$$\omega_2 = \omega_o + \Delta\omega\left(1 - \frac{t^2}{T^2}\right) \qquad (3.23)$$

---

* Even though the assumptions leading to Eq.(3.22) are not valid if we are very close to the crossing point, Eq.(3.22) seems able to describe partially the behavior in that region as well. This can be seen from the fact in that region $\alpha(t)\simeq 0$, therefore $E_1 \simeq (1+\cos 2J)/2$, $E_2 \simeq (1-\cos 2J)/2$. That is E_1 and E_2 show the oscillatory exchange of energy between these two resonators which is similar to those observed in Fig.3.3.

where $\Delta\omega$ and T are two parameters at our disposal and t is assumed to be finite so that ω_2 is always positive.

The quadratic crossing is characterized by two crossings occurring at $t = \pm T$. If both crossings are done adiabatically, the energy we start with in one of the resonators will be switched to the other after the first crossing more or less like the linear crossing discussed above. However it will return to the original resonator after the second crossing as an unavoidable consequence of the unidirectional transfer ability of the adiabatic crossing. This can be demonstrated generally with our matrix formulism. Again it is assumed initially only resonator 2 is excited. Also assume at $t = -t_1$ and at time t $(\simeq t_1)$ $\omega_1 >> \omega_2$, i.e., the resonators are essentially decoupled at these two extremes. For small coupling coefficient c, we have

$$\begin{aligned} \alpha(-t_1) &\simeq \alpha(t) = \omega_1 - \omega_2 >> c \\ Y(-t_1) &\simeq Y(t) \simeq \alpha + c^2/\alpha >> c \end{aligned} \tag{3.24}$$

Substitute Eq.(3.24) into Eq.(3.20) it follows

$$\begin{pmatrix} E_1(t) \\ E_2(t) \end{pmatrix} \simeq \frac{1}{(Y^2(t)+c^2)^2} \begin{pmatrix} 2c^2Y^2(t)(1-\cos 2J) \\ c^4+Y^4(t)+2c^2Y^2(t)\cos 2J \end{pmatrix}$$

$$\simeq \begin{pmatrix} \frac{2c^2}{Y^2}(1-\cos 2J) \\ 1 + \frac{2c^2}{Y^2}\cos 2J \end{pmatrix} \simeq \begin{pmatrix} 0 \\ 1 \end{pmatrix} \tag{3.25}$$

as is expected. Therefore, without taking into account the detailed phase accumulation, the quadratic adiabatic crossing generally can not provide us a unidirectional energy transfer.

Like linear crossing case, there exist some specific instants after the crossing at which substantial energy transfer can be achieved if the accumulated phase and the coupling coefficients are of proper values at these moments. Again, these values are found by the same procedure of solving a matrix equation as in the linear case. Even though there are certain circumstances where cyclic unidirectional transfer can be achieved regardless of the accumulated phase value; for example, if the energy transferred after the first crossing is consumed before the second crossing takes place or the second crossing is so highly non-adiabatic that the retransfer cannot occur, it nevertheless points to the difficulty which may arise if a simple cyclic switching operation is desired. Further study of quadratic crossing is needed so that a practical design of unidirectional cyclic switch can be designed.

3.4 Some Possible Applications Using Coupled Superconducting FM Resonator Systems

In this section, we will propose two applications making use of the properties of a coupled FM resonant system. Superconducting FM resonators are considered so that the requirements imposed by the finite energy decay time can be found.

3.4.1 Characteristics of Energy Switching Devices

Obviously using coupled high-Q superconducting resonator system

as energy switching devices follows immediately from the discussions and analyses of Sec. 3.2 and Sec. 3.3. The electromagnetic energy in a fixed resonator can be relocated to another through the action of an FM resonator which is coupled to both initial and final resonators of either the same or different resonant frequencies.

Since the effective coupling is very strong only in the vicinity of the region where two decoupled frequencies are almost equal, the crossing can be regarded as linear to the first order of approximation. Eq.(3.5) shows that in order to achieve a high degree of transfer the factor $(\Delta\Omega)^2/(\frac{d\Omega}{dt})$ has to be maximized, where $\Delta\Omega$ is the minimal splitting between the two eigenfrequencies which occurs when the decoupled frequencies are equal to each other and is a function of the coupling coefficients only. $(\frac{d\Omega}{dt})$ is the rate of modulation. These are two factors which can be independently varied. For our discussion, weak coupling has been assumed all along which makes the minimal splitting $(\Delta\Omega)$ accordingly small. This in turn sets an upper limit on the modulation rate $d\Omega/dt$. Modulation exceeding this limit will destroy the unique properties of the adiabatic crossing upon which the whole switching scheme is based. In reality, it cannot be set arbitrarily too slow either because of the finite energy loss rate. If the former is slower than the latter, clearly the process becomes very ineffective. The optimal energy switching will depend on the resonator energy decay time τ_p, the modulation rate $\frac{d\Omega}{dt}$, and the minimum splitting $\Delta\Omega$. As long as $\Omega\tau_p >> 1$, the transfer efficiency of Eq.(3.4) is a good approximation. Under this condition, the requirement for greater than 95% efficiency in energy

switching is that

$$\left(\frac{d\Omega}{dt}\right) < \frac{1}{3}(\Delta\Omega)^2 \qquad (3.26)$$

The quantity $(\Delta\Omega)/(\frac{d\Omega}{dt})$ is the time necessary to sweep the frequency through a range equivalent to the minimal splitting between the two eigenfrequencies. Thus for this case this time must be $> 3/(\Delta\Omega)$. For example, the minimal splitting $(\Delta\Omega)$ for two resonators coupled through a constant capacitance C_o such as the one shown in Fig.3.2 is given by $\Delta\Omega \sim \Omega_b(C_o/C_b)$ where $\Omega_b = 1/\sqrt{LC_b}$. Assume this equivalent circuit representation is valid for a coupled microwave resonator system and further assume the energy decay time τ_p is 1 sec for superconducting resonators at 10 GHz (i.e., $\Omega_b/2\pi$ = 10 GHz). Obviously $\Omega_b\tau_p = 10^{11} >> 1$ and Eq.(3.26) is valid. For $C_o/C_b \sim 10^{-3}$, the minimum splitting is given by $\Delta\Omega \sim 6\times10^7$ sec^{-1} and the time it takes to sweep through $\Delta\Omega$ must be larger than $3/(\Delta\Omega) \sim 5\times10^{-8}$ sec which is the lower bound for the mechanical modulation time τ_m. The upper bound of course is the energy decay time τ_p. Because of the limitation of material strength, the fastest modulation time achievable is of order of 10^{-4} sec. Clearly both conditions can be amply satisfied. Thus coupled high Q superconducting FM resonator system can be used as a high efficiency switching device.

3.4.2 Characteristics of High Power Microwave Generators

An immediate variation of this energy switching scheme could be to "Q switch" a highly-moded superconducting resonator onto an antenna load to produce a very high power microwave pulses. This

is brought about by the fact that substantial energy switching can be accomplished within a very small fraction of the basic mechanical modulation time. This is not a surprising result since the interaction between two weakly coupled resonators is strong only when the decoupled eigenfrequencies are almost equal which occurs only for a very short period of time. This feature is also demonstrated by the systematic study of computer simulation. One of the examples has been previously shown in Fig.3.3. The results indicate the switching is essentially finished in one or two hundred cycles of the intrinsic oscillation centering around the crossing instant for a wide range of modulation rate and coupling strength. For resonators operated at X-band frequencies, this switching time is about 10^{-7} sec.

In Sec. 2.5.2 it is shown that the maximum energy density that can be stored inside a superconducting resonator with present superconductivity technology is about a kilojoule per cubic meter. An X-band device of $10^3 cm^3$ active volume will contain a joule of microwave energy which can be switched to an antenna rapidly producing a microwave pulse of about 10 megawatts and 100 ns duration. If the volume scaling is valid, one cubic meter active volume will contain one kilojoules of energy which can be switched to generate a 10 GW pulse.

3.5 Conclusions

In this chapter, the familiar notions of coupled resonant systems are extended to gain insight into the behavior of coupled ideal FM resonators. Practically this ideal case is approximately fulfilled by coupled high Q superconducting FM resonators. Therefore the potential applications derived from the ideal system are very

likely to be realized with actually available superconducting resonators. The proposed applications as energy switching devices and pulse generators based on the scheme discussed here are quite unique and novel without having an equivalent counterpart in the room temperature microwave technologies. A new field of applied superconductivity has been opened up by the introduction of highly frequency modulated superconducting resonators operated at high rf power level. However there are a great deal of actual operations still needed to be demonstrated before this new scheme can be considered as a successful technology.

References

1. C.Zener, Roy. Soc. Proc. 137, 696-702 (1932).

2. J.S.Cook, Bell Sys. Tech. J. 34, 807-822(1955).

3. R.B.Smith, J. Opt. Soc. Am. 66, 882-892 (1976).

4. R.A.Waldron, Ouart. J. Mech. and Appl. Math. 18, 385-404.

5. W.H.Louisell, Coupled Modes and Parametric Electronics (Wiley, N. Y. 1960).

Appendix A

ADIABATIC THEOREM

For simplicity and definiteness, an ideal electric L-C resonant circuit with a time dependent capacitor is used as a model system to illustrate the adiabatic theorem. As shown in Fig. A.1a, V(t) and I(t) are respectively the instantaneous voltage across the capacitor C(t) and the current through the inductor L. The resonant angular frequency is given by the usual relationship

$$\omega(t) = \frac{1}{\sqrt{L \cdot C(t)}} \equiv 2\pi f(t) \qquad (A.1)$$

The time variation of C(t) (therefore, $\omega(t)$) is assumed extremely slow so that the following condition is satisfied

$$\frac{1}{\omega(t)} \frac{d\omega(t)}{dt} << \omega(t) \qquad (A.2)$$

Define a complex quantity a(t) such that

$$a(t) = \frac{L}{2} (I(t) + j\omega(t)C(t)V(t)) \qquad (A.3)$$

Clearly a(t) depends on the instantaneous distributions of the current and charge in this circuit. If we take absolute square of this quantity,

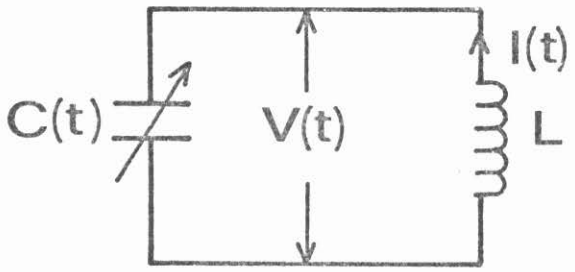

$$\omega = 1/\sqrt{LC}$$

$$a = \sqrt{L/2}(I + j\omega CV)$$

$$\frac{da}{dt} = (j\omega + \frac{1}{2\omega}\frac{d\omega}{dt})a - \frac{1}{2\omega}\frac{d\omega}{dt}\,a^*$$

Fig. A.1(a) An ideal circuit consisting of a fixed inductor L and a variable capacitor C for demonstrating the adiabatic theorem.

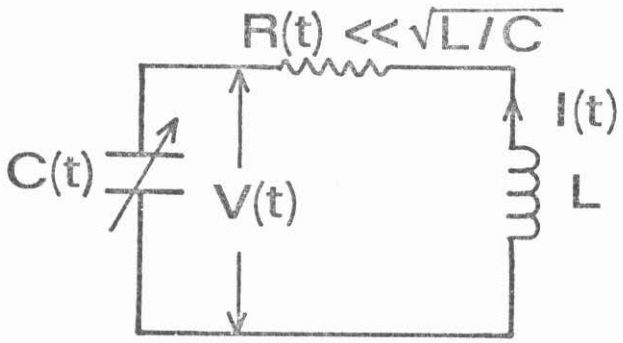

$$\omega = 1/\sqrt{LC}$$

$$a = \sqrt{L/2}\ (I + j\omega CV)$$

$$\frac{da}{dt} = (j\omega - R/2L + \frac{1}{2\omega}\frac{d\omega}{dt})a - (R/2L + \frac{1}{2\omega}\frac{d\omega}{dt})a^*$$

Fig. A.1(b) Same as Fig. A.1(a) except a time dependent dissipation is allowed.

$$|a(t)|^2 = \frac{1}{2} LI^2(t) + \frac{1}{2} C(t)V^2(t) \equiv W(t) \qquad (A.4)$$

where W(t) is the total electromagnetic energy of the circuit at any instant. It will be shown later, this quantity W(t) varies slowly with $\omega(t)$ if Eq.(A.2) is satisfied.

Maxwell equations and conservation of charges require

$$V(t) = - L \frac{dI(t)}{dt} \qquad (A.5)$$

$$I(t) = \frac{d}{dt} (C(t)V(t)) \qquad (A.6)$$

In terms of a(t), Eqs.(A.5) and (A.6) can be combined to give

$$\frac{da}{dt} = \left(j\omega + \frac{1}{2\omega} \frac{d\omega}{dt} \right) a - \left(\frac{1}{2\omega} \frac{d\omega}{dt} \right) a^* \qquad (A.7)$$

where a* is the complex conjugate of a. It follows immediately that

$$\frac{d|a|^2}{dt} \equiv \frac{dW}{dt} = \left(\frac{1}{\omega} \frac{d\omega}{dt} \right) W - \left(\frac{1}{\omega} \frac{d\omega}{dt} \right) \left(\frac{a^2+a^{*2}}{2} \right) \qquad (A.8)$$

The factor $\frac{1}{2}(a^2 + a^{*2}) \equiv \frac{1}{2} LI^2 - \frac{1}{2} CV^2$ is the difference between the instantaneous magnetic and electrical energy which can be of order of the total instantaneous energy itself. To evaluate this term, we need explicit expressions for a and a*. Eliminating I(t) from Eq.(A.5)

and Eq.(A.6), we have

$$\frac{d^2Q(t)}{dt^2} + \omega^2(t)Q(t) = 0 \qquad (A.9)$$

where $Q(t) = C(t)V(t)$. Eq.(A.9) can be solved within WKB approximation if Eq.(A.2) is satisfied. Under this condition $Q(t)$ is given by

$$Q(t) = \frac{Q_o}{\sqrt{\omega(t)}} \sin\left(\int_o^t \omega(t)dt + \theta_o\right) + O(s) \qquad (A.10)$$

Q_o and θ_o are constants which are determined by the initial conditions. $s \equiv \frac{1}{\omega^2}\frac{d\omega}{dt}$ is a very small dimensionless parameter characterizing the slowness of the adiabatic transformation.

With Eqs.(A.3), (A.5), (A.6) and (A.10), Eq.(A.8) can be written as

$$\frac{dW}{dt} - \frac{1}{\omega}\frac{d\omega}{dt}\cdot W = -\frac{W(0)}{\omega(0)}\omega^2\left(s\cdot\cos\left(2\int_o^t \omega dt + 2\theta_o\right) - \frac{s^2}{2}\sin\left(2\int_o^t \omega dt + 2\theta_o\right) + O(s^3)\right) \qquad (A.11)$$

where $W(0)$ and $\omega(0)$ are respectively the initial energy and frequency. If we average Eq.(A.11) over one cycle of the oscillation, the right hand side becomes vanishingly small because the averaged trigonometric terms are almost identically zero. Therefore

$$\overline{\frac{dW}{dt}} = \left(\overline{\frac{1}{\omega}\frac{d\omega}{dt}}\right)\overline{W} \qquad (A.12)$$

or

$$\overline{W} = \text{constant} \cdot \overline{\omega} \; * \qquad \text{(A.13)}$$

This is the statement of the adiabatic theorem. If dissipation is included, a time dependent resistance is added as shown in Fig.A.1b and Eqs.(A.7), (A.12) and (A.13) are respectively replaced by the following equations

$$\frac{da}{dt} = (j\omega - \frac{R}{2L} + \frac{1}{2\omega}\frac{d\omega}{dt})a - (\frac{R}{2L} + \frac{1}{2\omega}\frac{d\omega}{dt})a^* \qquad \text{(A.14)}$$

$$\overline{\frac{dW}{dt}} = (\overline{-\frac{R}{L} + \frac{1}{\omega}\frac{d\omega}{dt}})\overline{W} \qquad \text{(A.15)}$$

and

$$\overline{W} = \text{constant} \cdot \overline{\omega}(t) \cdot \exp(-\int_o^t \frac{dt}{\tau_p}) \qquad \text{(A.16)}$$

where $\tau_p \equiv \frac{L}{R}$ is the instantaneous energy decay time.

---

* Quantities with bars are the averaged values over one oscillating cycle.

Appendix B

A BRIEF DESCRIPTION OF THE ELECTROSTATIC TRANSDUCER

The electrostatic transducer used in our experiments consists of two parallel "plates" forming a capacitor as shown in Fig.2.1. One of the plates is the thin top plate of the reentrant resonator. The other is a metal disc of about one inch in diameter. A high voltage generated by the electronic circuit shown in Fig.B.1 is applied across this capacitor with the thin top plate always at ground potential. The high voltage is obtained from an audio signal at 2 KHz which is amplified and further boosted by a Stancor flyback transformer whose secondary is made to resonate around 2 KHz. A d.c. component is added to the a.c. voltage, so that the applied voltage is of the following form

$$V(t) = V_o + V_1 \sin(\omega_m t + \theta) \qquad (B.1)$$

where V_o and V_1 are respectively the d.c. and a.c. amplitudes; ω_m is close to the vibrational frequency and θ is the phase. For our experiments, V_o and V_1 were set equal to each other so that the voltage applied to the metal disc is always nonnegative. Voltage up to six kilovolts has been obtained with this method. At present, the limiting factors are the arcing inside the transducer and the instability of vibration when the applied voltage is too large.

The thin plate of the rf resonator will be driven to vibrate in its fundamental mechanical mode when the voltage of correct fre-

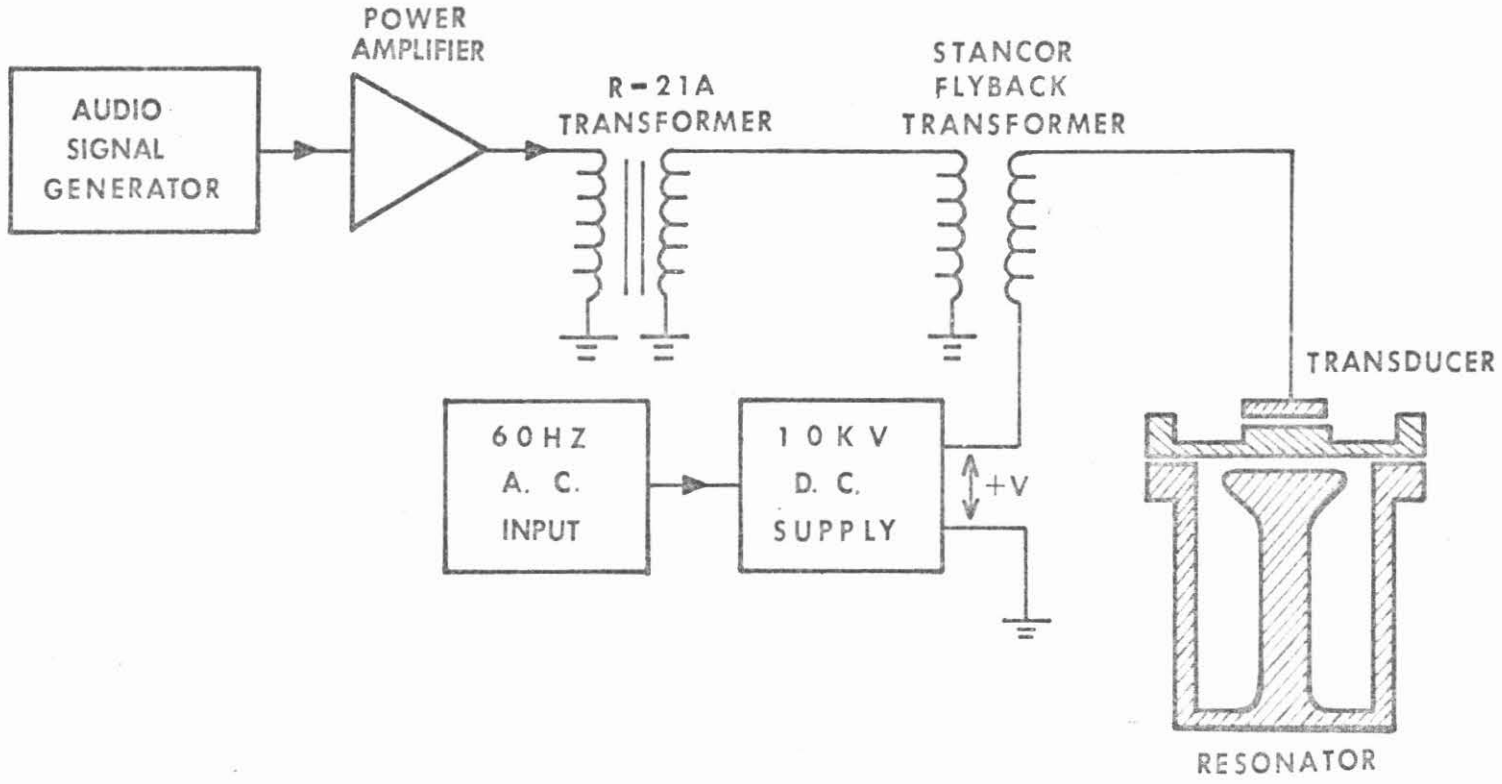

Fig. B.1 Block diagram showing the electronic arrangement used to generate high voltage transducer drive in the study of dynamic modulation.

quency is applied to it. This forced vibration is difficult to solve because of the somewhat odd geometry and the intrinsic nonlinearity of the vibration. It becomes clearer if we can describe the vibration in terms of its equivalent circuit. This is partially justified by noting that the vibrational amplitude within the thickened area is large and quite uniform due to its flexural rigidity. Outside that area the amplitude is much smaller. An effective mass can be calculated by properly weighting the mass distribution with the square of the corresponding vibrational velocity. Clearly, the effective mass comes mainly from the mass of the thickened area. For our transducer, it is estimated to be about 13 gms. Let x be the average vibrational amplitude within the thickened area. The equation of vibration is given by

$$\ddot{x} + \frac{\omega}{Q_m}\dot{x} + \omega^2 x = \frac{A}{m} \cdot \frac{\varepsilon_o}{2}\left(\frac{V(t)}{d-x}\right)^2 \qquad (B.2)$$

where Q_m is the mechanical quality factor for low amplitude; ω is the angular frequency; A and d are respectively the transducer area and static separation; ε_o is the permittivity of vacuum and V(t) is the applied voltage. The right hand side of Eq.(B.2) is the applied force per unit mass. For small vibrational amplitudes, Eq.(B.2) is reduced to ordinary linear forced vibration. In this limit, the quality factor Q_m of our transducer was found to be about 300 at room temperature and 3000 - 6000 at He temperature. Since we are interested in large amplitude vibrations, Eq.(B.2) becomes highly nonlinear. One dimensional approximation like Eq.(B.2) is inadquate to describe the vibration consistently. No effort has been made

toward optimizing the transducer design and operation because our experiments are currently limited by the coupling loading instead of the modulation range.

Appendix C

COUPLED MODE CALCULATION

Following conventional coupled mode formulism, let us assume $a_1(t)$, $a_2(t)$ are the mode amplitudes such that $E_1(t) \equiv |a_1(t)|^2$, and $E_2(t) \equiv |a_2(t)|^2$ are the energies associated with respective modes.

The "equations of motion" for $a_1(t)$ and $a_2(t)$ of an ideal system are given below:

$$\frac{da_1}{dt} = j\omega_1 a_1 + c_{12} a_2$$

$$\frac{da_2}{dt} = j\omega_2 a_2 + c_{21} a_1 \qquad (C.1)$$

The quantities ω_1, ω_2, c_{12} and c_{21} can be time dependent and in general are complex $j = \sqrt{-1}$. c_{12} and c_{21} are called coupling parameters.

Since total energy of the coupled system is $E(t) = E_1(t) + E_2(t)$, we have

$$\frac{dE(t)}{dt} = j(\omega_1 - \omega_1^*) |a_1|^2 + j(\omega_2 - \omega_2^*) |a_2|^2$$

$$+ 2 \cdot R_e \cdot (c_{12} + c_{21}^*) a_1^* a_2 \qquad (C.2)$$

Assume ω_1 and ω_2 are real, and energy is conserved, then it requires

$$c_{12} + c_{21}^* = 0$$

If ω_1 and ω_2 are complex, the amplitudes a_1 and a_2 can grow or diminish in addition to the energy exchange between them. For a system involving changing of constraint parameter, the mechanical energy can be added to or extracted from the system therefore the total energy may not be conserved. However in the adiabatic limit, the change of energy is so slow that within a not too long period of time the change is very small too. In Appendix A we have shown for an ideal case this is adequately taken into account by making ω's real and time dependent. If dissipation exists, ω's become complex. Since we are interested in systems of very small dissipation only, the physics remains essentially the same if we assume ω's are real in the following analysis.

For a small change δt in time t, from Eq.(C.1) we have

$$\begin{pmatrix} a_1(t+\delta t) \\ a_2(t+\delta t) \end{pmatrix} = \begin{pmatrix} 1+j\omega_1\delta t & c_{12}\delta t \\ c_{21}\delta t & 1+j\omega_2\delta t \end{pmatrix} \begin{pmatrix} a_1(t) \\ a_2(t) \end{pmatrix} \qquad (C.3)$$

Our goal is to find a matrix for a finite time change, say from $t = 0$ to $t = t_o$. Imagine the time interval t_o is divided into a large number n of elementary time interval δt so in the limit as $n \to \infty$, $\delta t \to 0$ that $n \cdot \delta t \to t_o$.

Define a matrix A as follows:

$$A(t,\delta t) = \begin{pmatrix} 1 + j\omega_1\delta t & c_{12}\delta t \\ c_{21}\delta t & 1 + j\omega_2\delta t \end{pmatrix} \qquad (C.4)$$

Therefore

$$\begin{pmatrix} a_1(t_o) \\ a_2(t_o) \end{pmatrix} = \underset{\substack{\delta t \to 0, n \to \infty \\ n\delta t \to t_o}}{\text{Limit}} \prod_{p=1}^{n} A_p \begin{pmatrix} a_1(0) \\ a_2(0) \end{pmatrix} \qquad (C.5)$$

where A_p is the matrix appropriate for pth time element δt.

To evaluate the matrix product, let us diagonalize A first. If

$$L \equiv PAP^{-1}$$

with

$$P = \begin{pmatrix} p & q \\ r & s \end{pmatrix}$$

$$P^{-1} = \frac{1}{\Delta}\begin{pmatrix} s & -q \\ -r & p \end{pmatrix}$$

$$\Delta \equiv ps - qr \neq 0$$

Set offdiagonal elements of L to zero, we have

$$\frac{p}{q} = j\left(\alpha + \sqrt{\left(\frac{\alpha}{2}\right)^2 - c_{12}c_{21}}\right)/c_{12} \equiv jY/c_{12}$$

$$\frac{s}{r} = -j\left(\alpha + \sqrt{\left(\frac{\alpha}{2}\right)^2 - c_{12}c_{21}}\right)/c_{21} \equiv -jY/c_{21} \qquad (C.6)$$

where

$$\alpha = \omega_1 - \omega_2$$

$$Y = \frac{(\omega_1 - \omega_2)}{2} + \sqrt{\left(\frac{\omega_1 - \omega_2}{2}\right)^2 - c_{12}c_{21}}$$

and

$$P = \begin{pmatrix} p & q \\ r & s \end{pmatrix} = \begin{pmatrix} \lambda_1 Y & -j\lambda_1 c_{12} \\ j\lambda_2 c_{21} & \lambda_2 Y \end{pmatrix}$$

$$P^{-1} = \frac{1}{\Delta}\begin{pmatrix} \lambda_2 Y & j\lambda_1 c_{12} \\ -j\lambda_2 c_{21} & \lambda_1 Y \end{pmatrix} \qquad (C.7)$$

λ_1, λ_2 are multipliers to be determined later. We have also

$$\Delta = \lambda_1\lambda_2(Y^2 - c_{12}c_{21})$$

$$L = \begin{pmatrix} L_{11} & 0 \\ 0 & L_{22} \end{pmatrix}$$

with

$$L_{11} = 1 + j\delta t\left(\frac{\omega_1 + \omega_2}{2}\right) + j\delta t\sqrt{\left(\frac{\omega_1 - \omega_2}{2}\right)^2 - c_{12}c_{21}}$$

$$L_{22} = 1 + j\delta t\left(\frac{\omega_1 + \omega_2}{2}\right) - j\delta t\sqrt{\left(\frac{\omega_1 - \omega_2}{2}\right)^2 - c_{12}c_{21}}$$

It will be proved later that in most cases the following

relationship is approximately valid,

$$\lim_{\substack{n\to\infty \\ \delta t\to 0}} \prod_{p=1}^{n} A_p = \lim_{\substack{n\to\infty \\ \delta t\to 0}} \left(P_n^{-1} \left(\prod_{p=1}^{n} L_p \right) P_i\right) \qquad (C.8)$$

Since L_p's are diagonal, it can be shown easily that

$$\prod_{p=1}^{n} L_p = \begin{pmatrix} \prod_{p=1}^{n} L_{11,p} & 0 \\ 0 & \prod_{p=1}^{n} L_{22,p} \end{pmatrix}$$

where $L_{11,p}$ is the matrix element L_{11} corresponding to pth time element δt and there

$$\lim_{\substack{\delta t\to 0 \\ n\to\infty}} \prod_{p=1}^{n} L_p = \exp\left(\frac{j}{2}\int_o^t (\omega_1+\omega_2)dt\right)\begin{pmatrix} e^{jJ} & 0 \\ 0 & e^{-jJ} \end{pmatrix} \qquad (C.9)$$

where $$J = \int_0^t \sqrt{\left(\frac{\omega_1-\omega_2}{2}\right)^2 - c_{12}c_{21}}\, dt$$

Thus $$\begin{pmatrix} a_1(t_o) \\ a_2(t_o) \end{pmatrix} = F\cdot T\begin{pmatrix} a_1(0) \\ a_2(0) \end{pmatrix} \qquad (C.10)$$

with $$F = \exp\left(\frac{j}{2}\int_o^t (\omega_1 + \omega_2)dt\right)$$

$$T = P^{-1}(t_o)\begin{pmatrix} e^{jJ} & 0 \\ 0 & e^{-jJ} \end{pmatrix} P(0) \qquad (C.11)$$

We shall examine the validity of Eq.(C.8) next.

Since $L = PAP^{-1}$, $A = P^{-1}LP$

$$P_n^{-1}\left(\prod_{p=1}^{n} L_p\right)P_1 = P_n^{-1}(L_n L_{n-1} \cdots\cdots L_n)P_1$$

$$= P_n^{-1}(P_n A_n P_n^{-1} \cdots\cdots P_1 A_1 P_1^{-1})P_1$$

$$= An\left(\prod_{p=1}^{n} \cdot P_{p+1}^{-1} P_p A_p\right)$$

Thus if

$$P_{p+1}^{-1} P_1 = I \qquad (C.12)$$

where I is the unit matrix, we would have

$$\prod_{p=1}^{n} A_p = P_n^{-1}\left(\prod_{p=1}^{n} L_p\right)P_1 \qquad (C.13)$$

and Eq.(C.8) would be identically true.

To investigate the condition for the validity of Eq.(C.12), let's write

$$A_p = A(t)$$

$$P_p = P(t)$$

$$P_{p+1} = P(t + \delta t)$$

Eq.(C.12) implies if we can replace $P^{-1}(t+\delta t)P(t)A(t)$ by $A(t)$ as $\delta t \to 0$, then Eq.(C.8) would be valid.

This substitution is legitimate if the zero-order terms in δt in the diagonal elements of $P^{-1}(t+\delta t)P(t)$ are equal to 1 and off-diagonal elements are equal to zero, and if terms in δt in the elements of $P^{-1}(t+\delta t)P(t)$ approach zero much faster than terms in δt in A(t) in the limit $\delta t \to 0$ as demonstrated below.

Using Eq.(C.7)

$$P^{-1}(t+\delta t)P(t) = \frac{1}{\Delta}\begin{pmatrix} (\lambda_2+\delta\lambda_2)(Y+\delta Y) & j(\lambda_1+\delta\lambda_1)(c_{12}+\delta c_{12}) \\ -j(\lambda_2+\delta\lambda_2)(c_{21}+\delta c_{21}) & (\lambda_1+\delta\lambda_1)(Y+\delta Y) \end{pmatrix}$$

$$\cdot\begin{pmatrix} \lambda_1 Y & -jc_{12}\lambda_2 \\ j\lambda_2 c_{21} & \lambda_2 Y \end{pmatrix}$$

$$\equiv\begin{pmatrix} Q_{11} & Q_{12} \\ Q_{21} & Q_{22} \end{pmatrix}$$

where $\delta\lambda_1 = \left(\frac{\partial\lambda_1}{\partial t}\right)\delta t$ etc.

and to the first order

$$Q_{11} = 1 + (Y^2\lambda_1\delta\lambda_1 + \lambda_1\lambda_2 Y\delta Y - c_{12}c_{21}\lambda_2\delta\lambda_1 - \lambda_1\lambda_2 c_{21}\delta c_{12})/\Delta$$

$$Q_{22} = 1 + (Y^2\lambda_2\delta\lambda_2 + \lambda_1\lambda_2 Y\delta Y - c_{12}c_{21}\lambda_1\delta\lambda_2 - \lambda_1\lambda_2 c_{12}\delta c_{21})/\Delta$$

$$Q_{12} = (j\lambda_1\lambda_2 Y c_{12})\left(\frac{\delta c_{12}}{c_{12}} + \frac{\delta\lambda_1}{\lambda_1} - \frac{\delta Y}{Y} - \frac{\delta\lambda_2}{\lambda_2}\right)/\Delta$$

$$Q_{21} = (-j\lambda_1\lambda_2 Y c_{21})\left(\frac{\delta c_{21}}{c_{21}} + \frac{\delta\lambda_2}{\lambda_2} - \frac{\delta Y}{Y} - \frac{\delta\lambda_1}{\lambda_1}\right)/\Delta$$

The zeroth order terms in Q give the identity matrix.

For the first-order terms of Q_{11} and Q_{22} to vanish, we require

$$\begin{aligned} \frac{\delta\lambda_2}{\lambda_2} Y^2 + Y\delta Y - c_{12}c_{21}\frac{\delta\lambda_1}{\lambda_1} - c_{21}\delta c_{12} = 0 \\ \frac{\delta\lambda_1}{\lambda_1} Y^2 + Y\delta Y - c_{12}c_{21}\frac{\delta\lambda_2}{\lambda_2} - c_{12}\delta c_{21} = 0 \end{aligned} \qquad \text{(C.14)}$$

and for Q_{12} and Q_{21} to vanish

$$\begin{aligned} \frac{\delta c_{12}}{c_{12}} + \frac{\delta\lambda_1}{\lambda_1} - \frac{\delta Y}{Y} - \frac{\delta\lambda_2}{\lambda_2} = 0 \\ \frac{\delta c_{21}}{c_{21}} + \frac{\delta\lambda_2}{\lambda_2} - \frac{\delta Y}{Y} - \frac{\delta\lambda_1}{\lambda_1} = 0 \end{aligned} \qquad \text{(C.15)}$$

In general, it is impossible to find λ_1 and λ_2 so that Eqs. (C.14) and (C.15) are satisfied simultaneously unless $\delta c_{12}/c_{12} = \delta c_{21}/c_{21} = \delta Y/Y$ which is unlikely to happen for practical modulations. However if the changes of c_{12}, c_{21}, ω_1 and ω_2 in time are so slow that the following adiabatic conditions are satisfied:

$$\frac{1}{\omega}\left|\frac{\partial c_{12}}{\partial t}\right| << |c_{12}|$$

$$\frac{1}{\omega}\left|\frac{\partial c_{21}}{\partial t}\right| << |c_{21}| \qquad \text{(C.16)}$$

$$\frac{1}{\omega}\frac{\partial \omega_1}{\partial t} << \omega_1$$

$$\frac{1}{\omega}\frac{\partial \omega_2}{\partial t} << \omega_2$$

where ω is the frequency of the order of the smaller frequency between ω_1 and ω_2 at that instant. In this limit, it can be shown that

$$P^{-1}(t+\delta t)P(t)A(t) \simeq A(t) \qquad \text{(C.17)}$$

and Eq.(C.8) becomes approximately true.

The conditions of Eq.(C.16) are amply satisfied for most practical cases; in particular, a weakly coupled microwave system with mechanical modulation such as the one under our study.

Furthermore, these conditions impose no new restriction on our

theory because they are already implicitly implied in Eq.(C.1). When these conditions hold, Eqs.(C.14) and (C.15) can be regarded as approximately satisfied and exact values for λ_1 and λ_2 are not too crucial. It turns out to be convenient to make

$$\lambda_1 = \lambda_2 = \frac{1}{\sqrt{Y^2 - c_{12}c_{21}}} \tag{C.18}$$

so that Matrix P assumes the following form

$$P = \frac{1}{\sqrt{Y^2 - c_{12}c_{21}}} \begin{pmatrix} Y & -jc_{12} \\ jc_{21} & Y \end{pmatrix} \tag{C.19}$$

The assignment of λ_1 and λ_2 as given by Eq.(C.18) is not completely random however, because for the case of constant coupling parameters (i.e., for contant c_{12} and c_{21}), these indeed provide a very good approximation for Eq.(C.17).

Thus we can express the Eqs.(C.10) and (C.11) as

$$\begin{pmatrix} a_1(t_o) \\ a_2(t_o) \end{pmatrix} = F \cdot T \begin{pmatrix} a_1(0) \\ a_2(0) \end{pmatrix}$$

with $$F = \exp\left(\frac{j}{2} \int_0^{t_o} \left(\frac{\omega_1 + \omega_2}{2} \right) dt \right) \tag{C.20}$$

$$T = \frac{1}{N}\begin{pmatrix} Y(t_o)Y(0)e^{jJ} - c_{12}(t_o)c_{21}(0)e^{-jJ} & (-j)(c_{12}(0)Y(t_o)e^{jJ} - c_{12}(t_o)Y(0)e^{-jJ}) \\ -j(c_{21}(t_o)Y(0)e^{jJ} - c_{21}(0)Y(t_o)e^{-jJ}) & -c_{12}(0)c_{21}(t_o)e^{jJ} + Y(t_o)Y(0)e^{-jJ} \end{pmatrix} \quad (C.21)$$

where

$$N = ((Y^2(t_o)-c_{12}(t_o)c_{21}(t_o))(Y^2(0)-c_{12}(0)c_{21}(0)))^{1/2}$$